VRIJE UNIVERSITEIT

The Geodesic Deviation Method and Extreme Mass-Ratio Systems

Theoretical methods and application to the calculation of gravitational waves

ACADEMISCH PROEFSCHRIFT

ter verkrijging van de graad Doctor aan
de Vrije Universiteit Amsterdam,
op gezag van de rector magnificus
prof.dr. L.M. Bouter,
in het openbaar te verdedigen
ten overstaan van de promotiecommissie
van de faculteit der Exacte Wetenschappen
op donderdag 15 december 2011 om 09.45 uur
in de aula van de universiteit,
De Boelelaan 1105

door

Gideon Koekoek

geboren te Amsterdam

promotoren: prof.dr. J.F.J. van den Brand,
prof.dr. J.W. van Holten.

This work was carried out at Nikhef as part of the research programma of the "Stichting voor Fundamenteel Onderzoek der Materie (FOM)", which is financially supported by the "Nederlandse Organisatie voor Wetenschappelijk Onderzoek (NWO)".

Contents

1 The basic machinery of General Relativity **9**
- 1.1 Introduction . . . 9
- 1.2 Gravity as curvature . . . 10
- 1.3 The geodesic equations . . . 12
- 1.4 Isometries and Killing vectors . . . 14
- 1.5 Dynamics and production of gravitational waves . . . 16
- 1.6 The energy and momentum of gravitational waves . . . 19
- 1.7 The EMRI system & outline of the thesis . . . 22
- 1.8 Summary . . . 23

2 The geodesic deviation method **25**
- 2.1 Introduction . . . 25
- 2.2 Basics of the Schwarzschild spacetime . . . 26
  - 2.2.1 Geodesic equations, constants of motion, and the circular orbit . . . 26
  - 2.2.2 Implicit solutions for general closed orbits . . . 28
  - 2.2.3 Another parametrisation of bound orbits . . . 30
  - 2.2.4 The necessity for orbital functions as functions of proper time . . . 31
- 2.3 The geodesic deviation method . . . 32
- 2.4 The first-order deviations . . . 34
  - 2.4.1 Calculating the first-order deviations . . . 34
  - 2.4.2 The epicycle expansion . . . 37
  - 2.4.3 The inclusion of the secular constants . . . 39
- 2.5 The second-order deviations . . . 40
  - 2.5.1 The Poincaré resonance and the Poincaré-Lindtsted method . . . 40
  - 2.5.2 Recalculating the first-order deviations . . . 42
  - 2.5.3 Calculating the second-order deviations . . . 43
  - 2.5.4 Collecting the results: the epicycle expansion to second order . . . 46
  - 2.5.5 The constants of integration . . . 47
- 2.6 Summary . . . 48

3 Results: bound geodesic motion **51**
- 3.1 Introduction . . . 51
- 3.2 Boundary conditions . . . 52

3.2.1 Using the constants of integration . . . 52
3.2.2 Conditions on the first-order expansion . . . 52
3.2.3 Conditions on the second-order expansion . . . 54
3.3 Explicit examples . . . 55
3.3.1 A worked example: $e = 0.1$, $a = 10M$ . . . 55
3.3.2 Further examples: $e = 0.1$, various values for a . . . 57
3.3.3 Further examples: various values for e and a . . . 59
3.4 The relationship between accuracy and eccentricity . . . 61
3.5 Increasing the accuracy . . . 63
3.6 Summary . . . 64

4 The Zerilli-Moncrief/Regge-Wheeler formalism 65
4.1 Introduction . . . 65
4.2 The Zerilli-Moncrief/Regge-Wheeler formalism . . . 66
4.2.1 Outline of the formalism . . . 66
4.2.2 Small deviations from a Schwarzschild spacetime . . . 66
4.2.3 The energy and angular momentum of the gravitational waves . . . 70
4.3 The Lousto-Price algorithm . . . 71
4.3.1 Outline of the algorithm . . . 71
4.3.2 Tortoise coordinates . . . 72
4.3.3 Integration over a single grid cell . . . 74
4.4 The source functions and geodesic deviations . . . 77
4.5 Summary . . . 79

5 Results: gravitational waves 81
5.1 Introduction . . . 81
5.2 The accuracy of the method . . . 82
5.2.1 The intrinsic error of the code . . . 82
5.2.2 The inaccuracy due to the epicycle expansion . . . 84
5.3 Bound eccentric orbits . . . 87
5.3.1 An explicit example: $e = 0.1$, $a = 10M$ . . . 87
5.3.2 Power emitted for $e = 0.1$, various a . . . 90
5.3.3 Higher eccentricities . . . 91
5.4 Gravitational waves from an EMRI system with radiative self force . . . 94
5.5 Summary . . . 98

6 Conclusions & outlook 101

A Source terms for the second-order geodesic deviation equation 105

B Retrieving the original epicycle expressions 109

C Details of the bound orbits 111

D Integrations over a grid cell **117**

Summary **129**

Populair-wetenschappelijke samenvatting **135**

Acknowledgments **141**

Chapter 1

The basic machinery of General Relativity

1.1 Introduction

The General Theory of Relativity is the leading theory of gravity and the interplay between the presence and dynamics of matter and energy and spacetime [1], [2], [3], [4]. As such, it predicts many gravitational phenomena, most of which have been confirmed in a century of experiments. One of the last predictions of the theory that awaits experimental confirmation is the existence of gravitational waves. Currently, much effort is put into measuring the effect that astrophysical sources of gravitational waves has on earthbound detectors [5], [6] and a direct detection of gravitational waves is widely expected to be reported within the next few years. One of the most promising sources of gravitational waves is the binary system: two stars orbiting each other in close proximity, sending out gravitational waves in the process. In order to filter out the wave signal from the data taken from detectors, a good theoretical understanding and description of the waves is necessary. It is the object of this thesis to present a novel way to describe the motion of binary systems and the resulting gravitational waves. In order to do so, some theoretical background of the basics of General Relativity needs to be provided first; exactly this is the topic of this chapter.
The chapter is organized as follows. In section 1.2 a brief review of the basics of General Relativity is presented, which serves to define the relevant quantities and state the conventions used in this thesis. As part of this thesis concerns a new expansion scheme to solve for motion in a curved spacetime, sections 1.3 and 1.4 review the geodesic equations, the normalization of their solutions, and the existence of constants of motion, all of which will become relevant in later chapters. Sections 1.5 and 1.6 present an overview of the theory of gravitational waves, their production, and the energy they carry. Section 1.7 concentrates more fully on one of the sources as a primary candidate for the emission of measurable gravitational waves, and gives an overview of the theoretical work to be presented in this thesis. Finally, section 1.8 presents a summary.

1.2 Gravity as curvature

General Relativity is based on the premise that the effects of gravity can be interpreted as curvature of spacetime. This correspondence is strongly suggested by the *Weak Equivalence Principle*, the experimental observation that the effects of gravity are the same on every free falling (*i.e.* under influence of gravity alone) massive object, so that gravity can be interpreted not as a property of the objects themselves, but as a property of the underlying space and time, *i.e.* spacetime. More specifically, the premise is that Newton's First Law holds in the presence of gravity, but that the straight lines are curved by the underlying spacetime on which they are defined, and not by the action of some force. The Equivalence Principle also leads to the insight that there is principally no way to distinguish accelerated motion from local effects of gravity, as any difference in the way objects are influenced by gravity would reveal itself in a relative acceleration between two different free-falling massive objects.
As a result of this correspondence between gravity and the curvature of spacetime, the theory of General Relativity and the mathematical theory of differential geometry are intimately entwined and the two theories share a common language, *i.e.* that of tensors. In addition, the Equivalence Principle calls for a description that is independent of the coordinate system in which the laws of physics are formulated, which again leads to a description of curved spacetime in terms of tensors. In brief, all properties of a curved spacetime can be described in terms of the infinitesimal distance $d\tau$ between two separated points in the spacetime, by constructing the invariant *line element*[1]

$$d\tau^2 = -g_{\mu\nu}dx^\mu dx^\nu. \tag{1.1}$$

In here, the *metric* $g_{\mu\nu}$ (as well as its inverse $g^{\mu\nu}$, defined by $g_{\mu\nu}g^{\nu\lambda} = \delta^\lambda_\mu$) is a symmetric tensor that contains all geometric properties of the curved spacetime. This was even already apparent with the development of Special Relativity, when Minkowski was able to show that all of the results of Special Relativity could be understood in terms of a spacetime described, in Cartesian coordinates, by the metric

$$g_{\mu\nu} = \begin{pmatrix} -1 & 0 & 0 & 0 \\ 0 & 1 & 0 & 0 \\ 0 & 0 & 1 & 0 \\ 0 & 0 & 0 & 1 \end{pmatrix} \equiv \eta_{\mu\nu}, \tag{1.2}$$

which is known as the *Minkowksi metric*. Indeed, by forming the line element of Eq. (1.1) as the invariant spacetime distance between two events separated temporally by dt and spatially by dx^i, it is easy to show that $d\tau$ can be interpreted as the time between the two events as measured by an observer for whom the two events take place at the same

[1]Here and in the rest of this thesis, repeated indices are to be summed over. Further conventions used are that a latin index refers to a spatial component of a tensor, whereas a greek index refers to a spacetime component. Furthermore, the speed of light c and Newton's gravitational constant G are both set to unity; a result of this is that length, mass, and time are all measured in the same units.

position, and special relativistic time dilation then follows directly by dividing both sides of the line element by dt^2, yielding the well-known formula

$$\frac{d\tau}{dt} = \sqrt{1 - \left(\frac{d\vec{x}}{dt}\right)^2}. \tag{1.3}$$

All other basic results of Special Relativity follow similarly from the Minkowski metric. Inspired by this success in the use of geometry as well as by the Weak Equivalence Principle, it is natural to expect that also gravity can be described in terms of curved spacetime. The physics comes in when the curvature of spacetime is related to the presence and dynamics of energy and matter, which is described by the *Einstein field equations*

$$G_{\mu\nu} \equiv R_{\mu\nu} - \frac{1}{2} g_{\mu\nu} R = -8\pi T_{\mu\nu}. \tag{1.4}$$

The right hand side contains the *energy momentum tensor* $T_{\mu\nu}$, which describes the presence and dynamics of matter density and energy density; notably, the component T^{00} is the energy density and the components T^{0i} correspond to the momentum density. The left hand side defines the *Einstein tensor* $G_{\mu\nu}$, which is a combination of the *Ricci tensor* $R_{\mu\nu}$ and *Riemann scalar* R. These are two non-linear constructions of the metric tensor and its first and second derivatives, and are defined by

$$R_{\mu\nu} \equiv R^{\lambda}{}_{\mu\lambda\nu}, \qquad R \equiv g^{\mu\nu} R_{\mu\nu}, \tag{1.5}$$

and $R^{\lambda}{}_{\mu\nu\kappa}$ is the *Riemann tensor*, defined by

$$R^{\lambda}{}_{\mu\nu\kappa} \equiv \partial_\kappa \Gamma^{\lambda}_{\mu\nu} - \partial_\nu \Gamma^{\lambda}_{\mu\kappa} + \Gamma^{\eta}_{\mu\nu} \Gamma^{\lambda}_{\kappa\eta} - \Gamma^{\eta}_{\mu\kappa} \Gamma^{\lambda}_{\nu\eta}, \tag{1.6}$$

in which, finally, the *Christoffel symbol* $\Gamma^{\lambda}_{\mu\nu}$ is defined by

$$\Gamma^{\lambda}_{\mu\nu} \equiv \frac{1}{2} g^{\lambda\kappa} \left(\partial_\mu g_{\kappa\nu} + \partial_\nu g_{\mu\kappa} - \partial_\kappa g_{\mu\nu} \right). \tag{1.7}$$

The form of the Einstein field equations is motivated [3] by the mathematical fact that any measure of a curved spacetime must contain second or higher derivatives of the metric and/or products of first and higher order derivatives (as purely first derivatives of a metric can always be put to zero by a suitable choice of coordinates, whereas this cannot be done for second derivatives), and by the Helmholtz theorem, which states that a general tensor with two indices built up from second-order derivatives of the metric and/or products of first-order derivatives, is always of the form $a \cdot R_{\mu\nu} + b \cdot g_{\mu\nu} R$ for some constants a, b. The physics (to wit: the values of the constants a, b, along with the value -8π in Eq. (1.4)) comes in from the fact that gravity is produced by mass so that the curvature must be the result of a nonzero $T_{\mu\nu}$, and from the requirement that for small values of energy and momentum the Einstein field equations should return Newtonian gravity. Finally, the left hand side of the Einstein field equations obeys the condition $D_\alpha G^{\alpha\beta} = 0$, in which D_α is

the covariant derivative defined in the next section, denoting that the right hand side does so too:

$$D_\alpha T^{\alpha\beta} = 0. \tag{1.8}$$

Physically, this states that energy and momentum in a curved spacetime are covariantly conserved quantities; this means that the curvature of spacetime itself carries energy, the amount of which is determined by the choice of coordinate system.
The field equations constitute a set of ten non-linear coupled partial differential equations in the ten variables that make up the metric, and it is therefore not surprising that finding analytic solutions $g_{\mu\nu}$ is a daunting task. However, the Einstein field equations have the property built in that there is complete freedom in choosing a coordinate system and as such, finding a solution can be simplified by choosing an appropriate coordinate frame (a *gauge*). In the absence of the source term $T_{\mu\nu}$ some exact solutions to the Einstein field equations are known, one of them being the Minkowski metric of Eq. (1.2) and another the Schwarzschild metric, the latter of which will play a major part in this thesis and will be explicitly discussed in the next chapter.

1.3 The geodesic equations

Having described how the curvature of spacetime is determined by the presence and dynamics of matter and energy, the next topic is to see how the dynamics of matter and energy are determined by the curvature of spacetime. As mentioned before, one premise of General Relativity is that Newton's First Law still holds (*i.e.* mass tends to move in a straight line with a constant velocity when it is not acted upon by a force) and that the influence of gravity comes from straight lines being defined on a curved spacetime. Hence, motion under influence of gravity can be studied by investigating how Newton's First Law manifests itself in curved spacetime.
This question can be elegantly answered in the Lagrangian formulation of mechanics. In pre-relativity physics, all Newtonian motion can be written in the Lagrangian formulation by writing the *action* S as the integral of the Lagrangian L,

$$S = \int L(t, x(t), \dot{x}(t))dt, \qquad \dot{x} \equiv \frac{dx}{dt}, \tag{1.9}$$

and minimizing it by means of the Euler-Lagrange equations,

$$\frac{\partial L}{\partial x} - \frac{d}{dt}\left(\frac{\partial L}{\partial \dot{x}}\right) = 0, \tag{1.10}$$

the result of which will give the equation of motion of the system. For a free particle the Lagrangian is just equal to the Newtonian kinetic energy $K = \frac{1}{2}m\dot{x}^2$, and minimizing the action then gives the equation of motion

$$\frac{d}{dt}\left(m\dot{x}\right) = 0, \tag{1.11}$$

which states that a free particle of constant mass moves in a straight line with constant velocity, *i.e.* Newton's First Law. In General Relativity the requirement is that the action is invariant under general coordinate transformations so as to make the resulting equations of motion hold in all coordinate frames. An invariant version of the Newtonian Lagrangian for a free test mass then naturally suggests itself by making use of the invariant line element of Eq. (1.1), giving

$$S = \int \left(\frac{1}{2} m g_{\mu\nu} \frac{dx^\mu}{d\tau} \frac{dx^\nu}{d\tau} \right) d\tau. \tag{1.12}$$

This action can be minimized by the appropriate Euler-Lagrange equations,

$$\frac{\partial L}{\partial x^\alpha} - \frac{d}{d\tau} \left(\frac{\partial L}{\partial u^\alpha} \right) = 0, \qquad u^\alpha \equiv \frac{dx^\alpha}{d\tau}, \tag{1.13}$$

having defined the *four-velocity* u^α. The result is an invariant equation of motion in a curved spacetime, given by

$$\frac{d^2 x^\lambda}{d\tau^2} + \Gamma^\lambda_{\mu\nu} \frac{dx^\mu}{d\tau} \frac{dx^\nu}{d\tau} = 0, \tag{1.14}$$

in which the Christoffel symbol of Eq. (1.7) makes its natural entry. The resulting equation of motion is called the *geodesic equation* and it describes the way a mass m moves in a curved spacetime, or equivalently, under influence of gravity. Indeed, the fact that the mass m makes no appearance shows explicitly that geodesic motion in a given curved spacetime is the same for all massive objects, as dictated by the Weak Equivalence Principle.
It is conventional to write the geodesic equation as

$$\frac{Du^\alpha}{D\tau} = 0, \qquad \frac{DA^\lambda}{D\tau} \equiv \frac{dA^\lambda}{d\tau} + \Gamma^\lambda_{\mu\nu} u^\mu A^\nu, \tag{1.15}$$

where the *covariant derivative* of a tensor A^μ along the curve with tangent vector u^μ has been defined. It has the properties that it obeys the Leibniz rule of differentiation, that the covariant derivative of a metric tensor vanishes, and that the covariant derivative of a scalar equals its derivative in uncurved spacetime. Physically, the covariant derivative $DA^\mu/D\tau$ describes, via the first term, the infinitesimal change of a tensor A^μ due to a change in its argument as well as due to, via the second term, a change in the spacetime on which the tensor is defined. Exactly that last term is what can be, again by the Weak Equivalence Principle, ascribed to gravity. Indeed, the second term in Eq. (1.15) denotes a deviation from a straight line which is due to geometrical reasons.
In case there are external forces present, the right hand side of the geodesic equation will not be zero and some force term f^μ will be present. An example of this is the Lorentz force, a situation that is explicitly discussed in Refs. [2], [7].

It is straightforward to show that geodesic motion implies that the resulting four-velocity u^μ is normalized, *i.e.* that the scalar $g_{\mu\nu} u^\mu u^\nu$ has a constant value in time along the

geodesic. This follows by taking the derivative with respect to proper time, and using the fact that a derivative of a scalar equals its covariant derivative

$$\frac{d}{d\tau}\left(g_{\mu\nu}u^\mu u^\nu\right) = \frac{D}{D\tau}\left(g_{\mu\nu}u^\mu u^\nu\right) = 2g_{\mu\nu}u^\mu\frac{Du^\nu}{D\tau} = 0, \tag{1.16}$$

where also the various properties of the covariant derivative have been used. The outcome equals zero, as geodesic motion by definition makes the covariant derivative of the four-velocity vanish.
In case some external four-force f^μ is present, the motion will not be geodesic and the above result seems to suggest that in that case the four-velocity is generally not normalized. However, dividing both sides of the line-element of Eq. (1.1) by $d\tau^2$ shows that *all* motion (*i.e.* not just geodesic) is properly normalized, and, what's more, that the normalization constant is minus unity for all of these cases. This fact should therefore be considered a condition on the form a four-force f^μ can have in order to be in agreement with General Relativity. This condition can be made explicit by setting the right hand side of the geodesic equation Eq. (1.15) equal to f^μ and using this new equation of motion in Eq. (1.16); the result is that the four-force must obey the condition

$$g_{\mu\nu}u^\mu f^\nu = 0. \tag{1.17}$$

This condition states that the four components of the force f^μ are not all independent: it is always possible to write the temporal component f^0 purely in terms of the spatial components f^i and the metric $g_{\mu\nu}$. This is in agreement with physical interpretation: the temporal component u^0 of the four-velocity is a measure of the gravitational respectively special relativistic time dilation, which are determined by the position respectively the velocity, both of which in turn are determined by the spatial components f^i and the geometry of spacetime. Therefore, it was to be expected that f^0 dictating the temporal component u^0 is fully specified by the metric tensor and the spatial components f^i of the four-force. Exactly this is stated by Eq. (1.17).

1.4 Isometries and Killing vectors

The geodesic equation Eq. (1.15) forms a set of four coupled non-linear differential equations in the four variables $x^\mu(\tau)$, and is usually difficult to solve analytically. The *form* of the geodesic solutions, however, can be investigated by the symmetry properties of the spacetime as these are related to constants of geodesic motion. This will now be shown.
A metric is said to be *form-invariant* under a coordinate transformation

$$x^\mu \to x'^\mu \equiv x^\mu + \xi^\mu(x) \tag{1.18}$$

if the new metric $g'_{\mu\nu}$ has the same outcome for every set of values y in the new coordinates x'^μ as the original metric $g_{\mu\nu}$ had for the same set of values y in the old original coordinates x^μ. Physically, this means that the coordinate transform replaces the old metric by a new

one such that it is impossible to tell by substituting some set of values of coordinates whether the coordinate transformation has been done at all. Mathematically, this is stated as

$$g'_{\mu\nu}(x' = y) = g_{\mu\nu}(x = y). \tag{1.19}$$

A coordinate transformation of this type is called an *isometry* of the form-invariant metric. It should be noted that equal values y in different coordinate systems x^μ, x'^μ generally correspond to different points in spacetime; Eq. (1.19) thus is a statement about the indifference of the metric (and hence all geometric properties) in going from one point in spacetime to some other by the transformation Eq. (1.18), *i.e.* it is a statement of a symmetry of the spacetime. The name isometry is therefore aptly chosen, as it connects points on the manifold that have the same geometric properties.
As isometries are closely related to symmetries, akin to a similar situation in theories described by Lagrangians in which a symmetry corresponds to a conserved Noether current, there exists a constant of motion related to each symmetry. In what follows, it will first be derived under what criterion a vector ξ^μ constitutes an isometry of the spacetime, followed by the proof that for such ξ^μ, indeed a constant of motion exists.
Doing a coordinate transform $x^\mu \to x'^\mu$ changes a metric into a new one by the following transformation rule

$$g'_{\mu\nu}(x') = \frac{\partial x^\rho}{\partial x'^\mu}\frac{\partial x^\sigma}{\partial x'^\nu} g_{\rho\sigma}(x). \tag{1.20}$$

In the present case, the transformation is given infinitesimally by Eq. (1.18) which, to first order in ξ^μ, transforms the right hand side to

$$\begin{aligned} \frac{\partial x^\rho}{\partial x'^\mu}\frac{\partial x^\sigma}{\partial x'^\nu} g_{\rho\sigma}(x) &\approx \left(\delta^\rho_\mu - \partial_\mu \xi^\rho\right)\left(\delta^\sigma_\nu - \partial_\nu \xi^\sigma\right) g_{\rho\sigma}(x) \\ &\approx g_{\mu\nu}(x) - g_{\mu\sigma}(x)\partial_\nu \xi^\sigma - g_{\rho\nu}(x)\partial_\mu \xi^\rho. \end{aligned} \tag{1.21}$$

If the coordinate transform is an isometry, Eq. (1.19) applies and the left hand side of Eq. (1.20) equals $g_{\mu\nu}(x')$, which to first order becomes

$$g_{\mu\nu}(x') \approx g_{\mu\nu}(x) + \left(\partial_\alpha g_{\mu\nu}\right)\xi^\alpha. \tag{1.22}$$

Collecting these results, the condition for ξ^μ to be an isometry follows to be

$$g_{\mu\nu}(x)\partial_\nu \xi^\sigma + g_{\rho\nu}\partial_\mu \xi^\rho + \left(\partial_\alpha g_{\mu\nu}\right)\xi^\alpha = 0, \tag{1.23}$$

or, using $\xi_\mu \equiv g_{\mu\nu}\xi^\nu$ and by using a covariant notation,

$$D_\rho \xi_\sigma + D_\sigma \xi_\rho = 0, \qquad D_\nu A_\mu \equiv \partial_\nu A_\mu - \Gamma^\lambda_{\mu\nu} A_\lambda. \tag{1.24}$$

This well-known result is called the *Killing equation*; its solutions ξ^μ are called *Killing vectors* and, by construction, constitute a coordinate transformation Eq. (1.18) under which the metric is form invariant.

As mentioned, the existence of a Killing vector ξ^μ corresponds to the existence of a conserved quantity of a geodesic motion. This quantity is given by

$$g_{\mu\nu}u^\mu\xi^\nu, \tag{1.25}$$

as will now be proved explicitly by taking the derivative of this scalar with respect to proper time τ. The quantity is a scalar so a derivative can be freely replaced by a covariant derivative, and as covariant derivatives obey the usual Leibniz rule, the derivative becomes

$$\frac{d}{d\tau}\left(u^\mu\xi_\mu\right) = \frac{Du^\mu}{D\tau}\xi_\mu + u^\mu\frac{D\xi_\mu}{D\tau}. \tag{1.26}$$

For geodesic motion, the first term at the left hand side is zero due to Eq. (1.15), whereas the second term is zero by Eq. (1.24) when the vector ξ_μ is a Killing vector. It has then followed that for geodesic motion x^μ in a spacetime that has a Killing vector ξ^μ, indeed, $g_{\mu\nu}u^\mu\xi^\nu$ is a constant of motion along that geodesic.
A trivial yet important example of the use of Killing constants is the case a metric is independent of a coordinate x^α; in that case, $\xi_\mu = \delta^\alpha_\mu$ is an obvious solution to the Killing equation, and hence $g_{\mu\alpha}u^\mu$ is a constant of motion. For instance, the simple case of a Minkowski spacetime in Cartesian coordinates, Eq. (1.2), does not depend on any coordinate and it follows that the four components of the four-velocity u^α are all constants of motion. Physically, this is just Newton's First Law, which is the expected outcome considering the fact that the Minkowski spacetime corresponds to the absence of gravity and for geodesic motion no external forces are present.
It should be noted that in the presence of external forces, the Killing equation changes form, as the first term in Eq. (1.26) is then generally not zero: this is a manifestation of the fact that an external force generally breaks a symmetry. It is, however, generally still possible to find a ξ^μ that obeys the new version of the Killing equations and so constants of motion can still be found. As such, Killing vectors are hugely advantageous when investigating the equations of motion in curved spacetime, be they geodesic or not, as they provide knowledge of the solutions even if the actual solving is difficult. They will be used in that way in Chapter 2.

1.5 Dynamics and production of gravitational waves

The Theory of General Relativity leads to many predictions, including (but not limited to) the perihelion precession of the planets [1], the bending of light when passing the Sun and gravitational time dilation [8], and the expansion of the Universe [9], all of which have been confirmed by experimental observations [10]. One of the last standing predictions that awaits confirmation is the existence of *gravitational waves*: a propagating dynamical disturbance of spacetime that can exist even in the absence of matter and energy. In this respect, they are comparable to electromagnetic waves, which exist in the theory of electrodynamics even in the absence of charges or currents. In the case of gravity, this existence comes about because the true measure of curved spacetime is the Riemann tensor, whereas

the Einstein field equations fix only the Ricci tensor. Thus, physically non-trivial $g_{\mu\nu}$ can exist even when the Ricci tensor vanishes. The rest of this section will illustrate this by presenting the example of gravitational waves in a Minkowski spacetime; the (much more difficult) case of gravitational waves in the spacetime of a non-rotating black hole will be the topic of chapter 4.

In the absence of any external matter or energy $T_{\mu\nu} = 0$, one solution to the Einstein field equations Eq. (1.4) is the Minkowski metric as it indeed has a vanishing Ricci tensor and Riemann scalar. In addition, the Riemann tensor vanishes as well. Adding a small perturbation $h_{\mu\nu}$ to the Minkowski metric,

$$\eta_{\mu\nu} \to \eta_{\mu\nu} + h_{\mu\nu}, \tag{1.27}$$

shows that the resulting Einstein tensor $G_{\mu\nu}$ can, when linearized to first order in $h_{\mu\nu}$, be made to vanish by having $h_{\mu\nu}$ obey the differential equation

$$\frac{1}{2}\left(\eta^{\alpha\beta}\partial_\alpha\partial_\beta\bar{h}_{\mu\nu} - \partial_\nu\partial_\kappa\bar{h}^\kappa_\mu - \partial_\mu\partial_\kappa\bar{h}^\kappa_\nu + \eta_{\mu\nu}\partial_\rho\partial_\sigma\bar{h}^{\rho\sigma}\right) = 0, \tag{1.28}$$

in which $\bar{h}_{\mu\nu} \equiv h_{\mu\nu} - \frac{1}{2}\eta_{\mu\nu}h^\lambda_\lambda$. In contrast, the Riemann tensor resulting from Eq. (1.27) linearized to first order in $h_{\mu\nu}$ will *not* vanish, denoting the presence of a non-trivial gravitational field even in the absence of matter and energy.
General Relativity's inherent freedom to choose a coordinate frame allows $\bar{h}_{\mu\nu}$ to obey the gauge condition

$$\partial_\alpha\bar{h}^{\alpha\beta} = 0. \tag{1.29}$$

In this coordinate frame, which is denoted the *De Donder gauge*, the differential equation for $h_{\mu\nu}$ takes the form of the massless Klein-Gordon equation,

$$\frac{1}{2}\eta^{\alpha\beta}\partial_\alpha\partial_\beta\bar{h}_{\mu\nu} = \frac{1}{2}\left(-\partial_t^2 + \nabla^2\right)\bar{h}_{\mu\nu} = 0, \tag{1.30}$$

from which it can be inferred that the gravitational wave propagates with the speed of light. The De Donder gauge does not correspond to just one specific coordinate frame, but rather to a class of them as it is still possible to choose additional gauge conditions that do not spoil Eq. (1.29):

$$h^i_i = 0, \qquad h^{0\mu} = 0 \qquad \Rightarrow \qquad \bar{h}_{\mu\nu} = h_{\mu\nu}\,. \tag{1.31}$$

With this additional choice of coordinate frame, called the *transverse traceless gauge (TT-gauge)*, it is easy to show that the gravitational wave has only two polarizations and that it is transverse [3], [6]. Indeed, arbitrarily choosing the direction of propagation to be the z-direction, the gravitational wave in the TT-gauge has the general form

$$h_{\mu\nu} = \begin{pmatrix} 0 & 0 & 0 & 0 \\ 0 & h_+ & h_\times & 0 \\ 0 & h_\times & -h_+ & 0 \\ 0 & 0 & 0 & 0 \end{pmatrix}, \tag{1.32}$$

in which $h_+,\ h_\times$ are two arbitrary functions of the argument $(t-z)$, which explicitly denote the two polarizations.

So far, the presentation has only shown that gravitational waves can exist as perturbations on a Minkowski spacetime, but nothing has yet been said about their production. This will now be presented. To do so, an energy momentum tensor $T_{\mu\nu}$ must be introduced that will be the source of the gravitational waves. The Einstein field equations of Eq. (1.4) will then have a non-vanishing right hand side, but as the previous derivation only concerned the left hand side, the results leading to the equation of motion for $\bar{h}_{\mu\nu}$ still hold. The gravitational waves thus are found to obey, in the De Donder gauge, the inhomogeneous wave equation

$$\eta^{\alpha\beta}\partial_\alpha\partial_\beta\bar{h}_{\mu\nu} = -16\pi T_{\mu\nu}(t,\vec{x}). \tag{1.33}$$

These constitute a set of ten uncoupled linear differential equations and are straightforward to solve. The solution[2] is given by

$$\bar{h}^{\alpha\beta} = 4\int d\vec{x}\,'\frac{T^{\alpha\beta}(t-|\vec{x}-\vec{x}\,'|,\vec{x}\,')}{|\vec{x}-\vec{x}\,'|}. \tag{1.34}$$

This expression is exact, but can be greatly simplified by making a number of assumptions. For typical astrophysical sources, $T^{\alpha\beta}$ is some periodic function (or can be written as a sum of such functions, for example by a Fourier series), *i.e.* $T^{\alpha\beta}(t,\vec{x}) \propto a^{\alpha\beta}(\vec{x})\cos(\omega t)$ for some frequency ω characteristic to the source. If that is the case and the additional assumptions are made that, firstly, the gravitational wave has a wavelength much greater than the dimensions of the source and, secondly, that the source is observed from some radial distance r far away, $|\vec{x}-\vec{x}\,'|$ can be replaced by r and the gravitational wave is well approximated by

$$\bar{h}^{\alpha\beta} = \frac{4}{r}\int d\vec{x}\,'\ T^{\alpha\beta}(t-r,\vec{x}\,'). \tag{1.35}$$

As this expression holds in the TT-gauge, all $\bar{h}^{\alpha 0}$ vanish and the only components of the wave equation Eq. (1.33) that need to be considered are the ones that contain integrals of the spatial energy momentum tensors T^{ij}. By the fact that the conservation of the energy momentum tensor in a Minkowski spacetime reads $\partial_\alpha T^{\alpha\beta} = 0$ and by doing a partial integration, these integrals can be written as

$$\int d\vec{x}\ T^{ij} = \frac{1}{2}\frac{d^2}{dt^2}\int d\vec{x}\ x^i x^j T^{00}, \tag{1.36}$$

which allows for one last assumption: if the velocities in the source are much smaller than that of light, the energy in the source is almost completely given by the rest mass, allowing

[2]The wave equation is a second-order linear differential equation and therefore has two linearly independent solutions, only one of which is given here. The reason is that this solution describes a gravitational wave that propagates away from the source towards infinity, whereas the second solution describes one that travels from infinity towards the source. The latter is not produced by the source (rather: they are absorbed), and are therefore ignored.

to write $T^{00} = \mu(t, \vec{x})$, in which μ is the density of the rest mass present in the source. Finally, then, the gravitational wave h^{ij} is given by

$$\bar{h}^{ij} = \frac{2}{r}\ddot{I}^{ij}(t-r), \qquad I^{ij}(t) \equiv \int d\vec{x}\ \mu(t,\vec{x})\ x^i x^j, \tag{1.37}$$

in which the *second mass moment* $I^{ij}(t)$ of the source has been defined as a measure of the presence and dynamics of mass in the astrophysical source. The fact that the resulting gravitational wave depends on $\ddot{I}^{ij}(t)$ shows that they are produced by systems that contain masses that are accelerated with respect to each other.

As a result of the gravitational wave of Eq. (1.32) or Eq. (1.37), the perturbed Minkowski Eq. (1.27) metric leads to non-zero values of the Christoffel symbols in the geodesic equations Eq. (1.15), typically denoting a measurable influence of a gravitational wave by introducing a relative acceleration between a set of test masses. Indeed, it is on this principle that present day gravitational wave detectors are based [5], [6].

1.6 The energy and momentum of gravitational waves

The fact that a gravitational wave can produce a change in relative position between test masses indicates that gravitational waves carry energy and momentum. This is also suggested by the *Strong Equivalence Principle* which states that the effects of spacetime curvature should be the same not only for all massive objects (as already stated by the Weak Equivalence Principle), but for *all* physical phenomena, including gravity itself. This means that gravitational waves are themselves sources of spacetime curvature, and hence, via the Einstein field equations, that they carry energy and momentum. It should therefore be possible to assign an energy momentum tensor $T^{GW}_{\mu\nu}$ to gravitational fields, most notably to gravitational waves $h_{\mu\nu}$.
A prescription to do so comes from the realization that the energy of a gravitational wave must be an expression *quadratic* in $h_{\mu\nu}$, as an expansion of the Einstein field equations to second order in $h_{\mu\nu}$ will introduce extra terms in the equation of motion for the waves, physically corresponding to the effect the waves have on their own dynamics. Some care must be taken in defining the background metric on which the gravitational wave is imposed: it can not be taken to be a metric that solves the vacuum Einstein field equations (*e.g.* can not be taken to be the Minkowski metric) as this by definition assumes that no energy momentum is present, whereas the object is to find a non-zero expression for the energy momentum tensor $T^{GW}_{\mu\nu}$. Instead, the background metric must be taken to be some metric $g^B_{\mu\nu}$ that is close to a metric that solves the Einstein field equations in vacuum, but still carries some imprint of the curvature brought by the presence of the energy momentum of the gravitational wave $h_{\mu\nu}$. The expansion then is of the form

$$g_{\mu\nu} = g^B_{\mu\nu} + h_{\mu\nu}. \tag{1.38}$$

Substituting this in the Einstein field equations for a vacuum (*i.e.* for a spacetime outside of the source of the gravitational waves, and which is devoid of any energy and momentum other than that contained in the gravitational field itself), $R_{\mu\nu} = 0$, and expanding to second order in $h_{\mu\nu}$ then leads to the equation

$$R^B_{\mu\nu} + R^{(1)}_{\mu\nu} + R^{(2)}_{\mu\nu} = 0, \tag{1.39}$$

in which a superscript B, (1), (2), respectively, denotes that the tensor is calculated with the background metric, to first order in $h_{\mu\nu}$, or to second-order in $h_{\mu\nu}$, respectively. The term $R^{(1)}_{\mu\nu}$ can be made to vanish by requiring the gravitational wave $h_{\mu\nu}$ to solve the equation of motion

$$R^{(1)}_{\mu\nu} = 0, \tag{1.40}$$

and the remaining equation can be written as

$$R^B_{\mu\nu} - \frac{1}{2} g^B_{\mu\nu} R^B = -8\pi T^{GW}_{\mu\nu}. \tag{1.41}$$

This was written suggestively in the form of the Einstein field equation on the background metric $g^B_{\mu\nu}$, curved by the presence of the energy momentum tensor of the gravitational wave $h_{\mu\nu}$. This energy momentum tensor is given by

$$T^{GW}_{\mu\nu} = \frac{1}{8\pi} \left\langle R^{(2)}_{\mu\nu} - \frac{1}{2} g^B_{\mu\nu} R^{(2)} \right\rangle, \tag{1.42}$$

in which the brackets mean that the expression contained within them is to be averaged over a region of spacetime that is big compared to the typical scale of the dynamics of the gravitational wave $h_{\mu\nu}$; physically, this averaging expunges the expression of all dynamics of the gravitational wave that are either too small to change significantly within the region of spacetime over which is averaged, and so much bigger than this region that they can be replaced by their average of zero. In effect, only the dynamics remain that have the same typical length- or timescale as the region of spacetime over which is averaged.
The Ricci tensor $R^{(2)}_{\mu\nu}$ and corresponding Riemann scalar $R^{(2)}$ can straightforwardly (if tediously) be calculated by substituting Eq. (1.38) in the definitions Eq. (1.5) and truncating the outcomes to second order in the gravitational wave $h_{\mu\nu}$. The result is given by

$$\begin{aligned} R^{(2)}_{\mu\nu} \;=\; & \frac{1}{2} g^{\rho\sigma,B} g^{\alpha\beta,B} \left[\frac{1}{2} D^B_\mu h_{\rho\alpha} D^B_\nu h_{\sigma\beta} + \left(D^B_\rho h_{\nu\alpha} \right) \left(D^B_\sigma h_{\mu\beta} - D^B_\beta h_{\mu\sigma} \right) \right. \\ & + h_{\rho\alpha} \left(D^B_\nu D^B_\mu h_{\sigma\beta} + D^B_\beta D^B_\sigma h_{\mu\nu} - D^B_\beta D^B_\nu h_{\mu\sigma} - D^B_\beta D^B_\mu h_{\nu\sigma} \right) \\ & \left. + \left(\frac{1}{2} D^B_\alpha h_{\rho\sigma} - D^B_\rho h_{\alpha\sigma} \right) \left(D^B_\nu h_{\mu\beta} + D^B_\mu h_{\nu\beta} - D^B_\beta h_{\mu\nu} \right) \right], \end{aligned} \tag{1.43}$$

in which the superscript B on the covariant derivates denotes that they need to be calculated by using the metric Eq. (1.38). If, as an additional simplification, the waves are considered very far from their origin and are assumed to drop off with increasing distance

from their source, they can be expected to be very small, allowing all $g^B_{\mu\nu}$ in Eq. (1.42) to be replaced by the metric of the background spacetime in absence of any curvature due to the energy carried by gravitational waves. Typically, this assumption of large distance from the source not only means that the background spacetime loses the imprint of the curvature due to the energy momentum tensor $T^{GW}_{\mu\nu}$ of the gravitational waves, but also that it becomes Minkowskian (as will happen when, for example, the observer is far away from a black hole). Under that assumption, the equation of motion Eq. (1.40) becomes simply that of a gravitational wave in a Minkowski spacetime, Eq. (1.30), and the Minkowski-based results of section 1.5 apply. Thus, the covariant derivatives D^B_μ can be replaced by the covariant derivatives of Minkowski spacetime, which in Cartesian coordinates just equal ∂_μ; furthermore, the metric $g^B_{\mu\nu}$ can be replaced by $\eta_{\mu\nu}$ and, most notably, the gravitational waves $h_{\mu\nu}$ can be taken to be in the TT-gauge. The expression for the energy momentum tensor $T^{GW}_{\mu\nu}$ then simplifies drastically and becomes

$$T^{GW}_{\mu\nu} = \frac{1}{32\pi} \left\langle \partial_\mu h_{\alpha\beta} \partial_\nu h^{\alpha\beta} \right\rangle . \tag{1.44}$$

The component $T^{00,GW}$ corresponds to the energy density of the gravitational wave, as found within the small region of spacetime over which is averaged. Using the notation of the solutions Eq. (1.32), the energy density of the gravitational wave takes on the particularly simple form

$$T^{00,GW} = \frac{1}{16\pi} \left\langle \dot{h}^2_+ + \dot{h}^2_\times \right\rangle . \tag{1.45}$$

This expression is the key to calculate the energy carried away from astrophysical sources by gravitational waves and gives a handle on the long-term evolution of such sources due to gravitational wave emission. It is important to note that, as opposed to the previous section in which all results were based on the case of gravitational waves in a Minkowski spacetime, this section has only made the assumption of Minkowski spacetime at the very end when simplifying Eq. (1.42) to its final form of Eq. (1.44). Indeed, up until Eq. (1.42), $g^B_{\mu\nu}$ was allowed to be *any* vacuum solution to the Einstein field equations with additional curvature brought in by $T^{GW}_{\mu\nu}$ However, the assumption made of a Minkowski spacetime is generally well justified by observing the source from afar, as most spacetimes become asymptotically Minkowskian far away from matter or energy. The final expression Eq. (1.45) is therefore expected to hold far away from the source of the gravitational wave in any curved spacetime that is asymptotically Minkowskian. It should be noted, however, that the *expressions* of the gravitational waves $h_{\mu\nu}$ themselves are *not* the same as in a Minkowski spacetime, as they are influenced by the curvature as they propagate from the source to the observer. Specifically, $h_{\mu\nu}$ will no longer be a function of the source $T_{\mu\nu}$ in the manner of Eq. (1.37), even though its general form will still be given by Eq. (1.32) when viewed far away from the source. In chapter 4, the correct expressions for the gravitational wave polarizations h_+ and $h_\times$ will be given for a general source in the Schwarzschild spacetime of a non-spinning black hole.

1.7 The EMRI system & outline of the thesis

For present-day and near-future experimental observations of gravitational waves, one of the most promising sources is the binary system: two stars orbiting each other under influence of their gravitational field, sending out gravitational waves in the process. In this thesis the emphasis will be on an *extreme mass ratio inspiral* (EMRI), a binary system in which one of the two stars[3] is non-rotating and much heavier than the companion star. The calculational advantage of this system is that, up to excellent approximation, spacetime can be taken to be that of the black hole and the curvature that is brought in by the presence of the companion star can be neglected. If, in addition, the stars are far away from each other and move with velocities much lower than that of light, the orbit of the companion star can be calculated by simple Newtonian mechanics, and spacetime can be taken to be Minkowskian up to good approximation. In that simplified case, the results of the previous two sections apply, and the emitted energy per second P as measured far away from the source can be found by calculating the second mass moment $I^{ij}(t)$ by Newtonian means, calculating the resulting gravitational wave by Eq. (1.37), and the energy density of the wave by Eq. (1.45). The resulting power P is given by the *Peters-Mathews equation* [11] as

$$P = \frac{32\mu^2 M^3}{5a^5} f(e), \qquad f(e) = \frac{1}{(1-e^2)^{7/2}} \left(1 + \frac{73}{24}e^2 + \frac{37}{96}e^4\right), \tag{1.46}$$

in which M is the mass of the black hole, μ the mass of the companion star, a is the semi-major axis of the Newtonian orbit and e is its eccentricity; the last two parameters will be presented in section 2.2.
However, when the two stars in the EMRI system are in close proximity, the effects of curvature or high velocities can not be neglected and spacetime can not be taken to be approximately Minkowskian. Instead, the background spacetime must be taken to be that of the heavier star, which introduces two complications. Firstly, the orbit of the companion star cannot be described by Newtonian mechanics anymore and instead the geodesic equations Eq. (1.15) must be solved, and, secondly, the gravitational waves resulting from these orbits need to be calculated as perturbations of the non-Minkowskian spacetime, which is a far more challenging task than the simple Minkowskian case. The conventional way to proceed is by the *Post-Newtonian method*, in which both steps are done by expanding spacetime around a Minkowski metric, adding the effects of curvature and high velocities by a perturbation series of the form Eq. (1.27) taken to arbitrarily high order in $h_{\mu\nu}$. This method has been pursued to accurately include many higher order gravitational effects, including the effect of the gravitational waves on their own dynamics, and comparison with numerically calculated outcomes are excellent [6], [12]. However, the Post-Newtonian expansion loses accuracy when considering orbits close to the black hole. This is a direct consequence of the premise of the method, which assumes an expansion around a near-flat spacetime whereas spacetime close to a black hole is extremely curved.

[3]The heavier star will usually be called a black hole in this thesis, even though it could in principle be any spherically symmetric compact object, *e.g.* a neutron star or a white dwarf.

In this thesis an alternative method to describe geodesic motion in the EMRI system and the resulting gravitational waves will be presented, which, in contrast to the Post-Newtonian method, will be done in a fully relativistic way, *i.e.* in which no compromise on the background spacetime will be made whatsoever. Consequently, the resulting orbits and gravitational waves are expected to be accurate even when the two stars in the EMRI system are in extremely close proximity to each other. The background taken will be that of a spherically symmetric non-rotating black hole, *i.e.* the background spacetime will be described by the Schwarzschild metric, to be discussed in detail in the next chapter.

The outline of the thesis is as follows. In chapter 2, the Schwarzschild spacetime will be discussed in detail, and the geodesic motion of stars in bound orbits around black holes will be investigated. There, a new and improved expansion scheme will be introduced that allows for the calculation of bound orbits, taking fully into account all relativistic effects of the Schwarzschild spacetime.
Chapter 3 presents the agreement of this expansion scheme with the purely numerically calculated solutions to the geodesic equations, where it will be seen to be excellent for all but the most extreme natural cases. Most importantly, the expressions found will be explicit functions of time, as required for the calculation of gravitational waves.
In chapter 4, a formalism will be reviewed for the calculation of gravitational waves in a Schwarzschild spacetime, resulting in two differential equations that have the two polarizations of the gravitational waves as their solutions. The sources of these differential equations contain the motion of the orbiting star that produces the waves, and using the expansion scheme of chapter 2, these sources will be written down as explicit functions of time. The resulting differential equations are solved by a numerical algorithm, the details of which will be explained as well.
Chapter 5 collects the results from the previous chapters for orbits and gravitational waves, and presents the outcomes for the latter in both graphic and numerical detail by listing the results for the average emitted power and angular momentum for a large number of cases. It also investigates the effect the emission of gravitational waves has on the orbits.
Finally, chapter 6 presents the conclusions of the thesis, discusses the applicability of the methods presented to other physical cases, and presents an outlook for future research.

1.8 Summary

In this chapter, the basic results of General Relativity have been reviewed and the notational conventions have been introduced. It was motivated that gravity can, by means of the Equivalence Principle, be seen as the curvature of spacetime, and that this curvature is the result of the presence and dynamics of matter and energy. The way the curvature of spacetime influences the motion of test masses in the absence of external forces was discussed by using a Lagrangian formalism, the result being the geodesic equations, and the criterion for the existence of, and expression for, constants of motion was derived.
Furthermore, the basics of the theory of gravitational waves have been discussed, showing

explicitly that the Einstein field equations generally allow the existence of gravitational waves, and for the example of a Minkowski spacetime the general form of the gravitational waves has been derived along with an expression for the energy they carry. Finally, special emphasis was put on the EMRI system, a binary system of two stars orbiting each other with one of the two stars being much heavier than its companion, and it was discussed that a proper description of such a system requires the inclusion of relativistic effects due to curvature, a method to do so being the topic of this thesis.
Having laid down the basic theory of both geodesic motion in a curved spacetime and the way such motion leads to gravitational waves, the next steps will be to calculate the geodesic motion of the stars in a binary system in chapter 2, followed by a calculation of the gravitational waves emitted from such a system in chapters 4 and 5. To emphasize, in the following chapters no compromise will be made on the curvature of spacetime so as to keep all relativistic effects fully accounted for.

Chapter 2

The geodesic deviation method

2.1 Introduction

The Schwarzschild metric [13] is, without doubt, one of the most important results to come out of relativistic gravitational theory. It accurately describes the curved spacetime around a static spherical mass distribution, and, as was realized independently by Jebsen [14] and Birkhoff [15], it is the only metric that does so if it is assumed that the rest of spacetime is empty and is asymptotically Minkowskian. As many astrophysical objects, including the Sun, the Earth, and black holes, are static and spherical up to good approximation, it is not surprising that the Schwarzschild metric plays an important role in astrophysical research. Most notably, gravitational waves coming from such astrophysical objects have recently become important with the advent of sensitive gravitational wave detectors all over the world. A lot of theoretical research has gone into understanding the gravitational waves that originate from EMRI systems, and one of the first steps in modeling these systems is to calculate bound geodesic motion in a Schwarzschild spacetime. A novel way to do so is the topic of this chapter.
The chapter is organized as follows. In section 2.2 the basic results of the Schwarzschild spacetime are reviewed and the geodesic equations are derived, showing why it is impossible to find general geodesic orbits in the time domain. As such orbits in the time domain are required for the calculation of gravitational waves presented in chapter 4, section 2.3 will introduce the geodesic deviation method for calculating the orbits as an expansion series. In this method, it will be the orbit that is seen as a perturbation series rather than the curvature of spacetime. The first and second-order expressions of this series are derived in sections 2.4 and 2.5, respectively, and their general properties will be studied. The chapter ends by presenting a summary in section 2.6.

2.2 Basics of the Schwarzschild spacetime

2.2.1 Geodesic equations, constants of motion, and the circular orbit

The Schwarzschild metric is one of the very few known analytical solutions to the vacuum Einstein field equations and was the first to be found [13], almost immediately after Einstein published the General Theory of Relativity in 1916. It describes [16] the spacetime around a non-spinning spherical mass distribution M, and will play a major part in this thesis.
The metric of the Schwarzschild spacetime is given in Droste coordinates $(t,\, r,\, \theta,\, \varphi)$ by [17]

$$g_{\mu\nu} = \begin{pmatrix} -\left(1-\frac{2M}{r}\right) & 0 & 0 & 0 \\ 0 & \left(1-\frac{2M}{r}\right)^{-1} & 0 & 0 \\ 0 & 0 & r^2 & 0 \\ 0 & 0 & 0 & r^2\sin^2\theta \end{pmatrix}, \tag{2.1}$$

and its line element thus follows as

$$d\tau^2 = \left(1-\frac{2M}{r}\right)dt^2 - \left(1-\frac{2M}{r}\right)^{-1}dr^2 - r^2 d\theta^2 - r^2\sin^2\theta\, d\varphi^2. \tag{2.2}$$

The radial coordinate r has the physical interpretation of the circumference of a circular orbit divided by 2π. The way the line element is written here, it appears it features two singularities: at the r-values of $2M$ and 0, the line-element blows up to infinity. The first of these, however, is only a consequence of the choice of coordinate system; equivalent descriptions of the Schwarzschild spacetime are known that are perfectly smooth at $r = 2M$. This can not be done for the singularity at $r = 0$: no coordinate transformation exists that will make it go away. This means that the singularity at $r = 0$ is a true physical singularity.
Using the line-element Eq. (2.2), the basic machinery of General Relativity reviewed in chapter 1 can be used to obtain constants of motion and to derive the geodesic equations. From the fact that the Schwarzschild metric is static and spherically symmetric, *i.e.* that $g_{\mu\nu}$ does not depend on t or φ, section 1.4 reveals that there are four constants of motion, two of which are zero in an appropriate choice of coordinates. The remaining ones are conventionally labelled ε and ℓ,

$$\varepsilon = \left(1-\frac{2M}{r}\right)u^t, \qquad\qquad \ell = r^2\sin^2\theta\, u^\varphi. \tag{2.3}$$

By considering low-velocity motion of a test mass μ far away from the central mass M, the physical interpretation of ε and ℓ becomes clear: ε becomes equal to $1/\mu$ times the rest energy of the moving mass μ and ℓ becomes equal to $1/\mu$ times its angular momentum. The constants of motion ε and ℓ can therefore be considered as the *energy per unit mass* and *angular momentum per unit mass* of the test mass μ.

The line-element Eq. (2.1) gives rise to the following non-zero connection coefficients

$$\begin{aligned}
\Gamma^t_{tr} &= \frac{M}{r^2}\left(1-\frac{2M}{r}\right)^{-1}, \qquad \Gamma^\varphi_{\varphi r}=\frac{1}{r}, \qquad \Gamma^\varphi_{\varphi\theta}=\frac{\cos\theta}{\sin\theta},\\
\Gamma^r_{tt} &= \frac{M}{r^2}\left(1-\frac{2M}{r}\right), \qquad \Gamma^r_{rr}=-\frac{M}{r^2\left(1-\frac{2M}{r}\right)}, \qquad \Gamma^r_{\theta\theta}=-r\left(1-\frac{2M}{r}\right),\\
\Gamma^r_{\varphi\varphi} &= -r\sin^2\theta\left(1-\frac{2M}{r}\right), \qquad \Gamma^\theta_{r\theta}=\frac{1}{r}, \qquad \Gamma^\theta_{\varphi\varphi}=-\sin\theta\cos\theta,
\end{aligned} \tag{2.4}$$

which in turn give rise to the geodesic equations for geodesic orbits in the Schwarzschild spacetime,

$$\begin{aligned}
\frac{d^2t}{d\tau^2} &= -\frac{2M}{r^2\left(1-\frac{2M}{r}\right)}\left(\frac{dr}{d\tau}\right)\left(\frac{dt}{d\tau}\right),\\
\frac{d^2r}{d\tau^2} &= -\frac{M}{r^2}\left(1-\frac{2M}{r}\right)\left(\frac{dt}{d\tau}\right)^2+\frac{M}{r^2\left(1-\frac{2M}{r}\right)}\left(\frac{dr}{d\tau}\right)^2\\
&+ r\left(1-\frac{2M}{r}\right)\left(\frac{d\theta}{d\tau}\right)^2+r\left(1-\frac{2M}{r}\right)\sin^2\theta\left(\frac{d\varphi}{d\tau}\right)^2,\\
\frac{d^2\theta}{d\tau^2} &= -\frac{2}{r}\left(\frac{dr}{d\tau}\right)\left(\frac{d\theta}{d\tau}\right)+\sin\theta\cos\theta\left(\frac{d\varphi}{d\tau}\right)^2,\\
\frac{d^2\varphi}{d\tau^2} &= -\frac{2}{r}\left(\frac{dr}{d\tau}\right)\left(\frac{d\varphi}{d\tau}\right)-\frac{2\cos\theta}{\sin\theta}\left(\frac{d\theta}{d\tau}\right)\left(\frac{d\varphi}{d\tau}\right).
\end{aligned} \tag{2.5}$$

These constitute four coupled differential equations that, when solved, give the four coordinates (t, r, θ, φ) of a general geodesic orbit as a function of proper time, τ. It is, unfortunately, not possible to solve these equations for a general orbit. However, for a circular orbit such solutions do exist and can readily be found. A circular orbit is defined by the statement $r = R =$ constant and θ can be chosen to equal $\pi/2$; this choice constitutes the appropriate choice of coordinates mentioned before. Then all derivatives of the r- and θ coordinates vanish and thus the non-trivial geodesic equations reduce to

$$\frac{d^2t}{d\tau^2}=0, \qquad \frac{M}{R^3}\left(\frac{dt}{d\tau}\right)^2-\left(\frac{d\varphi}{d\tau}\right)^2=0, \qquad \frac{d^2\varphi}{d\tau^2}=0. \tag{2.6}$$

The first and last of these denotes that $dt/d\tau$ and $d\varphi/d\tau$ are constants; by comparing with the Killing expressions Eqs. (2.3), they can be identified as $\varepsilon/(1-\frac{2M}{R})$ and ℓ/R^2, respectively. The second of the geodesic equations then relates the two constants to each other as

$$\varepsilon^2=\frac{\ell^2}{RM}\left(1-\frac{2M}{R}\right)^2. \tag{2.7}$$

A second equation that relates the constants ε and ℓ follows from the normalisation of four-velocity, $g_{\mu\nu}u^\mu u^\nu=-1$, which gives

$$1-\frac{\varepsilon^2}{1-\frac{2M}{R}}+\frac{\ell^2}{R^2}=0. \tag{2.8}$$

Combining this with Eq. (2.7) then uniquely expresses the Killing constants (ε, ℓ) in terms of the radius R and the mass M of the black hole

$$\varepsilon_0 = \frac{(1-\frac{2M}{R})}{\sqrt{1-\frac{3M}{R}}}, \qquad \ell_0 = \sqrt{\frac{RM}{1-\frac{3M}{R}}}, \tag{2.9}$$

(in which the subscript 0 denotes that these expressions hold for the circular orbit).
The two differential equations Eq. (2.3) can now be solved and give the expressions for $t(\tau)$ and $\varphi(\tau)$. Collecting these with the two constant expressions for r and θ then gives the total solution for the circular orbit explicitly as functions of proper time τ as

$$t(\tau) = \sqrt{\frac{1}{1-3M/R}}\,\tau, \quad r(\tau) = R, \quad \theta(\tau) = \pi/2, \quad \varphi(\tau) = \frac{1}{R^{3/2}}\sqrt{\frac{M}{1-3M/R}}\,\tau. \tag{2.10}$$

This solution will play a major part in the approximation method introduced in section 2.3.

2.2.2 Implicit solutions for general closed orbits

As already mentioned, calculating the solutions for *non*-circular bound orbits is not as easy: general solutions for the geodesic equations are not known as functions of proper time τ. It is however possible to find *implicit* solutions, that express t, r and φ in terms of each other via elliptic integrals, or by doing numerical calculations. Starting point of either approach is the normalisation of four-velocity, Eq. (1.16). Using the Killing constants ε and ℓ of Eq. (2.3), the normalisation condition yields a non-linear differential equation for the r-coordinate,

$$\frac{\varepsilon^2-1}{2} = \frac{1}{2}\left(\frac{dr}{d\tau}\right)^2 + \frac{1}{2}\left(1-\frac{2M}{r(\tau)}\right)\left(1+\frac{\ell^2}{r^2(\tau)}\right) - \frac{1}{2}. \tag{2.11}$$

By defining a new constant E and two potential functions $V_{Newton}(r)$ and $V_{GR}(r)$ as follows

$$E \equiv \frac{\mu(\varepsilon^2-1)}{2}, \qquad V_{Newton} \equiv -\frac{\mu M}{r} + \frac{\mu\ell^2}{2r^2}, \qquad V_{GR}(r) \equiv -\frac{\mu M\ell^2}{r^3}, \tag{2.12}$$

where again μ denotes a test mass in geodesic orbit, this differential equation can be written as

$$E = \frac{\mu}{2}\left(\frac{dr}{d\tau}\right)^2 + V_{Newton} + V_{GR}. \tag{2.13}$$

By identifying the left hand side as an energy, this has almost the same form as the radial energy equation encountered in Newtonian gravitational theory [18], if not for two differences: firstly, the derivatives are here with respect to proper time τ instead of Schwarzschild time (whereas such a distinction does not exist in Newtonian theory), and secondly an extra term V_{GR} makes an entrance. The connection to Newtonian theory is readily made

by realizing that for low velocities and far away from the central mass M, firstly, the difference between proper time and Schwarzschild time becomes neglible, and, secondly, the term V_{GR} becomes much smaller than V_{Newton}, showing explicitly that geodesic orbits as predicted by Newtonian gravity are only a limiting case of the ones predicted by General Relativity.
From Eq. (2.13), many properties of geodesic orbits can be derived. For instance, the fact that the potential terms $V_{Newton} + V_{GR}$ can, for a class of values of ℓ, exhibit a potential well means that an orbiting test mass with a given constant energy E can get trapped in a bound orbit, moving between a minimum radius (the *periastron*) and a maximum radius (the *apastron*). As a special case, there is an energy E for which the system is in a permanent state of lowest potential energy and hence the radial velocity must be zero: this corresponds to the circular orbit explicitly calculated before. The radius R of this orbit with lowest potential energy can be easily calculated by minimizing $V_{Newton} + V_{GR}$, and gives

$$R = \frac{\ell^2}{2M}\left(1 + \sqrt{1 - 12\left(\frac{M}{\ell}\right)^2}\right), \tag{2.14}$$

(which could have also been concluded from the explicit solution, Eq. (2.10)). Finally, from this expression it also follows that there is a smallest circular orbit: R is smallest when the square root vanishes, which is the case for $\ell = \sqrt{12}M$; substituting this back in the remaining expression then gives this smallest radius to be $R = 6M$, a radius known as the *Innermost Stable Circular Orbit* (ISCO).
Many more properties of geodesic orbits can be derived from Eq. (2.11) or Eq. (2.13) when either is combined with the Killing relations Eq. (2.3); an excellent study of these is given in the standard work by Chandrasekhar, Ref. [19]. For instance, the chain rule, Eq. (2.3) and Eq. (2.11) or Eq. (2.13) give a differential equation for φ as a function of r as

$$\begin{aligned}\frac{d\varphi}{dr} &= \pm\frac{\ell}{r^2}\left(\varepsilon^2 - \left(1 - \frac{2M}{r}\right)\left(1 + \frac{\ell^2}{r^2}\right)\right)^{-\frac{1}{2}} \\ &= \pm\frac{\ell}{r^2}\sqrt{\frac{2}{\mu}}\left(E - V_{Newton} - V_{GR}\right)^{-\frac{1}{2}}, \end{aligned} \tag{2.15}$$

where the overall sign depends on whether the geodesic has an increasing r coordinate with increasing φ (*e.g.* during the time a test mass moves from periastron to apastron) or decreasing r coordinate with increasing φ (*e.g.* during the time a test mass moves from apastron to periastron). This differential equation yields the shape of the geodesic orbit, as it relates the radial distance to the black hole to angle traversed by the test mass.
It follows from this equation that the orbits *precess*, by which it is meant that the angular distance between two successive periastra is not 2π as it is in the Newtonian theory. This follows by doing the explicit integration of Eq. (2.15) from one periastron to the next (taking due care of the correct overall sign) and noting that the integral would have yielded exactly 2π if the relativistic term V_{GR} had not been there. Including this term yields a

bigger outcome, the excess defining the famous *periastron shift* $\delta\varphi$. In the limit of low velocities and weak gravitational fields, the periastron shift comes out as [4]

$$\delta\varphi = 6\pi \left(\frac{M}{\ell}\right)^2, \tag{2.16}$$

per orbital revolution; an exact integral expression for the periastron shift will be presented momentarily. As is well-known, this result was already derived by Einstein himself (albeit in a different way, as he did not have the knowledge of the full Schwarzschild solution) and constituted the first quantitative experimental verification of General Relativity as it accurately describes the well-measured periastron shift of the planet Mercury [1].

2.2.3 Another parametrisation of bound orbits

The shape of the bound orbits can be further investigated by expressing it in terms of two new orbital parameters (a, e) rather than the parameters (ε, ℓ) used up till now. This is done by relating the orbital functions r and φ to each other in yet another way. By using Eq. (2.3), Eq. (2.11) can be written in a form that does just that,

$$\begin{aligned} \ell^2 \left(\frac{d}{d\varphi}\frac{1}{r}\right)^2 &= \varepsilon^2 - \left(1 - \frac{2M}{r}\right)\left(1 + \frac{\ell^2}{r^2}\right), \\ &= \frac{\mu}{2}\left(E - V_{Newton} - V_{GR}\right). \end{aligned} \tag{2.17}$$

In Newtonian gravity, the term V_{GR} would not be present, and this equation would be solved by

$$r = \frac{a}{1 + e\cos y}, \tag{2.18}$$

in which the variable y is just the angular coordinate φ with a possible constant phase φ_0, and the parameters (a, e) are related to (ε, ℓ) given by

$$\varepsilon^2 = \frac{M}{a}\left(e^2 - 1\right) + 1, \qquad \ell^2 = aM. \tag{2.19}$$

In that approximation, e represents the eccentricity of the elliptic orbit, and $(1 - e^2)a$ is the length of the semi-major axis[1]. Periastra are reached when y is an even multiple of π, whereas apastra are reached when y is an odd multiple of π. In the relativistic case, however, the term V_{GR} cannot be dropped and this means that the proposed solution Eq. (2.18) only solves the full shape equation Eq. (2.17) in case the new variable y is related nontrivially to the angular coordinate φ. Indeed, Eq. (2.17) with the term V_{GR} kept in place implies that the two variables are related by the nontrivial differential equation

$$\left(\frac{dy}{d\varphi}\right)^2 = 1 - \frac{2M}{a}\left(3 + e\cos y\right), \tag{2.20}$$

[1] In the rest of this thesis, they will be referred to as such even when considering relativistic cases.

and the (a, e) are related to (ε, ℓ) via

$$\varepsilon^2 = \frac{\left(\frac{a}{M} - 2 - 2e\right)\left(\frac{a}{M} - 2 + 2e\right)}{\frac{a}{M}\left(\frac{a}{M} - 3 - e^2\right)}, \qquad \ell^2 = \frac{a^2}{\frac{a}{M} - 3 - e^2}. \tag{2.21}$$

For large $a \gg M$ the second term of Eq. (2.20) is negligeable and the solution is found to be $y = \varphi - \varphi_0$, which, when substituted in Eq. (2.18), returns the relation between r and φ as is found for non-relativistically bound orbits. Physically, this means that far away from the mass M, orbits are accurately described by Newtonian gravity, as expected. However, in case a is of the same order of magnitude as M, the solution of Eq. (2.20) no longer yields a linear relationship between the parameter y and the orbital angle φ, and as a result Eq. (2.18) shows that successive periastra are no longer reached when φ is a multiple of 2π. This, again, constitutes the periastron shift $\delta\varphi$ mentioned before.
An integral expression for this periastron shift can now be derived by integrating the inverse of Eq. (2.20) from one periastron ($y = 0$) to the next ($y = 2\pi$). The result is

$$\Delta\varphi = 2\pi + \delta\varphi = \int_0^{2\pi} dy \, \frac{1}{\sqrt{1 - \frac{2M}{a}\left(3 + e\cos y\right)}}, \tag{2.22}$$

where $\delta\varphi$ is the advance of the periastron compared to the previous one. Finally, via $d\tau/dy = (d\varphi/d\tau)^{-1}(d\varphi/dy)$, Eq. (2.3) and Eq. (2.20), the proper time lapse between two successive periastra can also be written in integral form,

$$\Delta\tau = \frac{a^2}{\ell} \int_0^{2\pi} dy \, \frac{1}{\left(1 + e\cos y\right)^2 \left(1 - \frac{2M}{a}\left(1 + e\cos y\right)\right) \sqrt{1 - \frac{2M}{a}\left(3 + e\cos y\right)}}. \tag{2.23}$$

It follows that for circular orbits, $e = 0$, both $\delta\varphi$ and $\Delta\tau$ are completely fixed by a choice of the radius R of the orbit, making them *dependent* orbital characteristics. In contrast, for eccentric orbits, $e \neq 0$, the two orbital characteristics are completely *independent*, determined by the two independent parameters (a, e), or, equivalently, (ε, ℓ). This observation will be important later on, when discussing the accuracy of the first-order geodesic deviation method.

2.2.4 The necessity for orbital functions as functions of proper time

Eq. (2.15) and, equivalently, Eq. (2.17), happen to be solvable analytically in terms of elliptic functions, but the solution then still needs to be inverted to yield $r = r(\varphi)$, the result of which then needs to be substituted in Eq. (2.3) in order to find t and φ as functions of proper time τ. All of these steps are conventionally done numerically, as there is little hope to find analytical expressions. This is unfortunate; some subsequent applications of geodesic orbits explicitly require the orbits to be known as functions of time. This includes the application that will be discussed in chapter 4, in which the gravitational waves will

be calculated of a system of a test mass orbiting a black hole. It is therefore necessary to find a way to calculate orbits in the time-domain.
Methods to do so exist in the form of the Post-Newtonian expansions discussed in section 1.7, in which the orbits are first considered in a near-Minkowskian spacetime, perturbatively adding corrections due to non-zero curvature and velocities close to that of light. In contrast, in the *geodesic deviation method* to be presented in detail below, it will be the *geodesics* that are written as an expansion series; the curvature of the background spacetime will be taken into full account. The advantage of such a method is that no compromise is made on relativistic effects anywhere in the spacetime: strongly relativistic effects are built in from the outset and results are expected to suffer little from loss of accuracy when considered close to the black hole or when velocities are high. The geodesic deviation method is the topic of the next section.

2.3 The geodesic deviation method

The premise of the geodesic deviation method is to start with a simple geodesic $\bar{x}^\mu$ that is known in analytical form in the time-domain and to subsequently add corrections so as to turn it into a more general orbit:

$$x^\mu = \bar{x}^\mu + \sigma n^\mu + \frac{1}{2}\sigma^2\left(k^\mu - \bar{\Gamma}^\mu_{\lambda\nu} n^\lambda n^\nu\right) + \ldots, \tag{2.24}$$

in which σ is some expansion parameter related to the corrections n^μ and k^μ by the covariant definitions

$$n^\mu = \left.\frac{\partial x^\mu}{\partial \sigma}\right|_{\sigma=0}, \qquad k^\mu = \left.\frac{\partial n^\mu}{\partial \sigma}\right|_{\sigma=0} + \bar{\Gamma}^\mu_{\lambda\nu} n^\lambda n^\nu, \tag{2.25}$$

and $\bar{\Gamma}^\mu_{\lambda\nu}$ is the connection along the zeroth order geodesic $\bar{x}^\mu(\tau)$. The parameter σ is defined to be the physical distance between the perturbed orbit and the original geodesic at $\tau = 0$ as

$$d\sigma^2 = \left. g_{\mu\nu} dx^\mu dx^\nu \right|_{\tau=0}. \tag{2.26}$$

The corrections n^μ, k^μ are found by demanding the total solution Eq. (2.24) of simple geodesic plus corrections be a geodesic itself, or, in other words, that the true geodesic and its approximation are part of a congruence $x^\mu[\tau, \sigma]$ of neighboring geodesics [20]. Thus, by substituting the expansions Eq. (2.24) in the geodesic equation Eq. (1.15), the *geodesic deviation equations* are found to be manifestly covariant differential equations for n^μ and k^μ [3], [21]

$$\frac{D^2 n^\mu}{D\tau^2} - \bar{R}_{\lambda\nu\kappa}{}^\mu \bar{u}^\mu \bar{u}^\lambda n^\nu = 0, \tag{2.27}$$

$$\frac{D^2 k^\mu}{D\tau^2} - \bar{R}_{\lambda\nu\kappa}{}^\mu \bar{u}^\mu \bar{u}^\lambda k^\nu = D_\rho \bar{R}_{\lambda\nu\kappa}{}^\mu \left(\bar{u}^\kappa \bar{u}^\lambda n^\nu n^\rho - \bar{u}^\nu \bar{u}^\rho n^\kappa n^\lambda\right) + 4\bar{R}_{\lambda\nu\kappa}{}^\mu \bar{u}^\lambda n^\nu \frac{Dn^\kappa}{D\tau}, \tag{2.28}$$

in which $\bar{u}^\mu$ is the four-velocity of the starting point geodesic, $\bar{u} \equiv d\bar{x}^\mu/d\tau$, and $\bar{R}_{\lambda\nu\kappa}{}^\mu$ is the Riemann tensor calculated from the spacetime metric $\bar{g}_{\mu\nu} \equiv g_{\mu\nu}(\bar{x}^\mu)$ along this geodesic. The geodesic deviation equation Eq. (2.27) can be seen as the definition of the Riemann tensor, and it assigns to it a physical interpretation: the Riemann tensor is a measure of the curvature of spacetime which can be investigated by observing the change in the relative distance between two neighboring geodesics[2]. In contrast, in the geodesic deviation method the logic is reversed: here, the curvature of spacetime is taken as given, and instead it is one of the geodesics that is calculated assuming the other one to be known.

By defining

$$m^\mu \equiv k^\mu - \bar{\Gamma}^\mu_{\lambda\nu} n^\lambda n^\nu, \tag{2.29}$$

and writing out the Riemann tensors, the geodesic deviation equations can be written in a non-manifestly covariant (but more tractable) form

$$\frac{d^2 n^\mu}{d\tau^2} + 2\bar{u}^\lambda \bar{\Gamma}_{\lambda\nu}{}^\mu \frac{dn^\nu}{d\tau} + \bar{u}^\kappa \bar{u}^\lambda \partial_\nu \bar{\Gamma}_{\kappa\lambda}{}^\mu \, n^\nu = 0, \tag{2.30}$$

$$\frac{d^2 m^\mu}{d\tau^2} + 2\bar{u}^\lambda \bar{\Gamma}_{\lambda\nu}{}^\mu \frac{dm^\nu}{d\tau} + \bar{u}^\kappa \bar{u}^\lambda \partial_\nu \bar{\Gamma}_{\kappa\lambda}{}^\mu \, m^\nu = S^\mu[n], \tag{2.31}$$

in which the source $S^\mu[n]$ of the second-order geodesic deviation equation depends on the first-order solution and is given as

$$S^\mu[n] \equiv -2\bar{\Gamma}_{\lambda\nu}{}^\mu \frac{dn^\lambda}{d\tau}\frac{dn^\nu}{d\tau} - 4\partial_\kappa \bar{\Gamma}_{\lambda\nu}{}^\mu \, \bar{u}^\lambda n^\kappa \frac{dn^\nu}{d\tau} - \partial_\sigma \partial_\kappa \bar{\Gamma}_{\lambda\nu}{}^\mu \bar{u}^\lambda \bar{u}^\nu n^\sigma n^\kappa. \tag{2.32}$$

An important feature to note is that the left hand sides of the geodesic deviation equations Eqs. (2.30), (2.31) for n^μ, m^μ, are identical: the only difference between the first and second-order deviation equation is the presence of a source term $S^\mu[n]$ in the latter. This pattern continues when taking the method to third or higher orders, as the geodesic deviation equation for each order will have the exact same left hand side and will only differ from the previous order in the presence of extra source terms that depend on the solutions of the lower order deviation equations. However, even though deriving the geodesic deviation equations of the third and higher orders is straightforward, this will not be pursued in this thesis.

The geodesic deviation method can be applied to a number of spacetimes and by using a number of simple geodesics as starting point of the expansion [21], [24], [7], [25], [26]. In the rest of this chapter, the focus will be on the case of a Schwarzschild spacetime with a circular orbit of radius R as the zeroth order contribution $\bar{x}^\mu(\tau)$, but the methodological observations hold quite generally. The reason to use a circular orbit as the starting point of the expansion is that, as will be explicitly demonstrated in chapter 5, *all* bound geodesic orbits tend to circularize under the emission of gravitational waves, and hence that all eccentric orbits will ultimately be well-described by small deviations from the circular case.

[2]From an experimental point of view: measure the relative motion of two test masses in free fall.

2.4 The first-order deviations

2.4.1 Calculating the first-order deviations

The presentation will now be specialized to the description of bound geodesic motion in a Schwarzschild spacetime, starting from a circular orbit. For this case, the connections of Eq. (2.4) apply with the radial coordinate r set to a constant R, and the four-velocities are given by the derivatives of the circular solution Eq. (2.10). As the coordinate θ was set to $\pi/2$ in the coordinate system in which all motion is planar, the problem can be reduced from a four-dimensional to a three-dimensional one. For motions in the equatorial plane, then, Eq. (2.30) takes the form

$$\begin{pmatrix} \frac{d^2}{d\tau^2} & \alpha\frac{d}{d\tau} & 0 \\ \beta\frac{d}{d\tau} & \frac{d^2}{d\tau^2} - \kappa & -\gamma\frac{d}{d\tau} \\ 0 & \eta\frac{d}{d\tau} & \frac{d^2}{d\tau^2} \end{pmatrix} \begin{pmatrix} n^t \\ n^r \\ n^\varphi \end{pmatrix} = 0, \tag{2.33}$$

in which

$$\begin{aligned} \alpha &= \frac{2M}{R^2\left(1-\frac{2M}{R}\right)}\frac{1}{\sqrt{1-\frac{3M}{R}}}, \quad \beta = \frac{2M}{R^2}\frac{1-\frac{2M}{R}}{\sqrt{1-\frac{3M}{R}}}, \quad \gamma = 2\sqrt{\frac{M}{R}}\frac{1-\frac{2M}{R}}{\sqrt{1-\frac{3M}{R}}}, \\ \eta &= \frac{2}{R^2}\sqrt{\frac{M}{R}}\frac{1}{\sqrt{1-\frac{3M}{R}}}, \quad \kappa = \frac{3M}{R^3}\frac{1-\frac{2M}{R}}{1-\frac{3M}{R}}. \end{aligned} \tag{2.34}$$

This is a set of three coupled linear second-order differential equations that needs to be solved. For systems with constant coefficients (as is the case here), a method to do so exists in linear algebra [27], but only applies to systems of differential equations that are of *first* order. The current system is not first order, but can be made so by defining

$$\dot{n}^\mu \equiv \tilde{n}^\mu, \tag{2.35}$$

and rewriting the system of three coupled second-order differential equations into a system of six first-order differential equations. Defining a vector $\vec{x}$ as

$$\vec{x} \equiv \begin{pmatrix} \tilde{n}^t \\ \tilde{n}^r \\ \tilde{n}^\varphi \\ n^t \\ n^r \\ n^\varphi \end{pmatrix}, \tag{2.36}$$

the system Eq. (2.33) can be written equivalently as

$$\dot{\vec{x}} = \Lambda\vec{x}, \qquad \Lambda \equiv \begin{pmatrix} 0 & -\alpha & 0 & 0 & 0 & 0 \\ -\beta & 0 & \gamma & 0 & \kappa & 0 \\ 0 & -\eta & 0 & 0 & 0 & 0 \\ 1 & 0 & 0 & 0 & 0 & 0 \\ 0 & 1 & 0 & 0 & 0 & 0 \\ 0 & 0 & 1 & 0 & 0 & 0 \end{pmatrix}, \tag{2.37}$$

which is now a system of six coupled first-order differential equations. Linear algebra [27] then states that the general solution to this set is given by

$$\vec{x} = \sum_i \vec{v}_i e^{\lambda_i \tau}, \tag{2.38}$$

in which λ_i are the eigenvalues of the matrix Λ and $\vec{v}_i$ the corresponding eigenvectors.
Finding the eigenvalues is a standard exercise: setting the determinant of the matrix $(\Lambda - \lambda_i \mathbf{1}_6)$ to zero gives the characteristic equation that has the eigenvalues as its solutions:

$$\lambda^4 \left(-\lambda^2 + \kappa + \alpha\beta - \gamma\eta\right) = 0. \tag{2.39}$$

It follows that there are four zero modes, $\lambda = 0$, and two generally non-zero values, $\lambda_\pm = \pm\sqrt{\kappa + \alpha\beta - \gamma\eta}$. The latter will be considered first. Anticipating that these correspond to periodic solutions $n^\mu_{per}(\tau)$ to the system (indeed, these are *required*, as hyperbolic solutions would destroy the assumption of the geodesic deviation method that the deviations n^μ are small), the exponentials in Eq. (2.38) will be written in imaginary form by writing $\lambda_\pm = \pm i\omega$, with ω the eigenfrequency of the oscillations as

$$\omega = \sqrt{\eta\gamma - \alpha\beta - \kappa} = \sqrt{\frac{M}{R^3}\frac{1 - \frac{6M}{R}}{1 - \frac{3M}{R}}}. \tag{2.40}$$

This indicates that the solution indeed corresponds to periodic solutions when $R > 6M$, and will correspond to hyperbolic solutions when $R < 6M$. This is in agreement with section 2.2.2, where it was remarked that any orbit that lies (partially) within the ISCO at $6M$ will not be bounded and will spiral into the black hole. Although the geodesic deviation equation can be solved for such cases too, the following will concentrate on bound orbits, *i.e.* the assumption is made that $R > 6M$.
The eigenvector corresponding to the eigenvalue $\lambda_\pm$ is found to be

$$\vec{v} \propto \frac{1}{\eta}\begin{pmatrix} \pm i\omega\alpha \\ \omega^2 \\ \pm i\omega\eta \\ \alpha \\ \mp i\omega \\ \eta \end{pmatrix}. \tag{2.41}$$

Returning to the form of the solution Eq. (2.38) and taking only the last three components, the expressions for $n^\mu_{per}(\tau)$ follow as a sum of complex exponentials

$$n^\mu_{per}(\tau) = \vec{n}^\mu_+ e^{i\omega\tau} + \vec{n}^\mu_- e^{-i\omega\tau}, \qquad \vec{n}^\mu_\pm \propto \frac{1}{\eta}\begin{pmatrix} \alpha \\ \mp i\omega \\ \eta \end{pmatrix}, \tag{2.42}$$

which can be turned into real oscillatory functions by choosing the two proportionality constants appropriately. Additionally, the constants will be chosen such that $t(0) = 0, \varphi(0) = 0$ and that the radial function starts at an extremal value (*i.e.* the orbits will have a periastron or apastron at $\tau = 0$). The periodic solutions are then found to be

$$n^t_{per}(\tau) = -\frac{\alpha}{\omega} n^r_c \sin(\omega\tau), \qquad n^r_{per}(\tau) = n^r_c \cos(\omega\tau), \qquad n^\varphi_{per}(\tau) = -\frac{\eta}{\omega} n^r_c \sin(\omega\tau), \tag{2.43}$$

for any value of the constant n^r_c.
As for the zero-valued solutions of Eq. (2.39), these correspond to secular solutions n^μ_{sec} described by the linear functions

$$n^\mu_{sec} = v^\mu \tau + \Delta^\mu_n, \tag{2.44}$$

with

$$v^r = 0, \qquad \kappa\, \Delta^r_n = \beta v^t - \gamma v^\varphi. \tag{2.45}$$

The value $v^r = 0$ is a choice, made to accommodate the physical requirement that the motion described is bounded: a non-zero value for v^r would have been unacceptable as it would correspond to an orbit that in- or decreases linearly in time. This would not only describe orbits that are unbounded (contrary to the object of the calculation), but it is also contrary to the requirement that the deviations n^μ remain small. However, non-zero values for v^t and v^φ do not cause such problems and are perfectly allowed. In fact, such solutions are required for at least two reasons. Firstly, as will be explained in section 2.5.1, the source terms in the higher-order geodesic deviation equations generate Poincaré resonances which have to be removed by such secular terms. Secondly, the periodic solutions suffer from the problem that the angle and proper time lapse between periastra can not be matched correctly for eccentric orbits, as will be explained at the end of this section; this mismatch accumulates and grows without bound in due course of time, unless corrected by the secular contributions Eq. (2.44).
A choice of values for the parameters Δ^t_n and Δ^φ_n only change the origin of t and φ and are therefore arbitrary. In view of the initial conditions to have $t(0) = 0$ and $\varphi(0) = 0$, these are taken to be $\Delta^t_n = \Delta^\varphi_n = 0$. As Δ^r_n then is the only remaining relevant component, from here on it will for simplicity be written as $\Delta^r_n = \Delta_n$.

The sum of the periodic solutions and secular solutions forms the most general solution to the system Eq. (2.33). However, they still need to obey the normalization condition of four-velocity, Eq. (1.16). To first order this condition takes the form

$$\bar{g}_{\mu\nu}\bar{u}^\mu \frac{Dn^\nu}{D\tau} = 0 \tag{2.46}$$

It follows immediately that the periodic contribution to the solution automatically obeys this condition, and that the secular contribution only does so under the constraint

$$\varepsilon_0 v^t - \ell_0 v^\varphi = 0, \tag{2.47}$$

in which ε_0 and ℓ_0 are the energy per unit mass and angular momentum per unit mass of the circular orbit, *i.e.* they are given by Eq. (2.9). Taking into account Eq. (2.45), the expressions for v^t and v^φ can be decoupled and are

$$v^t = \frac{\alpha\kappa}{\alpha\beta - \eta\gamma}\,\Delta_n, \quad v^\varphi = \frac{\eta\kappa}{\alpha\beta - \eta\gamma}\,\Delta_n. \tag{2.48}$$

It then follows that application of the normalization condition for σ, Eq. (2.26), implies

$$n^r(0) = n^r_{per}(0) + n^r_{sec}(0) = n^r_c + \Delta_n = \sqrt{1 - \frac{2M}{R}}. \tag{2.49}$$

Combining all results, the solutions for the first-order perturbed geodesics describing bound motion become

$$\begin{aligned}
t(\tau) &= \left(\frac{1}{\sqrt{1-\frac{3M}{R}}}\right)\tau - \frac{\alpha}{\omega}\,\sigma n^r_c \sin(\omega\tau) + \left(\frac{\alpha\kappa}{\alpha\beta-\gamma\eta}\,\sigma\Delta_n\right)\tau, \\
r(\tau) &= R + \sigma n^r_c \cos(\omega\tau) + \sigma\Delta_n, \\
\varphi(\tau) &= \left(\sqrt{\frac{M}{R^3}}\frac{1}{\sqrt{1-\frac{3M}{R}}}\right)\tau - \frac{\eta}{\omega}\,\sigma n^r_c \sin(\omega\tau) + \left(\frac{\eta\kappa}{\alpha\beta-\gamma\eta}\,\sigma\Delta_n\right)\tau.
\end{aligned} \tag{2.50}$$

To summarize, these expressions by construction solve the geodesic equations to first order in σ, the geodesic deviation equations to first order in σ, and have a four-velocity that is properly normalized to first order in σ. They contain three constants that can freely be assigned values: the circular radius R, the normalization parameter σ, and the secular constant Δ_n.

2.4.2 The epicycle expansion

A number of observations can now be made. Firstly, the form of the solution Eq. (2.50) has a graphical interpretation very akin to the ancient Ptolemean system of *epicycles*, which was proposed to explain the apparent motion of the planets as seen from Earth [28]. For this reason, the expansion Eq. (2.50) (and its higher order extensions calculated later on) will be referred to as the *epicycle expansion*; the deviations themselves will be referred to as the epicycles. Secondly, it can be noted that the epicycle frequency ω differs from the frequency of the zeroth order circle by a factorthat depends on the ratio M/R, the result of which naturally accounts for the well-known periastron shift as discussed in section 2.2. Finally, it can be seen from the radial expansion $r(\tau)$ that the dimensionless constants

$\sigma\Delta_n/R$ and $\sigma n_c^r/R$ assume the role of the expansion parameters in the radial coordinate. They are related via Eq. (2.49), and have the following physical interpretations: the former is a measure of the correction that is made to the radius of the perfectly circular orbit on which the epicycle is placed, whereas the latter is a measure of the ratio of the sizes of the circular orbit and the epicycle.

The parameters Δ_n and σ will now be related to observable quantities. This can be done by noting that the radial distances of the periastra r_{pa} and apastra r_{aa} of the orbit occur at proper times τ_n such that $\omega\tau_n = n\pi$. It thus follows that

$$r_{pa} = R + \sigma\left(\Delta_n + n_c^r\right), \qquad r_{aa} = R + \sigma\left(\Delta_n - n_c^r\right). \tag{2.51}$$

Inverting these equations yields

$$\sigma n_c^r = \frac{1}{2}\left(r_{pa} - r_{aa}\right), \qquad \sigma\Delta_n = \frac{1}{2}\left(r_{pa} + r_{aa}\right) - R. \tag{2.52}$$

In view of Eq. (2.49), σ takes the value

$$\sigma = \frac{r_{pa} - R}{\sqrt{1 - \frac{2M}{R}}}. \tag{2.53}$$

From Eqs. (2.52) it follows immediately that the expansion parameters $\sigma\Delta_n/R$ and $\sigma n_c^r/R$ are directly related to the eccentricity of the epicycle expansion, making it effectively an expansion in the eccentricity. This is, of course, in agreement with the premise of the geodesic deviation method, as it assumed that the bound geodesic does not deviate too much from a perfectly circular orbit. It can also be seen from Eq. (2.53) that the size of the expansion parameter is determined not only by (via the numerator) the eccentricity of the orbit but also by (via the denominator) the radius R of the zeroth order circle. It can therefore be expected that the accuracy of the epicycle expansion will also have some dependence on the distance to the black hole and indeed this is found to be the case in the explicit examples in section 3.3. Based on the form of the denominator, however, this dependence is expected to be small for orbits for which $R > 6M$ and will be most significant only for orbits closest to the ISCO. It therefore does not contradict the statement that the accuracy of the epicycle expansion suffers little from close proximity to the black hole.

To end this section, the energy and angular momentum per unit of mass for the epicycle expansion Eqs. (2.50) can be calculated by a substitution in Eq. (2.3) and truncating the results to first order in σ:

$$\ell = \ell_0 + \sigma\ell_n\,, \qquad\qquad \varepsilon = \varepsilon_0 + \sigma\varepsilon_n\,, \tag{2.54}$$

in which ℓ_0 and ε_0 are the angular momentum per unit mass and energy per unit mass for the circular orbit, as given by Eq. (2.9), and the first-order corrections are given by

$$\ell_n = \left(\frac{1}{2}\sqrt{\frac{R}{M}}\frac{\omega^2R^2}{\sqrt{1-\frac{3M}{R}}}\right)\Delta_n\,, \qquad \varepsilon_n = \left(\frac{1}{2}\frac{\omega^2R}{\sqrt{1-\frac{3M}{R}}}\right)\Delta_n. \tag{2.55}$$

It is important to note that the fact that the energy per unit mass and angular momentum per unit mass come out as *constants* to first order in σ, is evidence that the expressions Eq. (2.50) are indeed solutions to the geodesic equations to this order, as required by Killing's theorem as explained in section 1.4. Had they not been (by, *e.g.*, a principal error in the method) a residual time dependence would have been likely to emerge in the expressions for ε_n and ℓ_n.

2.4.3 The inclusion of the secular constants

The first-order solutions consist of periodic terms and secular terms, the latter of which are parametrized by the constant Δ_n. Earlier work [21], [24] on the system Eqs. (2.30), (2.31) (as well as on the analogous system for the Kerr metric, [25]) dismissed these secular contributions as they were not thought to have any physical importance. At first glance this does indeed seem to be the case: any geodesic orbit in the Schwarzschild spacetime can always (up to orientation) be parametrized by only two constants (*e.g.* (a, e), or (ℓ, ϵ)), whereas the introduction of the secular constant Δ_n indicates that, alongside the constants R and σ, the epicycle-approximated orbit can be parametrized by three, making the secular constant Δ_n appear superfluous. This issue will be addressed in section 2.5.5.
A second reason the literature did not include the secular constant is that it appears in the radial first-order epicycle expansion Eq. (2.50) as a correction to the radius R of the zeroth order circle, and it seems as if it might therefore just as well be absorbed in this radius from the outset. This, however, is not true, as the expression Eq. (2.40) for the epicycle frequency ω depends only on the radius R and not on the secular constant, so that the choice not to include the constant in the radius allows to fix the radius and epicycle frequency independently. This can also be concluded from the expressions for the energy per unit mass and angular momentum per unit mass of the first-order expansion, Eq. (2.55), as this equation shows explicitly that the values of (ε, ℓ) are unchanged from the circular values ε_0, ℓ_0 if the secular contributions vanish: $\Delta_n = v^t = v^\varphi = 0$. However, in general changes of these values are *required* when describing non-circular orbits, as in that case ε and ℓ should be independent parameters whereas, as remarked at the end of section 2.2.3, circular orbits have dependent values of ε and ℓ.
This observation has a physical interpretation as well: the two parameters ε and ℓ determine the angle as well as the time lapse between successive periastra, as shown explicitly in Eqs. (2.22) and (2.23). Therefore, in general, one has to choose a non-zero value for the secular contributions Δ_n, in order to have the first-order epicycle expansion have the right periastron shift and proper time lapse when describing non-circular motion. Omission of the secular constant will therefore yield an epicycle orbit that does not reach the successive periastra angles at the right proper time. This results in a lag or overshoot compared to the true orbit, and this error will accumulate in time.
It is for this reason that the secular solutions to Eq. (2.30) are not dismissed. Indeed, only after including the secular contributions do the solutions accurately approximate closed geodesics, with deviations from purely numerically calculated geodesics being typically a few percent and usually much less, as will be demonstrated in the examples in chapter 3.

2.5 The second-order deviations

2.5.1 The Poincaré resonance and the Poincaré-Lindtsted method

In the previous section, the epicycle expansion has been calculated up to first order and it has been argued that the secular constant is necessary to make the expansion as accurate as possible. The price that has to be paid for this increased accuracy is the appearance of *Poincaré resonances* when going to second or higher order: the higher-order solutions turn out to be singular. This comes about because the secular contributions Δ_n at first order lead to oscillatory terms in the right hand side of Eq. (2.31) that have a frequency ω of the same value as the eigenvalue of the differential matrix in the left hand side[3]. To make this more precise, the source terms $S^\mu[n]$ at the right hand side of Eq. (2.31) will be of the form

$$S^\mu[n] = A^\mu_c \cos 2\omega\tau + A^\mu_s \sin 2\omega\tau + B^\mu_c \cos\omega\tau + B^\mu_s \sin\omega\tau + C^\mu, \tag{2.56}$$

in which the terms $\propto B^\mu_{c,s}$ have frequencies that have the same value as the eigenvalues of the differential matrix that is the left hand side of Eq. (2.31). These two frequencies resonate with each other, producing infinite solutions. Had the secular contributions been omitted, the terms $\propto B^\mu_{c,s}$ would have vanished and the only oscillatory terms that would appear in $S^\mu[n]$ would have had frequencies that are non-unity integer multiples of the frequency ω so no resonances occur.
The resolution of this kind of singular behaviour in the perturbative treatment of non-linear oscillators was realized long ago by Lindtsted and Poincaré [29], [30] (for a modern presentation, see *e.g.* [31]). Briefly, the dependence of the frequency on the amplitude of an anharmonic oscillator is not properly taken into account by the naive perturbative treatment. An improved perturbation theory can be developed in which both the amplitude and the frequencies of the perturbative solutions are made to depend on the expansion parameter σ, so as to cancel singular behaviour of the final solutions. Thus, the claim is that the Poincaré resonances can be dealt with by recognizing that the frequency of the solutions need to be seen as an expansion series itself,

$$\omega \to \bar\omega \equiv \omega + \sigma\omega_1 + \frac{1}{2}\sigma^2\omega_2 + \ldots, \tag{2.57}$$

in which the correction terms $\omega_1, \omega_2, \ldots$ can be chosen such that the Poincaré resonances vanish. This is possible because a derivative of an oscillatory first-order term n^μ will introduce an overall factor of $\bar\omega$ in that term rather than ω, effectively introducing higher order contributions. These then can be seen as contributions to the second-order deviation

[3]The reason that the frequency of the offending source terms is the same as the eigenvalue of the second-order differential matrix, is that the first and second-order geodesic deviation equations have the same left hand side, *i.e* the same differential matrix. Thus, a frequency ω introduced by the differential matrix of a deviation equation at one order introduces (an integer multiple of) this frequency in the source terms of the higher order deviation equations.

equation, and as a result, the source $S^\mu[n]$ will now be supplemented with extra terms that are proportional to ω_1. By choosing ω_1 appropriately, these extra terms in the source can be used to cancel the offending ones $\propto B_c^\mu$ in $S^\mu[n]$, thus removing the Poincaré resonance. This procedure is known as the *Poincaré-Lindtsted method*.

The Poincaré-Lindtsted method will be put in mathematical form now, by deriving the geodesic deviation equations anew. This is necessary, as the method changes the form of the geodesic deviation equations due to the expansion Eq. (2.57). Starting point is as in section 2.3, *i.e.* starting from a simple geodesic $\bar{x}^\mu$ plus its deviations n^μ and m^μ and demanding their sum to be geodesic as well. Collecting Eqs. (2.30), (2.31), it follows that the geodesic equation is given by

$$\begin{aligned}\frac{Du^\mu}{D\tau} &= \sigma\left[\frac{d^2n^\mu}{d\tau^2} + 2\bar{u}^\lambda\bar{\Gamma}^\mu_{\lambda\nu}\frac{dn^\nu}{d\tau} + \bar{u}^\lambda\bar{u}^\kappa\partial_\nu\bar{\Gamma}^\mu_{\kappa\lambda}n^\nu\right]_{\bar{x}} \\ &\quad + \frac{1}{2}\sigma^2\left[\frac{d^2m^\mu}{d\tau^2} + 2\bar{u}^\lambda\bar{\Gamma}^\mu_{\lambda\nu}\frac{dm^\nu}{d\tau} + \bar{u}^\lambda\bar{u}^\kappa\partial_\nu\bar{\Gamma}_{\kappa\lambda}{}^\mu m^\nu - S^\mu[n]\right]_{\bar{x}} + ... = 0\end{aligned} \tag{2.58}$$

To account for the perturbation series in the frequency, a new time variable λ is defined as

$$\omega\lambda = \bar{\omega}\tau \equiv \left(\omega + \sigma\omega_1 + \frac{1}{2}\sigma^2\omega_2 + ...\right)\tau. \tag{2.59}$$

The expansion then takes the equivalent form

$$\begin{aligned}&\sigma\left[\frac{d^2n^\mu}{d\lambda^2} + 2\bar{u}^\lambda\bar{\Gamma}^\mu_{\lambda\nu}\frac{dn^\nu}{d\lambda} + \bar{u}^\kappa\bar{u}^\lambda\partial_\nu\bar{\Gamma}^\mu_{\kappa\lambda}n^\nu\right]_{\bar{x}} \\ &+ \frac{1}{2}\,\sigma^2\left[\frac{d^2m^\mu}{d\lambda^2} + 2\bar{u}^\lambda\bar{\Gamma}^\mu_{\lambda\nu}\frac{dm^\nu}{d\lambda} + \bar{u}^\kappa\bar{u}^\lambda\partial_\nu\bar{\Gamma}^\mu_{\kappa\lambda}m^\nu - \Sigma^\mu[n]\right]_{\bar{x}} + ... = 0,\end{aligned} \tag{2.60}$$

where the inhomogeneous source term for m^μ is changed to

$$\begin{aligned}\Sigma^\mu[n] &= -2\bar{\Gamma}^\mu_{\lambda\nu}\frac{dn^\lambda}{d\lambda}\frac{dn^\nu}{d\lambda} - 4\partial_\kappa\bar{\Gamma}^\mu_{\lambda\nu}\,\bar{u}^\lambda n^\kappa\frac{dn^\nu}{d\lambda} - \partial_\sigma\partial_\kappa\bar{\Gamma}^\mu_{\lambda\nu}\bar{u}^\lambda\bar{u}^\nu n^\sigma n^\kappa \\ &\quad - \frac{4\omega_1}{\omega}\,\frac{d^2n^\mu}{d\lambda^2} - \frac{4\omega_1}{\omega}\,\bar{\Gamma}^\mu_{\lambda\nu}\bar{u}^\lambda\frac{dn^\nu}{d\lambda},\end{aligned} \tag{2.61}$$

or, put more simply,

$$\Sigma^\mu[n] = S^\mu[n] - \frac{4\omega_1}{\omega}\,\frac{d^2n^\mu}{d\lambda^2} - \frac{4\omega_1}{\omega}\,\bar{\Gamma}_{\lambda\nu}{}^\mu u^\lambda\frac{dn^\nu}{d\lambda}, \tag{2.62}$$

where $S^\mu[n]$ is given by Eq. (2.32) with τ replaced by λ.
The sum between each set of square brackets of Eq. (2.60) needs to vanish separately,

so that each of the sums constitutes a new differential equation for the first, second, and higher order deviations n^μ, m^μ, ..., that replace the ones Eqs. (2.30), (2.31) derived before. The key differences are, firstly, that derivatives are with respect to λ rather than τ, and secondly, as promised, that the source $\Sigma[n]$ of the second-order deviation equation consists of extra terms compared to the original source $S^\mu[n]$ and that these terms are proportional to ω_1. As advocated, it is now possible to choose ω_1 and its higher-order generalizations so as to cancel the dangerous contributions in $S^\mu[n]$ that produce the Poincaré resonances. In what follows, this procedure will be demonstrated explicitly.

2.5.2 Recalculating the first-order deviations

One consequence of the Poincaré-Lindtsted method is that the addition of higher orders will change the expressions for the lower orders as well (as opposed to more conventional perturbation theories, in which lower order contributions are unchanged when higher order contributions are added): this manifests itself in the fact that adding of higher orders will change the frequency $\bar{\omega}$ at all previous orders as well. With every higher order added, therefore, it is necessary to recalculate the lower order contributions.
In the present case, it is easy to see how the first-order contributions are changed. The equation for the first-order deviations is the linear homogeneous equation that can be read off from the first line of Eq. (2.60) by setting it to zero:

$$\frac{d^2n^\mu}{d\lambda^2} + 2\bar{u}^\lambda\bar{\Gamma}^\mu_{\lambda\nu}\frac{dn^\nu}{d\lambda} + \bar{u}^\kappa\bar{u}^\lambda\partial_\nu\bar{\Gamma}^\mu_{\kappa\lambda}n^\nu = 0. \tag{2.63}$$

This is of exactly the same mathematical form as Eq. (2.30), the only difference being that τ has been replaced by λ. Hence, the solution will be of the same form as before, with τ replaced by λ, *i.e.*

$$\begin{aligned} n^t(\lambda) &= -\frac{\alpha}{\omega}\,n_c^r\sin\omega\lambda + \frac{\alpha\kappa\lambda}{\alpha\beta-\gamma\eta}\,\Delta_n, \\ n^r(\lambda) &= n_c^r\cos\omega\lambda + \Delta_n, \\ n^\varphi(\lambda) &= -\frac{\eta}{\omega}\,n_c^r\sin\omega\lambda + \frac{\eta\kappa\lambda}{\alpha\beta-\gamma\eta}\,\Delta_n, \end{aligned} \tag{2.64}$$

with $\omega\lambda = \bar{\omega}\tau$, showing that the epicycle frequency has been changed by terms of order σ and higher. It is also straightforward to check that the solution still normalizes the four-velocity, *i.e.* that it solves Eq. (2.46). It does so not just to first order in σ but *exactly*, as

$$\bar{g}_{\mu\nu}\bar{u}^\mu\frac{Dn^\nu}{D\tau} = \left(\bar{g}_{\mu\nu}\frac{Dn^\nu}{D\lambda}\right)\frac{d\lambda}{d\tau}, \tag{2.65}$$

where the expression between brackets vanishes for Eq. (2.64). This can be checked by a direct substitution, but also follows directly when it is recognized that the first-order

solutions obtained in this section are exactly those of section 2.4 with $\tau \to \lambda$, and as the latter were made to solve Eq. (2.46), the former will make the expression between brackets in Eq. (2.65) vanish.

Having obtained the first-order contributions anew, they can be used to calculate the source terms $\Sigma^\mu[n]$ for the second-order contributions, by substituting Eq. (2.64) in the source terms Eq. (2.61) of the second-order geodesic deviation equations. This provides expressions for Σ^μ of the form

$$\begin{aligned} \Sigma^t &= a^t \sin(2\omega\lambda) + b^t \sin(\omega\lambda), \\ \Sigma^r &= a^r \cos(2\omega\lambda) + b^r \cos(\omega\lambda) + c^r, \\ \Sigma^\varphi &= a^\varphi \sin(2\omega\lambda) + b^\varphi \sin(\omega\lambda). \end{aligned} \tag{2.66}$$

The coefficients (a^μ, b^μ, c^μ) are complicated expressions in terms of R and the first-order deviation parameters (n_c^r, Δ_n), and are given in Appendix A. In what follows, the resulting second-order deviation equations Eq. (2.60) will be solved, and the Poincaré resonance will be removed.

2.5.3 Calculating the second-order deviations

The second-order deviation equations can be read off from Eq. (2.60) by setting the second line equal to zero:

$$\frac{d^2 m^\mu}{d\lambda^2} + 2\bar{u}^\lambda \bar{\Gamma}^\mu_{\lambda\nu} \frac{dm^\nu}{d\lambda} + \bar{u}^\kappa \bar{u}^\lambda \partial_\nu \bar{\Gamma}^\mu_{\kappa\lambda} m^\nu = \Sigma^\mu[n], \tag{2.67}$$

with the sources given by Eq. (2.66). A natural Ansatz for the most general solution (respecting, as before, the boundary conditions $t(0) = 0, \varphi(0) = 0$ and the requirement that $r(\tau)$ should not grow unboundedly in time) is

$$\begin{aligned} m^t &= m_2^t \sin(2\omega\lambda) + m_1^t \sin(\omega\lambda) + w^t \lambda, \\ m^r &= m_2^r \cos(2\omega\lambda) + m_1^r \cos(\omega\lambda) + \Delta_m, \\ m^\varphi &= m_2^\varphi \sin(2\omega\lambda) + m_1^\varphi \sin(\omega\lambda) + w^\varphi \lambda, \end{aligned} \tag{2.68}$$

in which $m^\mu_{1,2}$, Δ_m, and w^μ are, at this point, arbitrary constants, to be solved for below. After a substitution in Eq. (2.67), Eq. 2.68 indeed solves the system if the coefficients $m^\mu_{1,2}$ obey the algebraic matrix equations

$$\begin{pmatrix} -4\omega^2 & -2\omega\alpha & 0 \\ 2\omega\beta & -(4\omega^2+\kappa) & -2\omega\gamma \\ 0 & -2\omega\eta & -4\omega^2 \end{pmatrix} \begin{pmatrix} m_2^t \\ m_2^r \\ m_2^\varphi \end{pmatrix} = \begin{pmatrix} a^t \\ a^r \\ a^\varphi \end{pmatrix}, \tag{2.69}$$

and

$$\begin{pmatrix} -\omega^2 & -\omega\alpha & 0 \\ \omega\beta & -(\omega^2+\kappa) & -\omega\gamma \\ 0 & -\omega\eta & -\omega^2 \end{pmatrix} \begin{pmatrix} m_1^t \\ m_1^r \\ m_1^\varphi \end{pmatrix} = \begin{pmatrix} b^t \\ b^r \\ b^\varphi \end{pmatrix}, \tag{2.70}$$

in which the greek constant coefficients of Eq. (2.34) have been reintroduced, and the secular contributions $w^t,\ w^\varphi, \Delta_m$ obey

$$\beta w^t - \gamma w^\varphi - \kappa\Delta_m = c^r. \tag{2.71}$$

The subtlety in solving these matrix equations is, that the determinant of the matrix of coefficients of the m_1^μ vanishes as a result of Eq. (2.40) and hence the matrix cannot generally be inverted to yield a finite solution: this is the source of the Poincaré resonance. The system Eq. (2.70) can be solved only for a specific set of values $b^\mu(\omega_1)$; for this to happen, the frequency shift ω_1 has to be chosen properly. The condition is the following: the left hand side of Eq. (2.70) can be made to vanish when it is left-multiplied by the zero mode

$$m_{0\,\mu} = (\beta, \omega, -\gamma)\,; \tag{2.72}$$

therefore the condition that the system is solvable is when the right hand side also vanishes when left-multipied by $m_{0\,\mu}$, *i.e* the condition on ω_1 is

$$\beta b^t + \omega b^r - \gamma b^\varphi = 0. \tag{2.73}$$

The coefficients b^μ are of the form

$$b^\mu = n_c^r \left(F^\mu \frac{\Delta_n}{R} - G^\mu \frac{\omega_1}{\omega} \right), \tag{2.74}$$

with (F^μ, G^μ) as given in appendix A, determined only by M and R. Substituting this form in the condition then gives the value ω_1 that makes the system Eq. (2.70) solvable:

$$\omega_1 = \frac{\beta F^t + \omega F^r - \gamma F^\varphi}{\beta G^t + \omega G^r - \gamma G^\varphi} \frac{\Delta_n}{R}\,\omega. \tag{2.75}$$

It should be noted, that the frequency shift ω_1 is proportional to the secular constant Δ_n and hence vanishes whenever $\Delta_n = 0$. This implies that in the absence of secular terms Δ_n at first order there is no need for the Poincaré-Lindtsted method. This is in full accord with the discussion of section 2.5.1, where it was already noted that the absence of secular terms at first order would mean that no Poincaré resonances would occur in the first place. Having chosen ω_1 as such, Eq. (2.70) can be inverted to yield

$$\begin{aligned} m_1^t &= -\frac{\eta b^t - \alpha b^\varphi}{\omega^2(\omega^2+\kappa)}\,\gamma + \frac{\beta b^t - \gamma b^\varphi}{(2\omega^2+\kappa)(\omega^2+\kappa)}\,\alpha, \\ m_1^r &= \frac{\beta b^t - \gamma b^\varphi}{\omega(2\omega^2+\kappa)}, \\ m_1^\varphi &= -\frac{\eta b^t - \alpha b^\varphi}{\omega^2(\omega^2+\kappa)}\,\beta + \frac{\beta b^t - \gamma b^\varphi}{(2\omega^2+\kappa)(\omega^2+\kappa)}\,\eta. \end{aligned} \tag{2.76}$$

In contrast, Eqs. (2.69) for m_2^μ can be inverted straightforwardly, with the result

$$\begin{aligned} m_2^t &= \frac{\alpha}{12\omega^4}\left(\beta a^t + 2\omega a^r - \gamma a^\varphi\right) - \frac{a^t}{4\omega^2}, \\ m_2^r &= -\frac{1}{6\omega^3}\left(\beta a^t + 2\omega a^r - \gamma a^\varphi\right), \\ m_2^\varphi &= \frac{\eta}{12\omega^4}\left(\beta a^t + 2\omega a^r - \gamma a^\varphi\right) - \frac{a^\varphi}{4\omega^2}. \end{aligned} \tag{2.77}$$

The Poincaré resonance has thus been removed, and a non-singular solution to Eq. (2.67) has been found. It still needs to have its resulting four-velocity normalized, and this will now be done.
Substituting the expansion Eq. (2.24) in the normalization condition Eq. (1.16) and truncating the outcome to second order in σ shows that solutions up to second order must satisfy the condition

$$\sigma\left(\bar{g}_{\mu\nu}\bar{u}^\mu\frac{Dn^\nu}{D\tau}\right) + \frac{\sigma^2}{2}\left(\bar{g}_{\mu\nu}\bar{u}^\mu\frac{Dk^\nu}{D\tau} + \bar{g}_{\mu\nu}\frac{Dn^\mu}{D\tau}\frac{Dn^\nu}{D\tau} + \bar{u}^\kappa\bar{u}^\lambda\bar{g}_{\rho\kappa}\bar{R}^\rho_{\mu\lambda\nu}n^\mu n^\lambda\right) = 0, \tag{2.78}$$

where $k^\mu = m^\mu + \bar{\Gamma}_{\lambda\nu}^{\ \ \mu}n^\lambda n^\nu$. It was already seen in section 2.5.2 that the first term vanishes identically if the solution Eq. (2.64) for $n^\mu(\lambda)$ is substituted. Upon using Eq. (2.27) the term of second order in σ in Eq. (2.78) vanishes if

$$\bar{g}_{\mu\nu}\bar{u}^\mu\frac{Dk^\nu}{D\tau} + \frac{1}{2}\frac{d^2n^2}{d\tau^2} = \frac{d}{d\tau}\left(\bar{g}_{\mu\nu}u^\mu k^\nu + \frac{1}{2}\frac{dn^2}{d\tau}\right) = 0, \tag{2.79}$$

where $n^2 = \bar{g}_{\mu\nu}n^\mu n^\nu$. At this point, replacing τ by λ would only introduce third order terms in σ, which will be discarded when truncating the epicycle expansion at second order; hence τ can be freely replaced by λ. After substitution of the explicit expressions for u^μ, n^μ and k^μ, Eq. (2.79) then reduces to

$$\begin{aligned} \varepsilon_0\frac{dm^t}{d\lambda} - \ell_0\frac{dm^\varphi}{d\lambda} &= 2\omega\left(\varepsilon_0 m_2^t - \ell_0 m_2^\varphi\right)\cos 2\omega\lambda + \omega\left(\varepsilon_0 m_1^t - \ell_0 m_1^\varphi\right)\cos\omega\lambda + \varepsilon_0 w^t - \ell_0 w^\varphi \\ &= -\frac{\omega^2(n_c^r)^2}{1-\frac{2M}{R}}\cos 2\omega\lambda - \frac{2\omega^2\Delta_n n_c^r}{1-\frac{2M}{R}}\cos\omega\lambda - \frac{3}{4}\frac{\omega^2(\Delta_n)^2}{1-\frac{3M}{R}}. \end{aligned} \tag{2.80}$$

The two relations that follow for $m_{1,2}^\mu$ by comparing the terms proportional to $\cos\omega\lambda$ and $\cos 2\omega\lambda$ are identities, implied by Eqs. (2.76) and (2.77); however, for the constant terms there is the constraint

$$\varepsilon_0 w^t - \ell_0 w^\varphi = -\frac{3}{4}\frac{\omega^2(\Delta_n)^2}{1-\frac{3M}{R}}. \tag{2.81}$$

Together with the relation Eq. (2.71) this can be used to express w^t and w^φ in terms of Δ_m and the lower-order parameters as

$$\begin{aligned} w^t &= -\frac{3}{4}\frac{\omega^2(\Delta_n)^2}{\left(1-\frac{3M}{R}\right)^{3/2}} - \frac{1}{2}\frac{R\,(c^r+\kappa\Delta_m)}{\left(1-\frac{2M}{R}\right)\sqrt{1-\frac{3M}{R}}}, \\ w^\varphi &= -\frac{3}{4R}\sqrt{\frac{M}{R}}\frac{\omega^2(\Delta_n)^2}{\left(1-\frac{3M}{R}\right)^{3/2}} - \frac{1}{2}\sqrt{\frac{R}{M}}\frac{(c^r+\kappa\Delta_m)}{\sqrt{1-\frac{3M}{R}}}, \end{aligned} \tag{2.82}$$

with c^r as given in Eq. (A.13). This concludes the calculation of the second-order geodesic perturbations.

2.5.4 Collecting the results: the epicycle expansion to second order

Adding the zeroth-order contributions of Eq. (2.10), first-order contributions of Eq. (2.64) and second-order contributions derived in section 2.5.3 gives the total epicycle expansion up to second order. These are collected here for convenience, and are given by

$$\begin{aligned} t(\tau) &= U_0^t\tau + U_1^t\sin(\bar\omega\tau) + U_2^t\sin(2\bar\omega\tau), \\ r(\tau) &= U_0^r + U_1^r\cos(\bar\omega\tau) + U_2^r\cos(2\bar\omega\tau), \\ \varphi(\tau) &= U_0^\varphi\tau + U_1^\varphi\sin(\bar\omega\tau) + U_2^\varphi\sin(2\bar\omega\tau), \end{aligned} \tag{2.83}$$

where to this order $\bar\omega = \omega + \sigma\omega_1$, and

$$U_0^t = \frac{1}{\sqrt{1-\frac{3M}{R}}} + \frac{\sigma\alpha\kappa\bar\omega\Delta_n}{\omega(\alpha\beta-\gamma\eta)} + \frac{\sigma^2\bar\omega w^t}{2\omega}, \qquad U_1^t = -\frac{\sigma\alpha n_c^r}{\omega} + \frac{1}{2}\sigma^2 m_1^t, \qquad U_2^t = \frac{1}{2}\sigma^2 m_2^t,$$

$$U_0^r = R + \sigma\Delta_n + \frac{1}{2}\sigma^2\Delta_m, \qquad U_1^r = \sigma n_c^r + \frac{1}{2}\sigma^2 m_1^r, \qquad U_2^r = \frac{1}{2}\sigma^2 m_2^r,$$

$$U_0^\varphi = \frac{1}{R}\sqrt{\frac{M}{R}}\frac{1}{\sqrt{1-\frac{3M}{R}}} + \frac{\sigma\eta\kappa\bar\omega\Delta_n}{\omega(\alpha\beta-\gamma\eta)} + \frac{\sigma^2\bar\omega w^\varphi}{2\omega}, \;\; U_1^\varphi = -\frac{\sigma\eta n_c^r}{\omega} + \frac{1}{2}\sigma^2 m_1^\varphi, \;\; U_2^\varphi = \frac{1}{2}\sigma^2 m_2^\varphi. \tag{2.84}$$

To summarize, these expressions by construction solve the geodesic equations to second order in σ, the geodesic deviation equations to second order in σ, and have their four-velocities properly normalized to second order in σ. There are now four constants that can freely be assigned values: the circular radius R, the normalization constant σ, and the first and second-order secular constants Δ_n and Δ_m. By using straightforward algebra, the U_i^μ

and the epicycle frequency $\bar{\omega}$ can be expressed solely in terms of these four parameters and the mass M of the black hole. The result is stated in Appendix A.

Finally, to end this section, the energy per unit mass ε and angular momentum per unit mass ℓ can be found by using the expressions Eq. (2.3) after substitution of Eq. (2.83) and evaluating the outcome to second order in σ. The results are:

$$\ell = \ell_0 + \sigma\ell_n + \frac{1}{2}\sigma^2\ell_m\,, \qquad \varepsilon = \varepsilon_0 + \sigma\varepsilon_n + \frac{1}{2}\sigma^2\varepsilon_m\,, \tag{2.85}$$

in which ε_0 and ℓ_0 are given by their previous expressions Eq. (2.9), ε_n and ℓ_n by Eq. (2.55), and ℓ_m and ε_m are given by

$$\begin{aligned}
\ell_m &= \left(\frac{3}{2}\frac{\sqrt{M}}{R^{3/2}}\frac{1+\frac{M}{R}}{\left(1-\frac{3M}{R}\right)^{3/2}} - \frac{3\omega}{\sqrt{1-\frac{6M}{R}}}\right)(n_c^r)^2 \\
&\quad + \left(\frac{1}{2}\sqrt{\frac{M}{R}}\frac{1-\frac{6M}{R}}{\left(1-\frac{3M}{R}\right)^{3/2}}\right)\Delta_m - \left(\frac{1}{4}\frac{\sqrt{M}}{R^{3/2}}\frac{1-\frac{12M}{R}}{\left(1-\frac{3M}{R}\right)^{5/2}}\right)\Delta_n^2\,, \\
\varepsilon_m &= -\left(\frac{M}{2R^3}\frac{1-\frac{9M}{R}+\frac{6M^2}{R^2}}{\left(1-\frac{3M}{R}\right)^{3/2}\left(1-\frac{2M}{R}\right)}\right)(n_c^r)^2 \\
&\quad + \left(\frac{M}{2R^2}\frac{1-\frac{6M}{R}}{\left(1-\frac{3M}{R}\right)^{3/2}}\right)\Delta_m - \left(\frac{M}{4R^3}\frac{4-\frac{39M}{R}+\frac{54M^2}{R^2}}{\left(1-\frac{3M}{R}\right)^{5/2}}\right)\Delta_n^2\,.
\end{aligned} \tag{2.86}$$

As in the first-order case, these expressions evaluate to *constants* to this order in σ, as is required by Killing's theorem for geodesic motion. Again, this is evidence that the expressions Eq. (2.83) are indeed solutions to the geodesic equations to second order in σ and that there is no principal error in the method.

2.5.5 The constants of integration

Having obtained the expressions for bound geodesic motion around a Schwarzschild black hole to zeroth, first and second order, it can be seen that every next order has a constant of integration more than the previous one. This is a general pattern: with every extra order σ^i introduced in the epicycle expansion, one new secular constant Δ_i makes its appearance. This is easily understood: with every order, the same system of coupled homogeneous differential equations Eq. (2.33) needs to be solved, and as the system is linear, the most general solution for this extra order contribution will contain six constants of integration. By the choice to have the resulting orbit start at $t = 0$, $\varphi = 0$ and at a periastron, $u^r = 0$, three of the constants of integration are immediately accounted for. Of the three remaining ones, one is used to set a constant in the secular solution for the radial coordinate to zero to prevent an unbounded linear in- or decrease of the radial coordinate, whereas a second is used to make sure that the total four-velocity of the resulting orbit is properly normalized.

Eventually, thus, only one constant of integration remains, manifesting itself in the form of a secular constant Δ_i. Together with the zeroth order epicycle parameters R and σ, the epicycle expansion up to i-th order in σ will contain $i+2$ constants of integration, i of which in the form of secular constants.
It thus follows that there can be arbitrarily many constants of integration, depending on the order to which the epicycle expansion is taken. This appears to be in contrast with the fact that, up to orientation, a geodesic orbit in the Schwarzschild spacetime can always be parametrized by only two constants, for which can be taken, *e.g.*, the two Killing constants of motion energy per unit mass ε and angular momentum per unit mass ℓ. However, there is no contradiction: it merely indicates that the constants of integration are related, and that all but two are superfluous in the sense that they are not strictly necessary to describe a given orbit. Indeed, regardless of the number of constants of integration, the epicycle expansion up to any order produces, ultimately, only two constants of motion (ε, ℓ). For example: even though the first-order epicycle expansion has three constants of integration, any choice of their values leads, via Eq. (2.55), to only two fixed values for ε and ℓ. Likewise, the second-order epicycle expansion has four constants of integration but any choice of their values leads, via Eq. (2.86), to only two fixed values for ε and ℓ.
However superfluous, the extra constants can be used as an advantage, as the use of the secular constants makes the approximation already accurate at low orders. Indeed, an example of this was already discussed in section 2.4.3, in which it was demonstrated that the inclusion of the secular constant Δ_n allows the epicycle expansion to have the right periastra properties already at first order, whereas this is not possible if Δ_n is omitted.
Also, from the fact that *all* constants of integration have been taken into account, it follows that the solutions presented are the *most general* solutions of the geodesic deviation equations to describe bound orbits in a Schwarzschild spacetime, up to the order calculated. By dismissing the secular constants Δ_i, the results stated in the literature only form a small subset of the most general solutions given here. It is therefore possible to choose the constants (Δ_n, Δ_m) such that the general solutions reduce to the ones stated in the literature. This is explicitly demonstrated in Appendix B.

2.6 Summary

In this chapter, the method of geodesic deviations has been introduced as a way to approximate geodesic motion in any spacetime. As such the method is a useful tool in many practical situations, and is particularly suited to describe geodesic orbits in an EMRI system. The method assumes that geodesic motion can be approximated by calculating the perturbations to a simple geodesic solution, for which differential equations have been derived to second order.
The method has been applied to the description of bound geodesic motion of a test mass around a Schwarzschild black hole, yielding an expansion series which resembles the ancient Ptolemy system and is consequently referred to as the epicycle expansion. It was found that the most general solution consists of oscillatory terms and secular contributions, the

latter of which are necessary to describe eccentric orbits accurately as their omission will result in a cumulative angular lag or overshoot of the resulting orbit as compared to the exact one. The secular contributions of the first-order solution were also shown to lead to Poincaré resonances in the higher orders. These were removed by means of the Poincaré-Lindtsted method, by taking into account that the frequency of the oscillatory part of the solution is itself an expansion series. In this way fully analytical expressions for the epicycle expansion up to second order have been presented, as well as expressions for the energy per unit mass and angular momentum per unit mass carried by the system.
In the next chapter, the epicycle expansion will be put to the test by quantitatively comparing the resulting orbits to the ones that are found when the geodesic equations are solved by purely numerical means.

Chapter 3

Results: bound geodesic motion

3.1 Introduction

In the previous chapter a covariant perturbation theory for orbits of test masses in curved spacetime has been constructed, based on the method of geodesic deviations. It has been applied in particular to motion in a Schwarzschild background geometry, and explicit expressions for bound orbits to second order have been obtained. Using these expressions for the orbits, it can now be investigated how well the resulting epicycle orbits compare with the ones that are obtained when the geodesic equations Eq. (2.5) are solved purely numerically. As advocated, the main advantage of the geodesic deviation method is the fact that the curvature of the spacetime is taken into full account, and hence it is expected that the epicycle approximated orbits will remain accurate even when considered very close to the black hole. In order to test this, this chapter will consider a series of explicit examples of various eccentricities and of decreasing semi-major axes, all the way to the innermost stable circular orbit (ISCO). The comparison to the purely numerically calculated orbits will be done for the epicycle expressions up to first order, and up to second order.
The chapter is organized as follows. Section 3.2 discusses how the epicycle expansion can be used most effectively by choosing the appropriate boundary conditions, and presents algebraic equations that ensure that the resulting orbits will have the correct physical characteristics at periastron. In section 3.3, a large number of examples will be worked out in detail and the resulting bound orbits will be compared to their purely numerical counterparts, showing explicitly the excellent approximation the epicycle expansion provides for orbits of limited eccentricity. The accuracy of the method is expected to decrease with increasing eccentricity, and this is investigated in section 3.4. Section 3.5 reflects on the results, and discusses a way to increase the accuracy even more still. Finally, section 3.6 lists the results of this chapter as a summary.

3.2 Boundary conditions

3.2.1 Using the constants of integration

In chapter 2 it was shown that, when describing bound geodesic motion around a Schwarzschild black hole, the most general solution to the geodesic deviation equations consists of periodic contributions and secular contributions, and that there is a total of $i+2$ constants of integration that can freely be assigned values. These constants of integration allow for as many boundary conditions to constrain the resulting orbit, and the question then presents itself how these should be chosen so as to yield the epicycle expansion that best approximates a given bound geodesic orbit. There are at least two ways to make use of the integration constants. One way is to first fix their values and to subsequently calculate the energy per unit mass and angular momentum per unit mass of the resulting orbit to see with which geodesic orbit it best agrees. In this program, any addition of an extra order to the expansion leads to a slightly different value of the two constants of motion, and hence will make the expansion approximate a different geodesic. Alternatively, it can be chosen to have the epicycle expansion describe a *fixed* geodesic, and to seek constants of integration that will make the epicycle expansion best approximate this orbit. In this program, any addition of an extra order to the expansion will make the accuracy better.
It is in this second way that the epicycle expansion will be employed in this thesis. In practice, this amounts to fixing the values for the $i+2$ constants of integration by appropriate boundary conditions, which are taken to be the physical characteristics of the geodesic orbit that is to be approximated. This will now be discussed.

3.2.2 Conditions on the first-order expansion

In the case of the first-order orbits, Eq. (2.50), there are three constants that need to be assigned values: (σ, R, Δ_n), which means that these functions can be subjected to three boundary conditions. The following will be used: the orbit must have a periastron shift $\delta\varphi$, have two successive periastra a proper time $\Delta\tau$ apart, and yield a radial periastron distance r_{pa}. The first two of these make sure that the approximated orbit will have an angular evolution that stays synchronized with the actual orbit in that their periastra agree in angular distance and in proper time; the latter of these makes sure that the periastra take place at the correct radial distance from the black hole. This choice of boundary conditions also ensures that there will be no cumulative discrepancy between the epicycle-approximated orbits and the exact ones.
From the radial expansion in Eq. (2.50) it can be seen that the periastra take place at times $\tau = 2\pi n/\omega$, n an even integer number; from the angular expansion in Eq. (2.50), the angular distance between successive periastra follows immediately. The three boundary

conditions then mathematically translate to the algebraic conditions

$$\begin{aligned}
\delta\varphi &= 2\pi\left(\frac{1}{\omega}\sqrt{\frac{M}{R^3}}\frac{1}{\sqrt{1-\frac{3M}{R}}}+\frac{1}{\omega}\frac{\eta\kappa}{\alpha\beta-\gamma\eta}\sigma\Delta_n-1\right),\\
\Delta\tau &= \frac{2\pi}{\omega},\\
r_{pa} &= R+\sigma\left(n_c^r+\Delta_n\right).
\end{aligned} \tag{3.1}$$

Thus, by supplying a desired periastra shift $\delta\varphi$, proper time lapse $\Delta\tau$ between successive periastra, and radial distance r_{pa}, these algebraic conditions can be solved for a set of epicycle parameters $(R,\ \sigma,\ \Delta_n)$ that yields an epicycle orbit with exactly the desired periastra characteristics.

Some observations can now be made. Firstly, to emphasize a previously made point again, it should be noted that Eq. (3.1) shows that it is impossible to independently fix the values $\delta\varphi$ and $\Delta\tau$ if the secular parameter Δ_n was chosen as zero, justifying once more that the secular contributions are necessary to accurately describe eccentric bound geodesics.
Secondly, it should be noted that no prior knowledge of the exact orbit is required other than the values of the energy per unit mass and angular momentum per unit mass, as these alone suffice to fix the values of the right hand sides of the conditions in Eq. (3.1). Indeed, the fact that all such physical characteristics can, by the methods of sections 2.2.2 and 2.2.3, be calculated from only two parameters (ε, ℓ) or (a, e), emphasizes explicitly the statement that the secular constants are related. Thus, it follows once again that there is no contradiction in having an arbitrary number of secular constants to describe a geodesic orbit in the Schwarzschild spacetime.
Finally, there is generally more than one set of parameters (R, σ, Δ_n) that solves the system Eq. (3.1). This can be made explicit by combining the second of the conditions with the explicit expression for the epicycle frequency, Eq. (2.40), as it yields a quartic equation in the radius R and so allows for up to four different values for the radius; the remaining two conditions subsequently fix the values for σ and Δ_n uniquely.

The question then presents itself which of the solution sets most accurately describes the exact bound orbit. The answer is provided by two observations. The first is, that the most accurate expansion is likely the one that converges the most quickly, *i.e.* is the expansion that has the smallest ratio of terms that are first order in σ and terms that are zeroth-order in σ. There is some ambiguity in this observation, as there is an expansion for the radial coordinate, one for the angular coordinate, and one for the temporal coordinate, and there is no guarantee that the fastest convergence in one also implies the fastest convergence in the others. Here, the choice will be made to let a fast convergence of the radial coordinate take priority; this is motivated by the observation that the Peters-Mathews equation Eq. (1.46) predicts a strong dependence of the emitted power on the radial accuracy of the orbit. Of course, the Peters-Mathew equation holds only for a Minkowski spacetime, but

a similar strong dependence is expected in the current case of a Schwarzschild spacetime by a simple dimensional analysis (and, indeed, this will be found to be the case in section 5.2.2).
The second observation that leads to a criterion for the most accurate approximation, is the fact that the secular contributions and oscillatory contributions to the radial expansion represent different physical characteristics of the resulting orbit. Indeed, as was already remarked in section 2.4.3, the secular contribution $\sigma\Delta_n$ serves as a correction to the zeroth-order radius R, whereas the oscillatory contribution corresponds to the epicycle that is placed on top of the resulting circular orbit. It is then natural to assume that the most accurate radial expansion is the one that starts out with the most accurate circle on which the epicycles are placed, *i.e.* the expansion that has a zeroth-order circular orbit R that needs the smallest correction $\sigma\Delta_n$.
Thus, collecting results, the solution set (R, σ, Δ_n) that is expected to yield the most accurate radial epicycle expansion is the set that for which the following inequality holds best:

$$\left|\frac{\sigma\Delta_n}{R}\right| \ll 1. \tag{3.2}$$

In choosing between the different solution sets (R, σ, Δ_n), it is this criterion that will be used in the worked examples of section 3.3.

3.2.3 Conditions on the second-order expansion

Moving on to the second order, the orbital functions Eq. (2.83) can be subjected to the same three boundary conditions as before, but this time an extra constant Δ_m appears that needs to be assigned a value. This means that a fourth boundary condition can be imposed, which will be chosen to fix the radial apastron distance r_{aa}. The four boundary conditions are formulated as algebraic conditions by observing that the periastra and apastra correspond to the extreme values of $r(\tau)$ in Eq. (2.83) and that these occur at times $\bar{\omega}\tau_n = n\pi$, n an integer number. From $\varphi(\tau)$ then follows the periastron shift, while $r(\tau)$ yields the radial distances of the periastra and apastra. The four boundary conditions thus translate to the following algebraic conditions:

$$\begin{aligned} \Delta\tau = \frac{2\pi}{\omega + \sigma\omega_1} \quad , \qquad & \delta\varphi = 2\pi\left(\frac{U_0^\varphi}{\omega + \sigma\omega_1} - 1\right), \\ r_{pa} = U_0^r + U_1^r + U_2^r \quad , \qquad & r_{aa} = U_0^r - U_1^r + U_2^r. \end{aligned} \tag{3.3}$$

Solving these conditions yields values for the parameters $(R,\ \sigma,\ \Delta_n, \Delta_m)$ that ensure that the resulting epicycle expansion has the desired periastra characteristics and the desired radial apastron distance.
However, as in the first-order case, there is generally more than one set of values that solves the boundary conditions Eq. (3.3). The question then presents itself which of these orbits most accurately describes the exact geodesic, and again the answer is provided by the observation that the most accurate expansion is likely the one that converges the most

quickly, *i.e.* is the expansion that has the smallest ratio of terms that are of successive order in σ. As in the first-order case, a fast radial convergence is prioritized, and again this is done in the way that physically corresponds to choosing the epicycle expansion that has the most accurate circular orbit on which the epicycles are placed.
Thus, from Eq. (2.84) it follows that the solution set $(R, \sigma, \Delta_n, \Delta_m)$ that is expected to yield the most accurate radial expansion is the one that has the fastest convergence of the coefficient U_0^r, which is the one for which the following two inequalities hold best:

$$\left|\frac{\sigma\Delta_n}{R}\right| \ll 1\,, \qquad \left|\frac{\frac{1}{2}\sigma^2\Delta_m}{\sigma\Delta_n}\right| \ll 1\,. \tag{3.4}$$

Obviously, in contrast to the first-order criterion Eq. (3.2), there are now *two* ratios that are to be considered, because there are now two correction terms to the zeroth-order contribution R to radius of the perfectly circular orbit. A second difference with the first-order criterion is that, now, also the coefficient U_1^r of the *periodic* contribution to the radial expansion contains a correction term. It therefore appears as if a criterion for the most accurate radial expansion could also be formulated by demanding that the coefficient U_1^r converges fastest, which is the case when the ratio $\left|\frac{1}{2}\sigma^2 m_1^r/\sigma n_c^r\right|$ is small. This, however, is not true due to the way the boundary conditions Eq. (3.3) were chosen; by subtracting the expressions for r_{pa} and r_{aa}, it follows immediately that the coefficient U_1^r is completely fixed and hence has the same value for *any* of the solution sets to Eq. (3.3). A fast convergence for the coefficient U_1^r can therefore not be used a discriminatory factor between the different solution sets.
In choosing between the different solution sets $(R, \sigma, \Delta_n, \Delta_m)$, it will be the criterion Eq. (3.4) that will be used in the worked examples of the next section. Indeed, in all cases considered in this thesis, this criterion trustfully leads to the second-order epicycle expansion with the highest radial accuracy.

3.3 Explicit examples

3.3.1 A worked example: $e = 0.1$, $a = 10M$

The epicycle expansion will now be worked out in full detail for one specific bound orbit. For this explicit example, an orbit will be considered that is parametrized by, in the parameters presented in section 2.2.3, an eccentricity e of 0.1 and value of a of $10M$. The mass M of the black hole is given in some unspecified units, so that in the same units the periastron distance r_{pa}, apastron distance r_{aa}, periastron shift $\delta\varphi$, and proper time lapse $\Delta\tau$ between successive periastra are given by

$$r_{pa} = 9.09091M, \qquad r_{aa} = 11.1111M, \qquad \delta\varphi = 3.6561, \qquad \Delta\tau = 266.105M, \tag{3.5}$$

having used the integrals stated in section 2.2.3. This orbit corresponds to an energy per unit mass and angular momentum per unit mass given by

$$\varepsilon = 0.956568, \qquad \ell = 3.78235M. \tag{3.6}$$

It should be noted that the fact that this orbit has a periastron shift greater than the Newtonian angular distance between periastra of 2π, is evidence of the very strong relativistic effect this close to the central mass. This orbit will now be constructed up to first and up to second order in epicycle perturbation theory.
In the case of the first-order orbits, Eq. (2.50), there are three constants that need to be assigned values: (R, σ, Δ_n). This means that these functions can be subjected to three boundary conditions to fix the orbit and for these the ones discussed in section 3.2.2 will be used: the orbit must have a periastron shift $\delta\varphi$, have two successive periastra a proper time $\Delta\tau$ apart, and yield a radial periastron distance r_{pa}. These three conditions mathematically translate to the algebraic conditions of Eq. (3.1), and by the criteria discussed in section 3.2.2, the following solution set (R, σ, Δ_n) and the associated value of n_c^r is selected:

$$\sigma = -1.15699M, \qquad R = 10.1274M, \qquad \Delta_n = 0.05047, \qquad n_c^r = 0.845359. \tag{3.7}$$

This gives the following expressions for the orbital functions $t(\tau), r(\tau), \varphi(\tau)$:

$$\begin{aligned} t(\tau) &= 1.19347\,\tau + 1.1998M\,\sin(\omega\tau), \\ r(\tau) &= 10.0690M - 0.978072M\,\cos(\omega\tau), \\ \varphi(\tau) &= 0.0373\,\frac{\tau}{M} + 0.3025\,\sin(\omega\tau), \end{aligned} \tag{3.8}$$

in which the epicycle frequency is given by

$$\omega = 0.0236\frac{1}{M}. \tag{3.9}$$

Using the expressions for the ε_n and ℓ_n from Eq. (2.55), the energy per unit mass and the angular momentum per unit mass of this epicycle orbit are

$$\varepsilon = 0.95642, \qquad \ell = 3.78710M, \tag{3.10}$$

which are at most a few tenths of a percent different from the exact values in Eq. (3.6).
Moving on to the second-order epicycle expansion, there are now four constants of integration $(R, \sigma, \Delta_n, \Delta_m)$ that need to be assigned values by imposing boundary conditions, and for these the ones discussed in section 3.2.3 will be used: the orbit must have a periastron shift $\delta\varphi$, have two successive periastra a proper time $\Delta\tau$ apart, yield a radial periastron distance r_{pa}, and an apastron distance r_{aa}. These conditions translate mathematically to the algebraic conditions of Eq. (3.3), and by using the criteria discussed in section 3.2.3, the following solution set $(R, \sigma, \Delta_n, \Delta_m)$ and associated value n_c^r is chosen as

$$\sigma = -0.97114M, \quad R = 10.0046M, \quad \Delta_n = -0.12613, \quad \Delta_m = 0.0228\frac{1}{M}, \quad n_c^r = 1.0206, \tag{3.11}$$

which give rise to the expressions for the orbital functions

$$\begin{aligned} t(\tau) &= 1.19346\,\tau + 1.23903M\,\sin((\omega+\sigma\omega_1)\tau) + 0.061333M\,\sin(2(\omega+\sigma\omega_1)\tau), \\ r(\tau) &= 10.1378M - 1.0101M\,\cos((\omega+\sigma\omega_1)\tau) - 0.036836M\,\cos(2(\omega+\sigma\omega_1)\tau), \\ \varphi(\tau) &= 0.0037351\,\frac{\tau}{M} + 0.312458\,\sin((\omega+\sigma\omega_1)\tau) + 0.0174545\,\sin(2(\omega+\sigma\omega_1)\tau), \end{aligned} \tag{3.12}$$

in which the frequencies are given by

$$\omega = 0.02389\frac{1}{M}, \qquad \sigma\omega_1 = -0.00028\frac{1}{M}, \qquad \omega + \sigma\omega_1 = 0.0236\frac{1}{M}. \tag{3.13}$$

From Eq. (2.86), the energy per unit mass and angular momentum per unit mass for this approximation to the orbit then follow as

$$\varepsilon = 0.95667, \qquad \ell = 3.78263M, \tag{3.14}$$

which are at most a few thousandths of a percent different from the exact values in Eq. (3.6).

Having found the epicycle expressions to first and second order, they can be compared to orbital functions $r(\tau)$ and $\varphi(\tau)$ as calculated by solving the geodesic equations Eq. (2.5) by purely numerical means. The results are presented in Figure 3.1. In the left panel, the radial function $r(\tau)$ up to first and second order is given divided by its purely numerical counterpart, as a function of proper time. As can be seen, the relative difference between the first-order approximation and its numerical counterpart is at most about 1.1%; introducing the second-order epicycle improves the relative difference to less than 0.05%. The right panel shows the absolute difference between the angular coordinate φ in the epicycle approximation (both to first and second-order) and in the numerical one. As can be seen, the first-order epicycle deviates from the purely numerical one by at most 0.029 radians during any period, whereas the second order deviates from the numerical one by at most 0.004 radians. Thus, it has now been seen that, for the orbit with eccentricity 0.1 and semi-major axis $10M$, both the first- and second-order epicycle expansions are excellent approximations of the numerical orbital functions $r(\tau)$ and $\varphi(\tau)$.

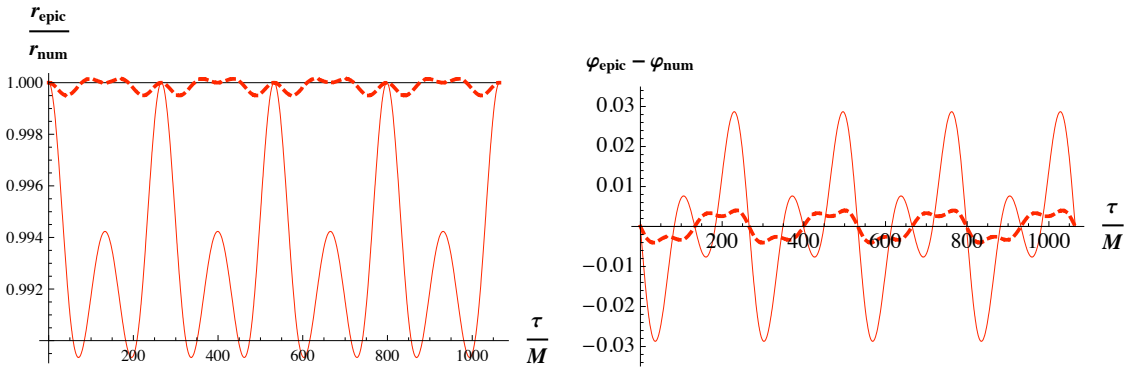

Figure 3.1: Left: The radial coordinate $r(\tau)$ in epicycle approximation up to first (solid curve) and second (dashed curve) order, divided by the numerical one, as a function of proper time τ. Right: The angular coordinate $\varphi(\tau)$ in radians in epicycle approximation up to first (solid curve) and second (dashed curve) order, minus the numerical one, as a function of the proper time τ.

3.3.2 Further examples: $e = 0.1$, various values for a

In the manner of the explicit example above, the accuracy of a whole series of orbits can be investigated, all of eccentricity $e = 0.1$ but decreasing value of a, so as to test the

claim that the epicycle approximations suffer very little from close proximity to the black hole. The physical characteristics of the orbits considered and the values of the epicycle parameters are listed in tables C.1, C.2 in appendix C, and the comparison with the purely numerically calculated orbits is presented in table 3.1 below. It lists the maximum relative difference between the epicycle-approximated orbital function $r(\tau)$ and its numerical counterpart, and the maximum absolute difference between the epicycle-approximated orbital function $\varphi(\tau)$ and its numerical counterpart. For the first-order epicycle approximation, it can be seen that the relative difference for the radial orbital function is typically of the order of 2% or less, and the absolute difference for the angular orbital function is of the order of a hundredth of a radian. For the second-order epicycle approximation, it can be seen that the relative difference of the radial orbital function is typically of the order of a hundredth of a percent, and the absolute difference of the angular function is of the order of a hundredth of a radian and usually much less still.
These results fully support the claim that the geodesic deviation method effortlessly approximates bound geodesic orbits, even those in close proximity to the black hole. Indeed, even the most extreme case considered of $a = 6.6M$ (which corresponds to an orbit that exactly grazes the ISCO at $r_{pa} = 6M$, and has a periastron shift of 15.019, *i.e.* the shift alone is more than two times the angular distance of 2π between successive periastra as predicted by Newtonian gravity) is still excellently approximated by the epicycle expansions, with the relative difference between the second-order radial function and its numerical counterpart being less than a quarter percent, and the absolute difference between the second-order angular function and its numerical counterpart less than 0.02 radians.
The table also demonstrates explicitly that the radial accuracies are virtually independent of distance to the black hole: over the course of the decreasing semi-major axis, the maximum relative radial difference increases only very slightly, and it is only at the orbits closest to the ISCO that the increase of relative radial difference becomes more significant. These observations fully agree with the discussion of section 2.4.2, where it was already predicted that the dependence of the accuracy on the distance would be very small and would only become more significant for the orbits closest to the ISCO.
As concerns the angular accuracy, the table demonstrates that the maximum absolute difference between the first-order epicycle approximation of the angular coordinate and its numerical counterpart is virtually independent from the distance to the black hole (save again from the orbits closest to the ISCO). In contrast, the accuracy of the second-order angular approximation does depend strongly on the distance to the black hole, as the maximum absolute difference increases by an order of magnitude.
These observations are not surprising, due to the way the boundary conditions were chosen. At first order, the boundary conditions were chosen to ensure the resulting orbit has the desired temporal, radial, and angular properties at periastron, giving rise to fixed accuracies for the radial and angular coordinates. At second order an extra boundary condition was chosen to further constrain one of the coordinates *in between* periastra as well. Here, the remaining boundary condition was used to fix the radial position of the apastron, greatly increasing the accuracy of the *radial* coordinate in between periastra, but offering no guarantee that the *angular* coordinate benefits from this choice as well.

$e = 0.1$	first-order epicycles		second-order epicycles	
a/M	max. rel. diff. r	max. abs. diff. φ	max. rel. diff. r	max. abs. diff. φ
20	1.05 %	0.018 rad	0.06 %	0.0015 rad
15	1.03 %	0.020 rad	0.06 %	0.0018 rad
10	1.08 %	0.029 rad	0.05 %	0.0040 rad
9.0	1.09 %	0.024 rad	0.05 %	0.0070 rad
8.5	1.04 %	0.042 rad	0.04 %	0.012 rad
8.0	1.21 %	0.058 rad	0.04 %	0.026 rad
7.5	1.47 %	0.028 rad	0.08 %	0.053 rad
7.0	1.52 %	0.040 rad	0.12 %	0.012 rad
6.6	2.20 %	0.022 rad	0.24 %	0.020 rad

Table 3.1: Accuracy of epicycle approximation for bound orbits of eccentricity $e = 0.1$ around a black hole of mass M and various values of a, as listed in the first column. The second column presents the maximum relative differences between the first-order epicycle radial orbital function $r(\tau)$ and its numerical counterpart; the third column presents the maximum absolute difference between the first-order epicycle angular orbital function $\varphi(\tau)$ and its numerical counterpart. The fourth and fifth columns present the same information for the second-order epicycle orbital functions. The smallest value of the semi-major axis a is chosen such, that the periastron of the resulting orbit exactly grazes the ISCO.

3.3.3 Further examples: various values for e and a

In the previous examples, the epicycle expansion was used to approximate an orbit of one fixed small eccentricity, and presented accurate results. As expected, the method suffers little from close proximity to the black hole: agreement with numerical outcomes were seen to be excellent for all values of a. In the following examples, the method will be used to approximate some more orbits for decreasing values of a, and this time for some different fixed values of the eccentricity: $e = 0.075$, $e = 0.15$ and $e = 0.2$. In this way, it can be investigated whether the conclusions of the $e = 0.1$ case presented in the previous section also hold for different eccentricities.
Appendix C lists the physical characteristics and the values of the epicycle parameters of these orbits in table C.3 and table C.4 for $e = 0.075$, in table C.5 and table C.6 for $e = 0.15$, and in table C.7 and table C.8 for $e = 0.2$. The results for the accuracy are presented in table 3.2 for $e = 0.075$, in table 3.3 for $e = 0.15$, and in table 3.4 for $e = 0.2$. These latter tables list the maximum relative difference between the epicycle approximation for the orbital function $r(\tau)$ and its numerical counterpart, and the maximum absolute difference between the epicycle approximated orbital function $\varphi(\tau)$ and its numerical counterpart.
In all cases, the same observations hold as in the examples of orbits of eccentricity $e = 0.1$: the accuracy of the radial first-order and second-order approximations, as well as the accuracy of the first-order angular approximation, have only a very small dependence on the distance to the black hole, whereas the angular second-order approximation becomes an order of magnitude less accurate as the semi-major axis decreases. The explanation for

these observations is the same as in the $e = 0.1$ case, and was already given in section 3.3.2.

$e = 0.075$	first-order epicycles		second-order epicycles	
a/M	max. rel. diff. r	max. abs. diff. φ	max. rel. diff. r	max. abs. diff. φ
20	0.589 %	0.00975 rad	0.0241 %	0.00061 rad
15	0.596 %	0.01106 rad	0.0228 %	0.00076 rad
10	0.606 %	0.01565 rad	0.0190 %	0.00168 rad
9.0	0.611 %	0.01882 rad	0.0170 %	0.00293 rad
8.5	0.617 %	0.02203 rad	0.0157 %	0.00487 rad
8.0	0.661 %	0.03029 rad	0.0138 %	0.00253 rad
7.5	0.802 %	0.01412 rad	0.0253 %	0.02559 rad
7.0	0.859 %	0.02370 rad	0.0385 %	0.00927 rad
6.45	1.573 %	0.06022 rad	0.1291 %	0.01090 rad

Table 3.2: Accuracy of epicycle approximation for bound orbits of eccentricity $e = 0.075$ around a black hole of mass M and various values of a, as listed in the first column. The second column presents the maximum relative differences between the first-order epicycle radial orbital function $r(\tau)$ and its numerical counterpart; the third column presents the maximum absolute difference between the first-order epicycle angular orbital function $\varphi(\tau)$ and its numerical counterpart. The fourth and fifth columns present the same information for the second-order epicycle orbital functions. The smallest value of the semi-major axis a is chosen such, that the periastron of the resulting orbit exactly grazes the ISCO.

$e = 0.15$	first-order epicycles		second-order epicycles	
a/M	max. rel. diff. r	max. abs. diff. φ	max. rel. diff. r	max. abs. diff. φ
20	2.373 %	0.04074 rad	0.2174 %	0.00431 rad
15	2.395 %	0.04650 rad	0.2111 %	0.00622 rad
12	2.414 %	0.05477 rad	0.2043 %	0.00847 rad
10	2.432 %	0.06827 rad	0.1974 %	0.01381 rad
9.0	2.467 %	0.08467 rad	0.1928 %	0.02348 rad
8.5	2.538 %	0.10191 rad	0.1888 %	0.03705 rad
8.0	2.860 %	0.14154 rad	0.1723 %	0.07486 rad
7.5	3.432 %	0.07101 rad	0.4520 %	0.14277 rad
6.9	3.650 %	0.09195 rad	0.7188 %	0.07175 rad

Table 3.3: Accuracy of epicycle approximation for bound orbits of eccentricity $e = 0.15$ around a black hole of mass M and various values of a, as listed in the first column. The second column presents the maximum relative differences between the first-order epicycle radial orbital function $r(\tau)$ and its numerical counterpart; the third column presents the maximum absolute difference between the first-order epicycle angular orbital function $\varphi(\tau)$ and its numerical counterpart. The fourth and fifth columns present the same information for the second-order epicycle orbital functions. The smallest value of the semi-major axis a is chosen such, that the periastron of the resulting orbit exactly grazes the ISCO.

$e = 0.2$	first-order epicycles		second-order epicycles	
a/M	max. rel. diff. r	max. abs. diff. φ	max. rel. diff. r	max. abs. diff. φ
20	4.27 %	0.075 rad	0.550 %	0.012 rad
15	4.30 %	0.085 rad	0.541 %	0.015 rad
12	4.33 %	0.101 rad	0.534 %	0.020 rad
10	4.38 %	0.127 rad	0.530 %	0.033 rad
9.0	4.47 %	0.159 rad	0.528 %	0.055 rad
8.5	4.64 %	0.192 rad	0.518 %	0.083 rad
8.0	5.31 %	0.262 rad	0.467 %	0.149 rad
7.5	6.22 %	0.137 rad	0.226 %	0.317 rad
7.2	5.80 %	0.090 rad	1.88 %	0.217 rad

Table 3.4: Accuracy of epicycle approximation for bound orbits of eccentricity $e = 0.2$ around a black hole of mass M and various values of a, as listed in the first column. The second column presents the maximum relative differences between the first-order epicycle radial orbital function $r(\tau)$ and its numerical counterpart; the third column presents the maximum absolute difference between the first-order epicycle angular orbital function $\varphi(\tau)$ and its numerical counterpart. The fourth and fifth columns present the same information for the second-order epicycle orbital functions. The smallest value of the semi-major axis a is chosen such, that the periastron of the resulting orbit exactly grazes the ISCO.

3.4 The relationship between accuracy and eccentricity

The results of the examples in the previous sections show that the accuracy of the epicycle approximation decreases with increasing eccentricity, supporting the observation made in 2.4.2 that the expansion parameter of the approximation is a measure of the eccentricity of the orbits considered. The pattern can be studied in more detail by taking the second-order epicycle approximation of the radial function of a series of bound orbits with fixed semi-major axis a and increasing values of the eccentricity e, and comparing each with its purely numerically calculated counterpart. It is then found that, for all values of the semi-major axis considered, the maximum relative difference of the radial function closely follows a power law of the eccentricity e, *i.e.*

$$(\text{max. rel. diff. } r) \propto e^b, \tag{3.15}$$

where the exponent b has a value of about 3.4. A typical example of this is presented in Figure 3.3 for a semi-major axis of $a = 10M$. The value of the exponent means that a doubling of the eccentricity leads to a decrease in accuracy of the radial approximation by a factor of $2^{3.4} \approx 10.6$, which amounts to about an order of magnitude. It is not surprising that the accuracy of the second-order epicycle expansion follows the same curve for all semi-major axes considered, as it had already been seen that the accuracy of the approximation is virtually independent of the distance to the black hole. The exponent value b of around 3.4 is therefore an *intrinsic* characteristic of the second-order epicycle expansion,

rather than of the particular examples considered.
A similar analysis can be done for the absolute difference between the second order epicycle approximation angular function and its purely numerically calculated counterpart, and it is found that the absolute difference roughly follows a power law of the eccentricity, as can be seen in Figure 3.3. The exponent is about 2.5 to 3, meaning that, roughly, the accuracy of the second order epicycle approximation decreases by a factor of about 5.7 to 8 when the eccentricity is doubled.

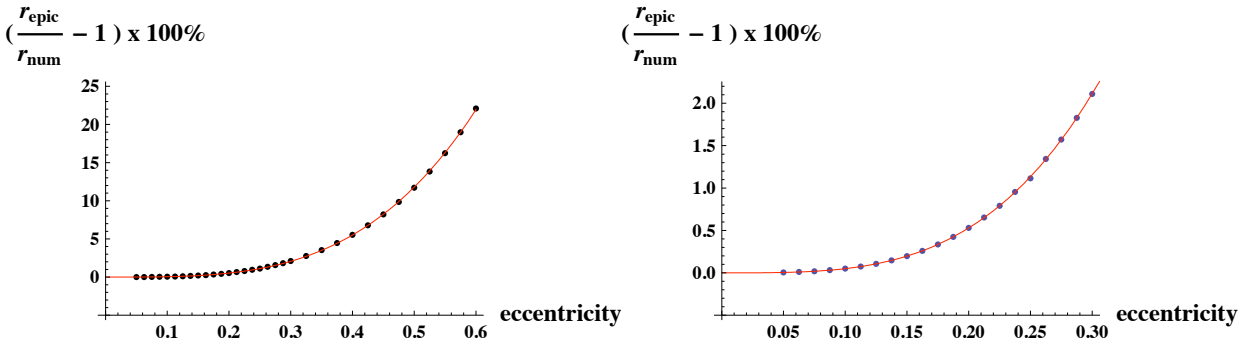

Figure 3.2: The maximum relative difference between the radial function in percents as calculated by the second-order epicycle approximation and its purely numerical counterpart, as a function of the eccentricity e for orbits with semi-major axis $a = 10M$. The left plot shows the eccentricity up to a value of 0.6; the right plot zooms in by showing eccentricities up to a value of 0.3. The semi-major axis is taken to be $a = 10M$ and the relative differences are given in percents. The data points are values obtained by the comparison as explained in the main text; the curve is the best fit through these points, given by $12.553M \cdot e^{3.413}$.

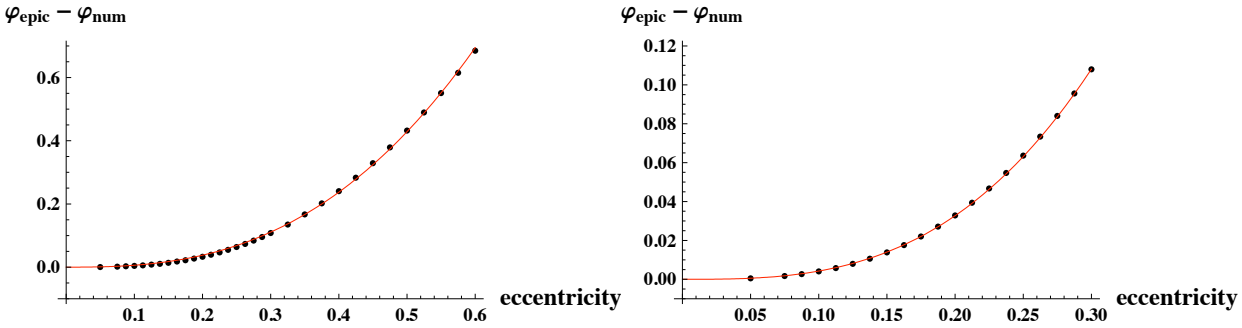

Figure 3.3: The maximum absolute difference between the angular function in radians as calculated by the second-order epicycle approximation and its purely numerical counterpart, as a function of the eccentricity e for orbits of semi-major axis $a = 10M$. The left plot shows the eccentricity up to a value of 0.6; the right plot zooms in by showing eccentricities up to a value of 0.3. The semi-major axis is taken to be $a = 10M$ and the absolute differences are given in radians. The data points are values obtained by the comparison as explained in the main text; the curve is the best fit through these points, which in the left plot is given by $2.69 \cdot e^{2.65}$, and in the right plot by $3.77 \cdot e^{2.95}$.

3.5 Increasing the accuracy

The examples presented show that the geodesic deviation method can be used to accurately describe eccentric bounded geodesics of a Schwarzschild black hole when the eccentricity is limited. The choice of boundary conditions used in this chapter focussed mostly on improving the accuracy of the radial function and, as such, the method effortlessly produces radial approximations that are accurate to a percent and usually much better still for orbits of eccentricity to about 0.2, even when describing orbits grazing the ISCO. The accuracy of the angular function, too, is excellent, and, in accord with the premise of the geodesic deviation method, the accuracies suffer little from close proximity to the black hole.
Going to orders of higher eccentricity reduces the accuracy of the epicycle expansion by about an order of magnitude for every doubling of the eccentricity; this too is in accord with the expectation, as it had been shown that the expansion parameter σ is related to the eccentricity of the orbits approximated. However, in chapter 5, it will be discussed that a test mass spiraling into a black hole will lose eccentricity due to the emission of gravitational waves, and hence will have its orbit better and better approximated by the epicycle expansion as it approaches the ISCO. It is therefore expected that the expansion up to second order will suffice to accurately describe all but the most extreme natural bound orbits.
There are, however, at least two reasons to consider taking the epicycle expansion up to third order or higher. Firstly, as discussed before, three of the four boundary conditions available at the second-order expansion are needed to guarantee that the right proper time, right angle, and right radial distance is reached *at* periastra, leaving only one boundary condition to constrain one of the coordinates *in between* the periastra. Here, the remaining boundary condition was used to fix the radial position of the apastron, greatly increasing the accuracy of the radial coordinate $r(\tau)$ in between periastra, but it is not guaranteed that the angular coordinate $\varphi(\tau)$ also increases in accuracy. However, an increase in the accuracy of the angular coordinate can be guaranteed by either choosing the remaining boundary condition to focus on constraining the angular coordinate $\varphi(\tau)$ rather than the radial $r(\tau)$, or by taking the epicycle expansion to third or higher order as every new order allows for one extra boundary condition. The latter option is preferable, because it allows for *both* the radial function and the angular function to be constrained between periastra.
A second reason to consider taking into account more terms in the epicycle expansion is as follows. The accuracy of the second-order epicycle expansion has here been checked by comparison with the purely numerical solutions to the geodesic equations, but it would be preferable to have some *intrinsic* measure of the accuracy of the expansion. This can be provided by taking the epicycle expansion to third or higher orders, as the ratio of the contributions of two subsequent orders gives a measure of the convergence (and therefore of the accuracy) of the expansion. Most notably, it is expected to yield a theoretical explanation for the observed fact that the exponent b in the power law for the accuracy of the radial function is about 3.4.
Thus, even though for all practical matters the epicycle expansion up to second-order gives excellent approximations of low eccentricity bound orbits, there is reason to take the

expansion to third or higher orders. It is recommended to take the epicycle expansion to fourth order: a third order expansion can be used to greatly increase the accuracy of the angular coordinate, whereas a fourth order can subsequently be used to offer an intrinsic measure of accuracy of the obtained results. With the method presented in this chapter, this is a tedious but straightforward exercise.

3.6 Summary

In this chapter, the epicycle expansion has been put to the test quantitatively by comparing the resulting orbits with the ones that are found when the geodesic equations are solved by numerical means. In order to do so, boundary conditions on the general first- and second-order epicycle expansions were formulated, which resulted in algebraic conditions on the constants of integration. These were formulated such that the resulting epicycle expansions yield orbits that have the correct physical characteristics at the moment of periastron, and, in case of the second-order epicycle expansion, additionally have the correct radial apastron distance as well. The epicycle expansions to first-and second-order were then tested by a detailed comparison with purely numerically calculated geodesic motion, showing excellent agreement all the way to the innermost stable circular orbit when eccentricities are up to about $e = 0.1$. Higher eccentricities decrease the accuracy of the epicycle expansion by about an order of magnitude for a doubling of the eccentricity, and this can be remedied by taking into account higher-order epicycles. This also has the advantage of allowing an intrinsic measure of the accuracy of the epicycle expansion.
Now it has been seen that the epicycle expansion yields accurate results, applications of the method are immediately foreseeable. Most notably, it opens up the possibility of removing one numerical step in calculating the gravitational radiation in a Schwarzschild background. A formalism to calculate gravitational radiation due to the motion of a test mass in a Schwarzschild background has been topic of research for many decades and was presented in a final form in Refs. [32], [33], but where that work had to rely on numerical descriptions of the geodesic orbits, the geodesic deviation method allows to replace that numerical step by an analytical one. This will be the topic of the next chapter.

Chapter 4

The Zerilli-Moncrief/Regge-Wheeler formalism

4.1 Introduction

In the previous chapters the geodesic deviation method has been used to find analytical expressions in the time domain for the geodesic orbits in a Schwarzschild spacetime; the orbits so obtained proved to accurately resemble the ones in the time domain that previously were only obtained numerically. What's more, the background metric was taken into full account, and hence the results were expected to stay accurate even when close to the central mass of the spacetime; this indeed was found to be the case. In the current chapter, these results will be combined with an existing formalism for the calculation of gravitational waves and again without making any compromise on the Schwarzschild spacetime. This formalism produces the gravitational waves as the solutions of two linear uncoupled differential equations for two scalar, which are called the Zerilli-Moncrief and the Regge-Wheeler functions. The differential equations so obtained are fully analytic but require the orbits to be known as a function of time. Such functions are provided by the geodesic deviation method, and the resulting differential equations will be derived in this chapter. Solving the differential equations for the Zerilli-Moncrief and Regge-Wheeler functions, however, still needs to be done numerically. A numerical algorithm used to solve the differential equations will be the second topic of this chapter.
This chapter is organized as follows. In section 4.2, the derivation of the differential equations for the Zerilli-Moncrief and Regge-Wheeler functions will be reviewed, along with the emission of energy and angular momentum by gravitational waves. Section 4.3 presents the algorithm used to numerically solve the Zerilli-Moncrief and Regge-Wheeler differential equations. In section 4.4, the sources for the differential equations will be calculated for geodesic motion by using the analytic expressions for the orbits as derived in chapter 2. Finally, section 4.5 lists the results of this chapter as a summary.

4.2 The Zerilli-Moncrief/Regge-Wheeler formalism

4.2.1 Outline of the formalism

The calculation of gravitational waves in a Schwarzschild spacetime proceeds in a way that is similar to the analogous case of the calculation in a Minkowski spacetime, which was presented in section 1.5. In principle, what needs to be done is to add a small perturbation $h_{\mu\nu}$ to the Schwarzschild metric and to linearize the Einstein tensor $G_{\mu\nu}$ to first order in $h_{\mu\nu}$, after which the resulting expression must be equated to the energy momentum tensor $T_{\mu\nu}$ that describes the source of the gravitational wave. Like in the Minkowski analogue, the result is a set of ten coupled differential equations that yields the ten components of the gravitational wave $h_{\mu\nu}$ as a function of the presence and dynamics of energy and mass. The key difference with the case of the Minkowski spacetime is that the resulting set of differential equations is much more complicated because the Einstein tensor contains covariant derivatives of the gravitational wave (whereas in the Minkowski case these can be replaced by the normal derivatives). As a result, the differential equations contain terms proportional to $h_{\mu\nu}$ (and its derivatives) with *non-constant* coefficients: the coefficients will generally depend on the radial coordinate r. Although some of these complicated terms can be gauged away by transforming to some convenient coordinate system (analogous to the De Donder gauge and TT-gauge), the remaining set of coupled differential equations still proves cumbersome.
It is therefore not surprising that it has taken many decades to reduce the system to a form that is more manageable, starting with a classic paper by Wheeler and Regge [34] in 1957 which, supplemented by contributions from many authors [35], [36], was presented in a final form in 2004 by Martel and Poisson [32], [33]. The key insights in the resulting formalism are the following: firstly, the fact that the Schwarzschild spacetime is spherically symmetric allows for a convenient rewriting of the differential equations in spherical harmonics, effectively removing the angular dependence from the system. Secondly, a number of convenient gauge transformations can be made to remove all unphysical degrees of freedom and leaving only the two polarizations of the gravitational wave.
In the following, the resulting formalism will be reviewed, leading, ultimately, to two uncoupled linear differential equations that have the two polarizations of the gravitational wave $h_{\mu\nu}$ as their solution.

4.2.2 Small deviations from a Schwarzschild spacetime

The premise of the formalism is to consider small deviations $h_{\mu\nu}$ from the metric $g_{\mu\nu}$ that describes the background spacetime,

$$g^p_{\mu\nu} \equiv g_{\mu\nu} + h_{\mu\nu}, \tag{4.1}$$

and to relate these to the energy momentum tensor $T_{\mu\nu}$ responsible for these perturbations. This can be done by perturbing the Einstein field equation for the total metric,

$$R^p_{\mu\nu} - \frac{1}{2} g^p_{\mu\nu} R^p = -8\pi T_{\mu\nu}, \tag{4.2}$$

to first order in the perturbation $h_{\mu\nu}$, while using that the background metric $g_{\mu\nu}$ is a vacuum solution, *i.e.* $R_{\mu\nu} = 0$. Doing so then relates the metric perturbation $h_{\mu\nu}$ to the energy momentum tensor via

$$\begin{aligned} &-\frac{1}{2} g_{\alpha\beta} D^\alpha D^\beta h_{\mu\nu} + \frac{1}{2} \left(D^\beta D_\nu h_{\beta\mu} + D^\beta D_\mu h_{\beta\nu} \right) \\ &-\frac{1}{2} D_\mu D_\nu h^\beta_\beta - \frac{1}{2} g_{\mu\nu} \left(D^\alpha D^\beta h_{\alpha\beta} - g_{\alpha\beta} D^\alpha D^\beta h^\kappa_\kappa \right) = -8\pi T_{\mu\nu}, \end{aligned} \tag{4.3}$$

in which the covariant derivatives D_α are defined by the background metric $g_{\mu\nu}$, and it is also this metric that is used for raising and lowering of indices. This expression holds regardless of the background spacetime (indeed, replacing all covariant derivatives by partial derivatives of an uncurved spacetime reduces the left hand side of this equation to the one that holds in a Minkowski spacetime, *i.e.* Eq. (1.28)), but as in the current context the spacetime has a spherical symmetry, the following splitting of the metric is allowed:

$$g_{\mu\nu} = \tilde{g}_{ab} \bigoplus r^2 \Omega_{AB}. \tag{4.4}$$

In this splitting, Ω_{AB} denotes the part of the metric that concerns the angular coordinates (denoted by upper case Latin indices), and $\tilde{g}_{ab}$ denotes the part that concerns the temporal-radial coordinates (denoted by lower case Latin indices). For example, for a Schwarzschild spacetime in the Droste coordinates introduced in section 2.2.1, the two parts of the metric are given by

$$\tilde{g}_{ab} = diag(-f(r), f(r)^{-1}), \qquad \Omega_{AB} = diag(1, \sin^2\theta), \tag{4.5}$$

in which, and in what follows, a shorthand notation is used,

$$f(r) \equiv 1 - \frac{2M}{r}. \tag{4.6}$$

As a next step, the perturbations $h_{\mu\nu}$ as well as the energy momentum tensor $T_{\mu\nu}$ will be decomposed in spherical harmonics, so as to decouple the angular parts of the system from the parts defining the evolution in t and r. The different elements of the metric have different behavior under angular rotations, and this reflects itself in the decomposition: the elements of $h_{\mu\nu}$ that behave as a scalar, vector, respectively tensor under spatial rotations must be decomposed in scalar (Y^{lm}), vector (Z^{lm}_A, X^{lm}_A), respectively tensorial (U^{lm}_{AB}, V^{lm}_{AB}, W^{lm}_{AB}) spherical harmonics. The definitions and the properties of these different types of spherical harmonics are well-known and can be found in, *e.g.*, Ref. [34].

The decomposition of the metric perturbations follows as

$$\begin{aligned} h_{ab} &= \sum_{lm} p_{ab}^{lm}(t,r)Y^{lm}(\theta,\varphi), \\ h_{aA} &= \sum_{lm} q_{a}^{lm}(t,r)Z_{A}^{lm}(\theta,\varphi) + h_{a}^{lm}(t,r)X_{A}^{lm}(\theta,\varphi), \\ h_{AB} &= \sum_{lm} r^2 \Bigg(K^{lm}(t,r)U_{AB}^{lm}(\theta,\varphi) + G^{lm}(t,r)V_{AB}^{lm}(\theta,\varphi) + h_{2}^{lm}(t,r)W_{AB}^{lm}(\theta,\varphi) \Bigg). \end{aligned} \tag{4.7}$$

The energy momentum tensor is similarly decomposed as

$$\begin{aligned} T^{ab} &= \sum_{lm} 8\pi Q^{ab,lm}(t,r)Y^{lm}(\theta,\varphi), \\ T^{a}{}_{A} &= \sum_{lm} \frac{4\pi}{r^2} \Bigg(Q^{a,lm}(t,r)Z_{A}^{lm}(\theta,\varphi) + P^{a,lm}(t,r)X_{A}^{lm}(\theta,\varphi) \Bigg), \\ T_{AB} &= \sum_{lm} \frac{4\pi}{r^4} \Bigg(r^2 Q^{\flat,lm}(t,r)U_{AB}^{lm}(\theta,\varphi) + Q^{\sharp,lm}(t,r)V_{AB}^{lm}(\theta,\varphi) + P^{lm}(t,r)W_{AB}^{lm}(\theta,\varphi) \Bigg). \end{aligned} \tag{4.8}$$

In these decompositions, all lower case Latin indices (a, b) are to be lowered and raised by using $\tilde{g}_{ab}$ and its inverse, and the upper case indices by using Ω_{AB} and its inverse. The mode indices (lm) will be dropped on the expansion coefficients for the sake of notational convenience.

It should be noted that these expansions in spherical harmonics have not introduced any physics: the scalar, vector, and tensorial spherical harmonics are known to form a complete set and hence *any* function can be decomposed in the manner of Eqs. (4.7) and (4.8). The physics is encapsulated in the question how to relate the ten coefficients $p_{ab}, q_a, h_a, K, G, h_2$ of the perturbation $h_{\mu\nu}$ to those $Q^{ab}, Q^a, Q^\flat, Q^\sharp, P^a, P$ of the energy momentum tensor $T_{\mu\nu}$. This can be answered by substituting the expansions for metric perturbation and energy-momentum tensor in the perturbed Einstein field equation Eq. (4.3) and working out the relationships between the various coefficients.

At first, the fact that the perturbed Einstein field equation yields ten equations and there are ten variables to solve for, it appears as if the system is exactly solvable. However, just like in the case of the analogous derivation in Minkowski spacetime as presented in section 1.5, this is not true, as General Relativity's inherent freedom to choose coordinate systems allows gauge transformations to be made. Ultimately, therefore, there are only two physical degrees of freedom, corresponding to the two polarizations of a gravitational wave.

Making use of the established results presented in [32], [33], the two degrees of freedom are encapsulated in two scalar functions, the *Zerilli-Moncrief (ZM)* and *Regge-Wheeler*

(RW) functions, which are provided by two uncoupled equations of motion for any energy momentum tensor:

$$\left(\tilde{g}^{ab}\tilde{D}_a\tilde{D}_b - V^l_{ZM}(r)\right)\Psi^{lm}_{ZM}(t,r) = S^{lm}_{ZM}(t,r), \tag{4.9}$$

$$\left(\tilde{g}^{ab}\tilde{D}_a\tilde{D}_b - V^l_{RW}(r)\right)\Psi^{lm}_{RW}(t,r) = S^{lm}_{RW}(t,r), \tag{4.10}$$

in which $\tilde{D}_a$ is the covariant derivative associated with the non-angular part $\tilde{g}_{ab}$ of the metric. The potential functions V_{ZM} and V_{RW} are given by

$$V^l_{ZM} = \frac{1}{r^2\Lambda^2(r)}\left(2\lambda^2\left(\lambda+1-\frac{3M}{r}\right)+\frac{18M^2}{r^2}\left(\lambda+\frac{M}{r}\right)\right), \tag{4.11}$$

$$V^l_{RW} = \frac{1}{r^2}\left(l(l+1)-\frac{6M}{r}\right), \tag{4.12}$$

in which the shorthand notations are used

$$\lambda \equiv \frac{1}{2}(l+2)(l-1), \qquad \Lambda(r) \equiv \lambda + \frac{3M}{r}. \tag{4.13}$$

The source functions $S^{lm}_{ZM,RW}$ carry all information of the energy momentum tensor $T_{\mu\nu}$ responsible for the production of the gravitational waves. They are given by

$$\begin{aligned} S^{lm}_{ZM} &= \frac{1}{(\lambda+1)\Lambda(r)}\Bigg(r^2\Big(f^2(r)\partial_r Q^{tt} - \partial_r Q^{rr}\Big) + r\left(\frac{\Lambda(r)}{f(r)}-1\right)Q^{rr} \\ &\quad + rf(r)Q^{\flat} - \frac{f(r)}{r\Lambda(r)}\Big(\lambda(\lambda-1)r^2 + (4\lambda-9)Mr + 15M^2\Big)Q^{tt}\Bigg) \\ &\quad + \frac{2}{\Lambda(r)}Q^r - \frac{1}{r}Q^{\sharp}, \\ S^{lm}_{RW} &= \frac{1}{r}\left(\frac{2}{r}\left(1-\frac{3M}{r}\right)P - f(r)\partial_r P + P^r\right). \end{aligned} \tag{4.14}$$

Solving the two equations of motion Eqs. (4.9), (4.10) then provides all information on the metric perturbation $h_{\mu\nu}$. Indeed, the relationship between the two polarisations and the Zerilli-Moncrief and Regge-Wheeler functions can be found to be [32]

$$h_+ - ih_\times = \frac{1}{r}\sum_{lm}\left(\Psi^{lm}_{ZM} - 2i\int_{-\infty}^{t}\Psi^{lm}_{RW}(t')dt'\right)\cdot V^{lm}_{AB}\bar{m}^A\bar{m}^B. \tag{4.15}$$

In the present case of an EMRI system, the interest lies in the gravitational waves produced by a test mass μ in a bound geodesic orbit around the black hole. For test masses, the energy momentum tensor is given by [3]

$$T_{\mu\nu} = \mu\int\left(\frac{1}{\sqrt{-g}}\cdot u_\mu u_\nu\cdot\delta^4(x^\alpha - x^\alpha_p(\tau))\right)d\tau, \tag{4.16}$$

in which g is the determinant of the background metric, $x_p^\alpha(\tau)$ denotes the four-position of the test mass. This energy momentum tensor leads, via inversion of Eq. (4.8) and the completeness properties of the spherical harmonics, to the following expressions for $Q^{ab}, Q^a, Q^\flat, Q^\sharp, P^a, P$ (which in the following will be referred to as *energy coefficients*),

$$\begin{aligned}
Q^{ab} &= \frac{8\pi\mu}{r^2}\frac{u^a u^b}{u^t} Y^{*lm}(\theta_p,\varphi_p)\delta(r-r_p(\tau)),\\
Q^a &= \frac{16\pi\mu}{l(l+1)}\frac{u^a u^A}{u^t} Z_A^{*lm}(\theta_p,\varphi_p)\delta(r-r_p(\tau)),\\
Q^\flat &= 8\pi\mu\frac{u^A u^B}{u^t} U_{AB}^{*lm}(\theta_p,\varphi_p)\delta(r-r_p(\tau)),\\
Q^\sharp &= 32\pi\mu\frac{(l-2)!}{(l+2)!}r^2\frac{u^A u^B}{u^t} V_{AB}^{*lm}(\theta_p,\varphi_p)\delta(r-r_p(\tau)),\\
P^a &= \frac{16\pi\mu}{l(l+1)}\frac{u^a u^A}{u^t} X_A^{*lm}(\theta_p,\varphi_p)\delta(r-r_p(\tau)),\\
P &= 16\pi\mu\frac{(l-2)!}{(l+2)!}r^2\frac{u^A u^B}{u^t} W_{AB}^{*lm}(\theta_p,\varphi_p)\delta(r-r_p(\tau)),
\end{aligned} \tag{4.17}$$

in which the subscript p refers to the position of the test mass μ in the Schwarzschild spacetime, and the superscript $*$ denotes the complex conjugate.
In the present case, all motion was taken to be geodesic and hence takes place in a plane, which was chosen to be $\theta_p = \pi/2$ in chapter 2. As a result of this, the spherical harmonics Y^{lm}, Z_A^{lm}, U_{AB}^{lm} and V_{AB}^{lm} vanish when $l+m$ is odd, whereas X_A^{lm} and W_{AB}^{lm} vanish when $l+m$ is even. This means that for $l+m$ even or, respectively odd, the only wave function that need to be calculated is the Zerilli-Moncrief or, respectively, Regge-Wheeler function[1]. Furthermore, the functions $r_p(\tau), \varphi(\tau)$ are given analytically, as the geodesic deviation method of chapter 2 has provided accurate orbital functions in the time domain. As such, the sources for the Zerilli-Moncrief and Regge-Wheeler equations of motion can be written down as fully analytical functions of time. The expressions are tedious in their resulting form. However, in section 4.4 they will be greatly simplified by making use of the fact that the Zerilli-Moncrief and Regge-Wheeler differential equations will be solved by splitting up spacetime in a grid of cells of finite size.

4.2.3 The energy and angular momentum of the gravitational waves

Once the Zerilli-Moncrief and Regge-Wheeler functions have been found, Eq. (4.15) can be used to produce the two polarisations of the gravitational wave $h_{\mu\nu}$. Additionally, the

[1]It is for this reason that, in the literature, the Zerilli-Moncrief functions is sometimes called the *even* function, whereas the Regge-Wheeler function is sometimes called the *odd* function. Some caution is called for, however, as the odd function and Regge-Wheeler function are sometimes related to each other by an integral.

power emitted in the form of gravitational waves follows from the Zerilli-Moncrief and Regge-Wheeler functions as well. In brief, an expression for the energy momentum carried by gravitational waves is found by taking the expansion Eq. (4.3) to second order in $h_{\mu\nu}$ and interpreting all second-order terms as part of a (pseudo-) tensor, that, following arguments in section 1.6, can be interpreted as the energy-momentum tensor $T^{GW}_{\mu\nu}$ belonging to the gravitational wave $h_{\mu\nu}$. Thus, Eq. (1.44) applies, and the energy momentum tensor of the gravitational wave is given by

$$T^{GW}_{\mu\nu} = \frac{1}{32\pi} < D_\mu h^{\alpha\beta} D_\nu h_{\alpha\beta} >, \tag{4.18}$$

in which the brackets denote an average over a region of spacetime large compared to the wavelength of the gravitational radiation. This expression allows for the calculation of the change $dE/dt \equiv P$ in energy as well as the change $dL/dt \equiv \dot{L}$ in angular momentum of a gravitational wave. Expressed in terms of the Zerilli-Moncrief and Regge-Wheeler functions, the power at spatial infinity is given by [32]:

$$P = \frac{1}{64\pi} \sum_{lm} \frac{(l+2)!}{(l-2)!} \left(|\dot{\Psi}^{lm}_{ZM}|^2 + 4|\Psi^{lm}_{RW}|^2 \right), \tag{4.19}$$

in which the overdot denotes a derivative with respect to Schwarzschild time, *i.e.* the time as measured by a stationary observer at spatial infinity. The change in angular momentum is found to be:

$$\frac{dL}{dt} = \frac{i}{128\pi} \sum_{lm} m \frac{(l+2)!}{(l-2)!} \left(\dot{\Psi}^{lm}_{ZM} \Psi^{*lm}_{ZM} + 4\Psi^{*lm}_{RW} \int_{-\infty}^{t} \Psi^{*}_{RW}(t')dt' \right) + c.c, \tag{4.20}$$

in which *c.c.* denotes the complex conjugate.

4.3 The Lousto-Price algorithm

4.3.1 Outline of the algorithm

The equations of motion Eqs. (4.9) and (4.10) for Ψ^{lm}_{ZM} and Ψ^{lm}_{RW} are notoriously difficult to solve analytically for general orbits. Although strides have been made [38] to do so and the current context only demands a solution for the case of a circular orbit plus geodesic deviations, at the present time they will be solved numerically. This is done by following the *Lousto-Price algorithm* presented in [39] and which was also used in [32], [33] (though other numerical methods are equally effective [40], [41]).
In brief, the Lousto-Price algorithm divides up a two-dimensional spacetime in cells of some user-defined size Δ (the exact definition of which will be stated momentarily). Each cell typically has a number of corners that correspond to spacetime pairs (t, r), at which the function $\Psi^{lm}_{ZM,RW}$ takes on particular values. These values are calculated by a discretized version of the wave equations, Eqs. (4.14), which connects the value of the wave $\Psi^{lm}_{ZM,RW}$ at

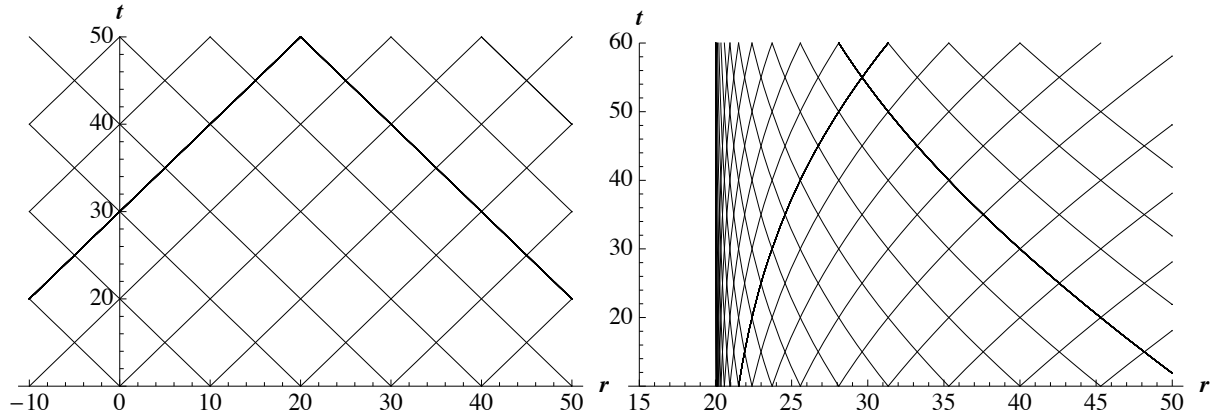

Figure 4.1: Left: The grid defined by lines of $d\tau = 0$ in a Minkowski spacetime, in some arbitrary units of t and r. Right: The grid defined by curves of $d\tau = 0$ in a Schwarzschild spacetime, in some arbitrary units of t and r and in which the mass of the black hole is taken to be $M = 10$ in the same units. In both grids, the vertical axis is the time direction, whereas the horizontal axis is the radial direction. The grid in Schwarzschild spacetime is characterized by cells of uneven size, and the presence of a vertical asymptote at the radial position of the horizon at $r = 2M$. By using the tortoise coordinate r_* rather than the Droste coordinate r, the Schwarzschild grid (right) can be made to look like the Minkowski grid (left).

one corner to those at the other corners. Thus, by supplying the values of $\Psi^{lm}_{ZM,RW}$ for some initial set of grid points (physically, this denotes supplying some initial gravitational wave at, *e.g.* $t = 0$), the Lousto-Price algorithm allows the iterative calculation of the values of $\Psi^{lm}_{ZM,RW}$ at other grid points of interest. Listing all values at some fixed spatial position r_{obs} for a sequence of subsequent times, constitutes the time evolution of the gravitational wave at that fixed spatial position r_{obs}.
In what follows, the algorithm will be presented in detail. Firstly, an appropriate way of splitting up the spacetime in grid cells will be discussed. After that, a way to discretize the wave equation will be presented, so as to express the value of $\Psi^{lm}_{ZM,RW}$ at the corners of a single cell in terms of each other.

4.3.2 Tortoise coordinates

There are, of course, in principle many ways to divide up a spacetime in a grid of cells. For example, for a Minkowski curvature, a natural choice is to split up spacetime in symmetric diamond shaped cells in the manner shown in the left panel of Figure 4.1. In that figure, the grid lines are defined by lines of the form

$$t \mp r = t_0 \tag{4.21}$$

in which the t_0 are arbitrary constants, the values of which are related to the size Δ of the individual cells. As such an equation is obtained from the Minkowski line element by setting $d\tau^2 = 0$, these lines are exactly the world lines followed by light (or any other influence that travels with the speed of light, such as, for example, gravitational waves).

In particular this means that an observer's causality triangle is trivially identified, and the discretization of the wave equation needs only consider equally spaced timesteps as all cells are equally spaced.
In a curved spacetime, splitting up the spacetime by using lines of constant $t \mp r$ will yield cells that, generally, have variable sizes depending on the position of the cells in the spacetime. For example, in the current case of the Schwarzschild spacetime, using such a choice of grid lines produces a grid as shown in the right panel of Figure 4.1. As can be seen, the cells are not equally shaped nor are the grid points at fixed distance from each other. What's more, the coordinate singularity at $r = 2M$ represents itself as an impractical vertical asymptote. Discretizing a Schwarzschild spacetime in such a way would prove cumbersome when implementing the algorithm as a numerical code.
It is therefore desirable to use General Relativity's inherent freedom to choose a coordinate system to transform to a system of coordinates in which the cells are equally sized throughout spacetime. From the Schwarzschild line element of Eq. (2.2) this can be achieved by setting $d\tau^2 = 0$ and integrating the result to yield an expression for t in terms of r:

$$\begin{aligned} d\tau^2 &= \left(1 - \frac{2M}{r}\right) dt^2 - \left(1 - \frac{2M}{r}\right)^{-1} dr^2 = 0, \\ \Rightarrow \quad dt &= \pm \int \left(1 - \frac{2M}{r}\right)^{-1} dr, \\ \Rightarrow \quad t &= \pm \left(r + 2M \ln\left(\frac{r}{2M} - 1\right)\right) + t_0, \end{aligned} \tag{4.22}$$

in which t_0 is an arbitrary constant. By defining the *tortoise coordinate* r_* as follows

$$r_* \equiv r + 2M \ln\left(\frac{r}{2M} - 1\right), \tag{4.23}$$

this relation between the spatial coordinate and time coordinate can be written in the form of Eq. (4.21), and thus suggests a natural way to divide the spacetime up in a grid of equally sized cells in the manner of the left panel of Figure 4.1.
This has several advantages: as setting $d\tau^2 = 0$ amounts to describing motion with the speed of light, the grid lines of constant $t \mp r_*$ correspond to the world lines followed by light, gravitational waves (or any other influence that travels with the speed of light). As such, in the tortoise coordinates (t, r_*) it is trivial to identify the triangle of causality for an observer at a fixed position r_{*obs}. Furthermore, the coordinate singularity at $r = 2M$ that appeared in the Droste coordinates of Eq. (2.2) has now been placed at minus infinity, effectively removing it from the system for all practical matters[2]. Finally, in tortoise coordinates the line element of the Schwarzschild spacetime takes a form that is symmetric in its radial and temporal coordinates, as

$$d\tau^2 = \left(1 - \frac{2M}{r}\right) dt^2 - \left(1 - \frac{2M}{r}\right) dr_*^2 - r^2 \Omega_{AB} dx^A dx^B. \tag{4.24}$$

[2]This echoes the comment made in section 2.2.1: the singularity at $r = 2M$ is merely a result of the coordinates chosen, so it does not represent any actual physics.

As a result of this symmetric appearance, the wave equation becomes of the form of a Klein-Gordon equation,

$$\left(-\partial_t^2 + \partial_{r_*}^2 - \bar{V}^l_{ZM,RW}(r)\right) \Psi^{lm}_{ZM,RW} = \bar{S}^{lm}_{ZM,RW}, \tag{4.25}$$

in which for notational convenience the subscript (ZM, RW) will be dropped for the time being, and

$$\bar{V}^l(r) \equiv \left(1 - \frac{2M}{r}\right) V^l(r), \qquad \bar{S}^{lm}(t,r) \equiv \left(1 - \frac{2M}{r}\right) S^{lm}(t,r). \tag{4.26}$$

Finally, the source function $\bar{S}^{lm}$ will be assumed to be of the general form

$$\bar{S}^{lm} = G^{lm}(r)\delta(r - r_p(t)) + F^{lm}(r)\partial_r\delta(r - r_p(t)). \tag{4.27}$$

This is motivated by Eqs. (4.14), which state that the source function is a sum of the energy coefficients of Eq. (4.17) and their derivatives with respect to the radial coordinate r. In section 4.4, this assumption will be justified and the epicycle expansion will be used to find explicit and analytical expressions for $F^{lm}(r)$ and $G^{lm}(r)$.
It will be in the form Eq. (4.25) that the wave equation will be discretized to allow an iterative integration. This will be done next.

4.3.3 Integration over a single grid cell

Having divided up the Schwarzschild spacetime in equal sized grid cells by transforming to tortoise coordinates (t, r_*), the next step in the Lousto-Price algorithm is to discretize the wave equation Eq. (4.25) so that it enables the calculation of the value of Ψ^{lm} at the top corner of a single cell when the values at the three other corners are known. This will be done by integrating the wave equation over a single grid cell by evaluating the following three expressions,

$$\int_{cell} \left(-\partial_t^2 + \partial_{r_*}^2\right) \Psi^{lm}\, dt dr_*\,, \qquad \int_{cell} \bar{V}^l(r)\Psi^{lm}\, dt dr_*\,, \qquad \int_{cell} \bar{S}^{lm}\, dt dr_*\,. \tag{4.28}$$

A picture of a single cell is shown in Figure 4.2, which serves to introduce the definition of the cell size parameter Δ and the various observables used in the presentation that follows. The first expression in Eq. (4.28) can be evaluated straightforwardly to yield

$$\begin{aligned}\int_{cell} \left(-\partial_t^2 + \partial_{r_*}^2\right) \Psi^{lm}\, dt dr_* = \; &- \; 2\Psi^{lm}(t, r_*) + 2\Psi^{lm}(t + \Delta, r_* - \Delta) \\ &+ \; 2\Psi^{lm}(t + \Delta, r_* + \Delta) - 2\Psi^{lm}(t + 2\Delta, r_*).\end{aligned} \tag{4.29}$$

This expression is an identity, as the derivatives and the integrations canceled each other by the basic rules of calculus.
In contrast, the second expression in Eq. (4.28) can not be evaluated exactly because it

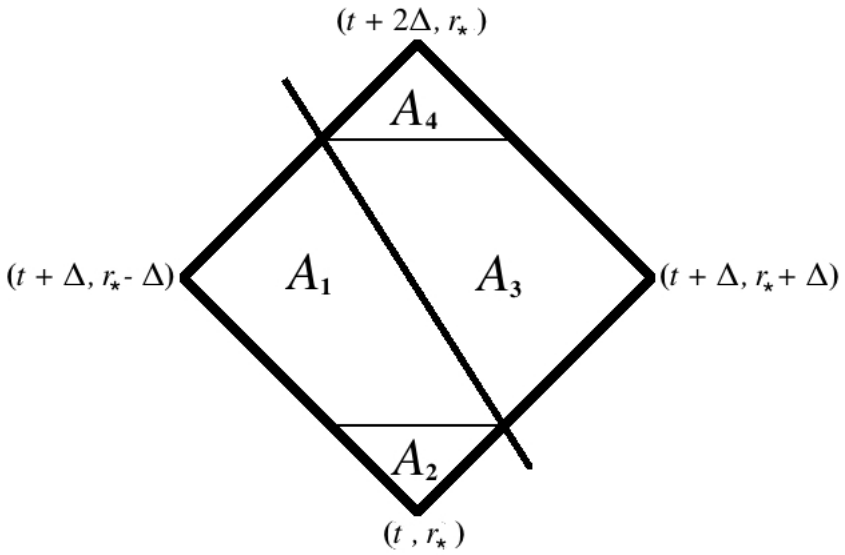

Figure 4.2: A single grid cell, traversed by the worldline of the test mass. The worldline splits up the cell in four areas, denoted A_1, A_2, A_3, A_4 in the manner shown. The total area of the cell is $2\Delta^2$ in tortoise coordinates.

requires the wave function to be known explicitly. This can be remedied by choosing the cell small enough so as to allow the assumption that the integrand changes very little throughout the cell, and hence the outcome of the integration is approximately equal to the average of the values at the four corners:

$$\begin{aligned}\int_{cell} \bar{V}^l(r)\Psi^{lm}\,dtdr_* \approx \Big(\quad &+ \quad \bar{V}^l(r_*)\Psi^{lm}(t,r_*) + \bar{V}^l(r_*)\Psi^{lm}(t+2\Delta,r_*) \\ &+ \quad \bar{V}^l(r_*-\Delta)\Psi^{lm}(t+\Delta,r_*-\Delta) \\ &+ \quad \bar{V}^l(r_*+\Delta)\Psi^{lm}(t+\Delta,r_*+\Delta) \quad \Big)\frac{1}{2}\Delta^2, \end{aligned} \tag{4.30}$$

where it has been used that the area of the cell is $2\Delta^2$, as can be seen in Figure 4.2.
In case the cell is traversed by the world line, the averaging procedure needs to be modified because the wave function Ψ^{lm} is not continuous over the area of the cell. This is because the world line itself is a discontinuity, and hence the wave function Ψ^{lm} takes on different values at either side of the line. In the Lousto-Price algorithm, this is remedied by applying a weighing procedure to the averaging: the world line is in each cel approximated by a straight line such that it splits up the cell in four pieces, as depicted in Figure 4.2. On each piece the wave function *is* continuous and the value of the integral can be calculated approximately. The latter is done by assuming that the function integrand is approximately constant on the piece so that it can be taken outside the integral. The outcome thus equals the area of the piece multiplied by the value of the function at the closest grid point. The

total average is then constructed as the sum of the four separate contributions, and the resulting expression is

$$\begin{aligned}\int_{cell} \bar{V}^l \Psi^{lm}\, dt dr_* &\approx \bar{V}^l(r_*)\Psi^{lm}(t, r_*)A_2 \\ &+ \bar{V}^l(r_*)\Psi^{lm}(t+2\Delta, r_*)A_4 \\ &+ \bar{V}^l(r_*-\Delta)\Psi^{lm}(t+\Delta, r_*-\Delta)A_1 \\ &+ \bar{V}^l(r_*+\Delta)\Psi^{lm}(t+\Delta, r_*+\Delta)A_3. \end{aligned} \tag{4.31}$$

The final expression in Eq. (4.28) needs only to be evaluated for the cells that are traversed by the world line of the test mass, as the delta function and its derivative trivially vanish when the zero point (*i.e.* the position of the test mass) does not lie inside the range of the integration. The evaluation of the integral for cells that are traversed is straightforward, albeit tedious, and is presented in appendix D. The result of the evaluation is an identity and is given by

$$\begin{aligned}\int_{cell} \bar{S}^{lm}\, dr_* dt &= \int_{t_b}^{t_t} dt \left(\frac{G^{lm}(r)}{f(r)} - \partial_r\Big(\frac{F^{lm}(r)}{f(r)}\Big)\right)\Bigg|_{r=r_p(t)} \\ &\pm \frac{F^{lm}(r_p(t_b))}{f^2(r_p(t_b))} \frac{1}{1 \mp \dot{r}_{*p}(t)}\Bigg|_{t=t_b} \\ &\pm \frac{F^{lm}(r_p(t_t))}{f^2(r_p(t_t))} \frac{1}{1 \pm \dot{r}_{*p}(t)}\Bigg|_{t=t_t}, \end{aligned} \tag{4.32}$$

in which an overdot denotes a derivative with respect to Schwarzschild time t, and in which t_b respectively t_t denote the Schwarzschild times at which the world line of the test mass enters the cell, respectively leaves the cell. The ambiguity in the signs of the boundary terms is resolved as follows: in the first boundary term, the upper sign must be chosen when the world line enters the cell from the right whereas the lower sign must be chosen when the world line enters the cell at the left. In the same way, in the second boundary term the upper sign must be chosen when the world line leaves the cell at the right, whereas the lower sign must be chosen when the world line leaves the cell at the left.
Combining the outcomes Eqs. (4.29), (4.30), (4.31), and (4.32) of the integrations of the different terms in the wave equation over an individual cell, yields an expression that relates the values of Ψ^{lm} at the four corners of the cell to each other. It is now possible to express the value $\Psi^{lm}(t+2\Delta, r_*)$ at the upper corner of a cell to the values $\Psi^{lm}(t+\Delta, r_* \pm \Delta)$, $\Psi^{lm}(t, r_*)$ at the three other corners of the cell. The result for cells that are not traversed by the world line of the test mass, is

$$\begin{aligned}\Psi^{lm}(t+2\Delta, r_*) = -\Psi^{lm}(t, r_*) &+ \frac{1 - \frac{\Delta^2}{4}\bar{V}^l(r_*-\Delta)}{1 + \frac{\Delta^2}{4}\bar{V}^l(r_*)}\Psi^{lm}(t+\Delta, r_*-\Delta) \\ &+ \frac{1 - \frac{\Delta^2}{4}\bar{V}^l(r_*+\Delta)}{1 + \frac{\Delta^2}{4}\bar{V}^l(r_*)}\Psi^{lm}(t+\Delta, r_*+\Delta), \end{aligned} \tag{4.33}$$

and for cells that are traversed by the world line, the result is

$$\begin{aligned}\Psi^{lm}(t+2\Delta,r_*) = &- \Psi^{lm}(t,r_*)\frac{1+\frac{A_2}{4}\bar{V}^l(r_*)}{1+\frac{A_4}{4}\bar{V}^l(r_*)} - \frac{\int_{cell}\bar{S}^{lm}(t,r)\,dtdr_*}{4+\bar{V}^l(r_*)A_4} \\ &+ \frac{1-\frac{A_1}{4}\bar{V}^l(r_*-\Delta)}{1+\frac{A_4}{4}\bar{V}^l(r_*)}\Psi^{lm}(t+\Delta,r_*-\Delta) \\ &+ \frac{1-\frac{A_3}{4}\bar{V}^l(r_*+\Delta)}{1+\frac{A_4}{4}\bar{V}^l(r_*)}\Psi^{lm}(t+\Delta,r_*+\Delta). \end{aligned} \tag{4.34}$$

By using Eqs. (4.33), (4.34) it is possible to iteratively calculate the value of Ψ^{lm} at every grid point in the spacetime, starting from a given set of values at some initial set of grid points. Of course, the only grid points at which the value need to be calculated are the ones that lie within the causality triangle of the observer at r_{*obs}.
This concludes the review of the Lousto-Price algorithm for the numerical integration of the Zerilli-Moncrief and Regge-Wheeler differential equations. In the usual presentation, the only assumption made on the form of the sources of the differential equations is that they are of the form of Eq. (4.27). In the literature, the functions G^{lm} and F^{lm} therein themselves are calculated numerically, as they require the coordinates of the test mass' world line be known as a function of time. In the present case, however, no need for such numerical calculation of the sources is necessary, as the geodesic deviation method has provided the world line as an analytical function of time in the form of the epicycle expansion of chapter 2. It is therefore possible to calculate the sources explicitly as analytical functions of time. This will be done next.

4.4 The source functions and geodesic deviations

The geodesic deviation method allows the calculation of the source functions $\bar{S}^{lm}_{ZM,RW}$ of the Zerilli-Moncrief and Regge-Wheeler functions. To do so, the energy coefficients of Eq. (4.17) need to be substituted in the general expressions for $\bar{S}^{lm}_{ZM,RW}$, Eq. (4.27), carefully separating all terms that contain the delta function from those that contain its derivative with respect to the radial coordinate r; the former terms will make up the function $G^{lm}_{ZM,RW}$, the latter terms the function $F^{lm}_{ZM,RW}$.
Naively (and correctly), this can be done by a straightforward substitution and working out the results, but this exercise is rather cumbersome due to the many derivatives. However, the work can be greatly simplified by making use of the fact that the source functions $\bar{S}^{lm}$ will, in the Lousto-Price algorithm, always be integrated over a cell. For such integrations the following rules hold:

$$\begin{aligned}\int_{cell}\Big(a(r)\delta(r-r_p(t))\Big)\,dtdr_* &= \int_{cell}a(r_p(t))\,\delta(r-r_p(t))\,dtdr_*\,, \\ \int_{cell}b(r)\partial_r\Big(a(r)\delta(r-r_p(t))\Big)\,dtdr_* &= \int_{cell}b(r)a(r_p(t))\,\partial_r\delta(r-r_p(t))\,dtdr_*\,,\end{aligned} \tag{4.35}$$

for any well-behaved functions $a(r)$, $b(r)$; this is discussed in more detail in Appendix D. The first of these rules is just the defining property of the delta function applied on a finite region of integration; the second rule states, simply put, that when a derivative is taken of some function $a(r)\delta(r - r_p(t)$, the integration over a cell allows the radial coordinate in the function $a(r)$ to be replaced by the zero point $r_p(t)$ of the delta function, whereas this does not happen for the radial coordinate in the function $b(r)$. This greatly simplifies the calculation of the functions $F(r)$ and $G(r)$ as now many of the derivatives need not to be taken.

There is, however, an even more stringent reason to use Eq. (4.35): it allows all the four-velocities in the energy coefficients to be replaced by the ones describing the geodesic motion. Before, in the general expression for $\bar{S}^{lm}$, the four-velocities were supposed to be the most general u^μ describing bound geodesic motion, and only *after* derivatives have been taken to obtain F^{lm} and G^{lm}, were they to be replaced by the ones describing the particular geodesic motion of interest. It is for this reason that, in the literature [45], [32], some time is spent to obtain general expressions for the four-velocities before evaluating the functions F^{lm} and G^{lm}. The use of the rule Eq. (4.35) circumvents this, as the direct replacement of many of the r by $r_p(t)$ replaces the general u^μ by those given by the epicycle expansion. The latter statement is true for geodesic motion, because the Killing constants of Eq. (2.3) state that the four-velocities u^t and u^φ are a function of solely the radial position $r_p(t)$; then also, by the normalization of four-velocity Eq. (1.16), u^r is a function of the radial position only. Thus, replacing the radial coordinate by $r_p(t)$ is equivalent to replacing all general four-velocities by the ones calculated to describe some specific geodesic motion.

For the Zerilli-Moncrief source, the functions F^{lm}_{ZM} and G^{lm}_{ZM} are then straightforwardly found to be given by the expressions

$$
\begin{aligned}
F^{lm}_{ZM}(r, r_p(t)) &= \frac{r^2}{(\lambda+1)\Lambda(r)}\frac{8\pi\mu}{r_p^2(t)}\cdot\left(\left(1-\frac{2M}{r}\right)^3 u_p^t \;-\left(1-\frac{2M}{r}\right)\frac{(u_p^r)^2}{u_p^t}\right)\cdot Y^{*lm}(\theta_p,\varphi_p),\\
G^{lm}_{ZM}(r_p(t)) &= \frac{8\pi\mu}{(\lambda+1)\Lambda(r_p(t))}\cdot\Bigg(r_p(t)\Big(\Lambda(r_p(t))-f(r_p(t))\Big)\frac{1}{r_p^2(t)}\frac{(u_p^r)^2}{u_p^t}\cdot Y^{*lm}(\theta_p,\varphi_p)\\
&\quad + r_p(t)f^2(r_p(t))\frac{(u_p^\varphi)^2}{u_p^t}\cdot U^{*lm}_{\varphi\varphi}(\theta_p,\varphi_p) - \frac{f^2(r_p(t))u_p^t}{r_p(t)\Lambda(r_p(t))}\\
&\quad \cdot\Big(\lambda(\lambda-1)r_p^2(t)+(4\lambda-9)Mr_p(t)+15M^2\Big)\cdot Y^{*lm}(\theta_p,\varphi_p)\Bigg)\\
&\quad + 32\pi\mu\cdot\frac{f(r_p(t))}{\Lambda(r_p(t))}\frac{1}{l(l+1)}\frac{u_p^r u_p^\varphi}{u_p^t}\cdot Z^{*lm}_{\varphi}(\theta_p,\varphi_p)\\
&\quad - 32\pi\mu\cdot f(r_p(t))\frac{(l-2)!}{(l+2)!}r_p(t)\frac{(u_p^\varphi)^2}{u_p^t}\cdot V^{*lm}_{\varphi\varphi}(\theta_p,\varphi_p).
\end{aligned}
\tag{4.36}
$$

For the Regge-Wheeler source, a similar calculation yields the functions F^{lm}_{RW} and G^{lm}_{RW}:

$$\begin{aligned} F^{lm}_{RW}(r, r_p(t)) &= -16\pi\mu \cdot \frac{f^2(r)}{r} r_p^2(t) \frac{(l-2)!}{(l+2)!} \frac{(u^\varphi_p)^2}{u^t_p} \cdot W^{*lm}_{\varphi\varphi}(\theta_p, \varphi_p), \\ G^{lm}_{RW}(r_p(t)) &= 32\pi\mu \cdot f(r_p(t)) \left(1 - \frac{3M}{r_p(t)}\right) \frac{(l-2)!}{(l+2)!} \frac{(u^\varphi_p)^2}{u^t_p} \cdot W^{*lm}_{\varphi\varphi}(\theta_p, \varphi_p) \\ &\quad + 16\pi\mu \cdot \frac{f(r_p(t))}{l(l+1) \cdot r_p(t)} \frac{u^r_p u^\varphi_p}{u^t_p} \cdot X^{*lm}_{\varphi}(\theta_p, \varphi_p). \end{aligned} \tag{4.37}$$

A number of observations can be made. Firstly, in the context of the Zerilli-Moncrief and Regge-Wheeler formalism, no further approximations have been made so that the expressions are all exact in terms of $r_p(t)$. Furthermore, they are completely known as analytical functions of time and the radial position. Finally, the expressions are very general: the only assumptions that have been made is that the motion takes place in a plane (so as to ignore all terms containing u^θ_p), that the motion is geodesic (so as to be able to conclude that the components of the four-velocity are fully fixed when the radial position is known), and that the geodesic motion is known as a function of time. Using the geodesic deviation method of the previous chapter, these assumptions are all automatically fulfilled and hence the source functions Eqs. (4.36), (4.37) are fully compatible with *any* expansion the geodesic deviation method produces, for example (but not limited to) the epicycle expansion. In the next chapter, this will be illustrated by using the source functions to calculate the gravitational waves emitted by an EMRI system.

4.5 Summary

This chapter described methods to calculate the production and propagation of gravitational waves in a Schwarzschild spacetime, taking into account the full Schwarzschild geometry. A formalism to do so is known in the literature and was briefly reviewed. It expands the energy momentum tensor of the physical source of the waves in spherical harmonics, and does so too for the gravitational waves. The coefficients in both expansions are then related to each other by an explicit substitution of the two expansions in the Einstein field equations, resulting in, ultimately, two uncoupled scalar differential equations that yield the two physical degrees of freedom of the gravitational wave as their solution: the Zerilli-Moncrief and Regge-Wheeler functions.
Solving these differential equations has to be done numerically, and the formalism to do so was reviewed as well. This algorithm first splits up the Schwarzschild spacetime in finitely sized cells, and then supplies a discretized version of the Zerilli-Moncrief and Regge-Wheeler differential equations that can be used to calculate the value of the solution at one corner of a cell if the values at the other corners are known. This allows an iterative calculation of the Zerilli-Moncrief and Regge-Wheeler function by means of a computer program, which was implemented in C++.
This algorithm was then combined with the analytical orbital functions provided by the

geodesic deviation method of chapter 2, producing expressions for the source functions of the Zerilli-Moncrief and Regge-Wheeler differential equations. The source functions so obtained are, in contrast with methods presented in the literature, completely analytically known as functions of time, and they are also very general: the only assumption made was that the described motion is geodesic and known as a function of time. As such, the source functions obtained can be used for *any* orbital expansion provided by the geodesic deviation method. The results of this chapter will next be applied to the EMRI system.

Chapter 5

Results: gravitational waves

5.1 Introduction

The previous chapters have dealt with methods to calculate the orbits in an extreme mass-ratio inspiral system and the resulting gravitational waves. Chapter 2 presented the formalism to accurately calculate geodesic orbits as a function of time, which were subsequently used in chapter 4 to find analytic expressions for the sources of the Zerilli-Moncrief and Regge-Wheeler equations. In the current chapter, these results will be collected and used to calculate gravitational waves emitted by the EMRI system, allowing a comparison of the methods of this thesis with the purely numerical ones presented in the literature. There are two sources of inaccuracy in this method, coming from the facts that the epicycle expansion is itself an approximation and that the numerical code relies on a finite cell-size. The distinction between the two sources of inaccuracy will be investigated and quantified in this chapter as well. Finally, this chapter will investigate how the geodesic orbits evolve under influence of the emission of gravitational radiation, so as to confirm the claim that the orbits become increasingly circular and thus that the Epicycle Expansion is increasingly justified.
This chapter is organized as follows. In section 5.2 the code will be tested for a number of orbits that are simple enough not to require the epicycle approximation, so as to make quantitive the intrinsic error that is a result of the numerical algorithm of the code. It will also be discussed how an estimate can be made of the inaccuracy in the gravitational waves due to the fact that the orbits supplied to the code come from the epicycle expansion. In section 5.3, the gravitational waves of a series of bound eccentric orbits modeled by the epicycle expansion will be calculated, resulting in values for the average power and angular momentum emitted by gravitational waves. Also, the values for the powers are compared to the values as predicted by the Peters-Mathews equation, showing where the latter gives a reasonable approximation. Section 5.4 investigates the influence of the emission of energy and angular momentum on the shape of the bound orbits. Finally, section 5.5 lists the results of this chapter as a summary.

5.2 The accuracy of the method

5.2.1 The intrinsic error of the code

It was discussed in chapter 4 that the Zerilli-Moncrief and Regge-Wheeler equations of motion can be solved by an iterative method provided by the Lousto-Price algorithm, which can be implemented as a computer code. A preliminary version of such a code written in the language C++ was presented in Ref. [42], where it was shown to accurately calculate the gravitational waves emitted when a test mass falls radially into a Schwarzschild black hole. Since then, the code has been generalized to allow the calculation of gravitational waves due to *any* motion of a test mass in the vicinity of a Schwarzschild black hole, and it is this version of the code that has produced all Zerilli-Moncrief and Regge-Wheeler functions to be presented in this chapter, along with the energy and angular momentum the resulting gravitational waves carry away from the EMRI system.
Before presenting these results, the intrinsic error of the code will be quantified. This will be done by investigating the class of circular orbits of various radii. This is a case well-studied in the literature by purely numerical approaches, as the circular orbit is known analytically as a function of time and thus allows for an *exact* calculation of the sources $\bar{S}^{lm}_{ZM,RW}$ of the Zerilli-Moncrief and Regge-Wheeler differential equations. Therefore, the resulting gravitational waves and the energy and angular momentum that they carry are not plagued by the question how accurate the sources are known; instead, the results form a direct measure of the accuracy of the numerical algorithm.
The literature presents at least two different ways to calculate the energy and angular momentum carried by gravitational waves emitted by a circular orbit. One is done in the frequency domain [43], [44], *i.e.* the calculation is done in Fourier space first and the outcomes are subsequently transformed back to the time domain. The second approach is in the time domain from the outset [32], [33] and follows the Lousto-Price algorithm presented in Chapter 4. The two approaches yield outcomes for the energy and angular momentum that have a relative difference typically less than a percent and usually much less still. These outcomes will be used for comparison with the results obtained by the methods described in this thesis.
Circular orbits of the following two radii will be used: $a = 7.9456M$ and $a = 46.062M$, and the energy per unit mass and angular momentum per unit mass carried by the gravitational waves will be calculated for a number of modes (l, m). The ratio between the companion star's mass μ and the black hole mass M will be set to $\mu/M = 10^{-5}$. The results are presented in table 5.1; it lists the power and change in angular momentum per unit mass for a number of modes for the cases $a = 7.9456M$ and $a = 46.062M$, and compares these to the values obtained in the literature. In obtaining these average values (and all other averages presented later in this chapter), the following equations are used

$$< \dot{E} > = \frac{1}{T} \int_t^{t+T} \dot{E}\, dt, \qquad < \dot{L} > = \frac{1}{T} \int_t^{t+T} \dot{L}\, dt\,, \tag{5.1}$$

in which T is the Schwarzschild time that elapses between one periastron and a next periastron.
The results listed in the table show that the code works correctly and that it accurately reproduces the energy and angular momentum sent out by the system: the total (*i.e.* summed over all modes) relative difference with the high-precision values stated in the literature is typically of the order of a few tenths of a percent. For the purposes of this thesis this accuracy suffices, for reasons that will be explained momentarily.

$a = 7.9456M$	Frequency domain		Time domain		This thesis	
mode	P	$\dot{L}$	P	$\dot{L}$	P	$\dot{L}$
$l = 2, \lvert m\rvert = 2$	$1.706 \cdot 10^{-4}$	$3.822 \cdot 10^{-3}$	$1.705 \cdot 10^{-4}$	$3.816 \cdot 10^{-3}$	$1.707 \cdot 10^{-4}$	$3.803 \cdot 10^{-3}$
$l = 2, \lvert m\rvert = 1$	$8.163 \cdot 10^{-7}$	$1.828 \cdot 10^{-5}$	$8.162 \cdot 10^{-7}$	$1.827 \cdot 10^{-5}$	$8.208 \cdot 10^{-7}$	$1.819 \cdot 10^{-5}$
$l = 3, \lvert m\rvert = 3$	$2.547 \cdot 10^{-5}$	$5.705 \cdot 10^{-4}$	$2.543 \cdot 10^{-5}$	$5.688 \cdot 10^{-4}$	$2.550 \cdot 10^{-5}$	$5.640 \cdot 10^{-4}$
$l = 3, \lvert m\rvert = 2$	$2.520 \cdot 10^{-7}$	$5.644 \cdot 10^{-6}$	$2.516 \cdot 10^{-7}$	$5.626 \cdot 10^{-6}$	$2.524 \cdot 10^{-7}$	$5.612 \cdot 10^{-6}$
$l = 3, \lvert m\rvert = 1$	$2.173 \cdot 10^{-9}$	$4.867 \cdot 10^{-8}$	$2.174 \cdot 10^{-9}$	$4.868 \cdot 10^{-8}$	$2.197 \cdot 10^{-9}$	$4.877 \cdot 10^{-8}$
$l = 4, \lvert m\rvert = 4$	$4.726 \cdot 10^{-6}$	$1.058 \cdot 10^{-4}$	$4.708 \cdot 10^{-6}$	$1.052 \cdot 10^{-4}$	$4.729 \cdot 10^{-6}$	$1.052 \cdot 10^{-4}$
$l = 4, \lvert m\rvert = 3$	$5.775 \cdot 10^{-8}$	$1.293 \cdot 10^{-6}$	$5.746 \cdot 10^{-8}$	$1.293 \cdot 10^{-6}$	$5.767 \cdot 10^{-8}$	$1.292 \cdot 10^{-6}$
$l = 4, \lvert m\rvert = 2$	$2.509 \cdot 10^{-9}$	$5.620 \cdot 10^{-8}$	$2.499 \cdot 10^{-9}$	$5.593 \cdot 10^{-8}$	$2.516 \cdot 10^{-9}$	$5.567 \cdot 10^{-8}$
total	$2.019 \cdot 10^{-4}$	$4.524 \cdot 10^{-3}$	$2.018 \cdot 10^{-4}$	$4.515 \cdot 10^{-3}$	$2.021 \cdot 10^{-4}$	$4.497 \cdot 10^{-3}$

$a = 46.062M$	Frequency domain		Time domain		This thesis	
mode	P	$\dot{L}$	P	$\dot{L}$	P	$\dot{L}$
$l = 2, \lvert m\rvert = 2$	$2.865 \cdot 10^{-8}$	$8.957 \cdot 10^{-5}$	$2.865 \cdot 10^{-8}$	$8.981 \cdot 10^{-6}$	$2.888 \cdot 10^{-8}$	$9.026 \cdot 10^{-6}$
$l = 2, \lvert m\rvert = 1$	$1.849 \cdot 10^{-11}$	$5.780 \cdot 10^{-9}$	$1.871 \cdot 10^{-11}$	$5.850 \cdot 10^{-9}$	$1.911 \cdot 10^{-11}$	$5.810 \cdot 10^{-9}$
$l = 3, \lvert m\rvert = 3$	$8.064 \cdot 10^{-10}$	$2.521 \cdot 10^{-7}$	$8.084 \cdot 10^{-10}$	$2.527 \cdot 10^{-7}$	$8.116 \cdot 10^{-10}$	$2.537 \cdot 10^{-7}$
$l = 3, \lvert m\rvert = 2$	$1.093 \cdot 10^{-12}$	$3.416 \cdot 10^{-10}$	$1.099 \cdot 10^{-12}$	$3.436 \cdot 10^{-10}$	$1.109 \cdot 10^{-12}$	$3.465 \cdot 10^{-10}$
$l = 3, \lvert m\rvert = 1$	$7.549 \cdot 10^{-14}$	$2.360 \cdot 10^{-11}$	$7.726 \cdot 10^{-14}$	$2.416 \cdot 10^{-11}$	$8.073 \cdot 10^{-14}$	$2.524 \cdot 10^{-11}$
$l = 4, \lvert m\rvert = 4$	$2.794 \cdot 10^{-11}$	$8.734 \cdot 10^{-9}$	$2.800 \cdot 10^{-11}$	$8.753 \cdot 10^{-9}$	$2.807 \cdot 10^{-11}$	$8.775 \cdot 10^{-9}$
$l = 4, \lvert m\rvert = 3$	$4.660 \cdot 10^{-14}$	$1.457 \cdot 10^{-11}$	$4.680 \cdot 10^{-14}$	$1.463 \cdot 10^{-11}$	$4.670 \cdot 10^{-14}$	$1.469 \cdot 10^{-11}$
$l = 4, \lvert m\rvert = 2$	$1.602 \cdot 10^{-14}$	$5.008 \cdot 10^{-12}$	$1.617 \cdot 10^{-14}$	$5.056 \cdot 10^{-12}$	$1.643 \cdot 10^{-14}$	$5.136 \cdot 10^{-12}$
total	$2.950 \cdot 10^{-8}$	$9.224 \cdot 10^{-6}$	$2.951 \cdot 10^{-8}$	$9.249 \cdot 10^{-6}$	$2.974 \cdot 10^{-8}$	$9.295 \cdot 10^{-6}$

Table 5.1: The power P and time derivative $\dot{L}$ of the angular momentum emitted by two systems of a test mass orbiting a black hole at radii of $a = 7.9456M$ and $a = 46.062M$, respectively, per mode as listed in the first column of each table (where $|m|$ denotes the sum of the two modes $\pm m$). The power and angular momentum as calculated in the literature in the frequency domain [43], [44] are given in the second and third column, and these values as calculated in the literature in the time domain [32], [33] are listed in the fourth and fifth column. The last two columns state the values as calculated by the methods of this thesis. The power is stated in units $(\mu/M)^2$ and the derivative of the angular momentum in units $\left(\mu^2/M\right)$, and their ratio used in these tables is given by $\mu/M = 10^{-5}$. The relative differences between the total (*i.e.* summed over all modes) outcomes of the three methods is of the order of a tenth of a percent.

5.2.2 The inaccuracy due to the epicycle expansion

Now that the intrinsic inaccuracy has been found to be of the order of 0.1%, any remaining inaccuracy in the gravitational wave is due to the fact that the orbital functions $r(\tau)$ and $\varphi(\tau)$ supplied to the code themselves have an error, as they are given by the epicycle expansion of chapter 2. Typically, when using expansion series, the accuracy of the series is provided by the series itself as the relative size of two subsequent terms is a measure of the convergence of the series. In the case of the epicycle expansion taken to second order, such a measure can only be formulated for the first-order expansion, as a measure for the accuracy to second-order requires a third-order to be calculated as well. However, the accuracy of the second-order epicycle expansion can be compared to the orbital functions as found by a purely numerical solution to the geodesic equations. Indeed, the accuracies so obtained were already listed in tables 3.1, 3.2, 3.3, and 3.4 for a large number of bound geodesic orbits.
Taking the accuracies of the orbital functions to be known, the subsequent question is how these translate to inaccuracies in the Zerilli-Moncrief and Regge-Wheeler functions. Of course, this can be answered again by extrinsic means, *i.e.* by comparing the resulting functions to the ones found when the Zerilli-Moncrief and Regge-Wheeler sources are supplied purely numerically (as is done in the literature). However correct, this is not necessary: the inaccuracy of the Zerilli-Moncrief and Regge-Wheeler functions is directly and straightforwardly related to the inaccuracy of the orbital functions.
Physically, this is because in the derivation of the Zerilli-Moncrief and Regge-Wheeler wave equations it was assumed that the gravitational waves $h_{\mu\nu}$ are small compared to the curvatue of the Schwarzschild spacetime, so as to be able to linearize the Einstein field equations. As a result, a deviation $\Delta\Psi^{lm}_{ZM,RW}$ of the wave function will propagate through the spacetime decoupled from $\Psi^{lm}_{ZM,RW}$ itself (*i.e.* there is no backreaction of the wave function on itself), and, what is more, the dynamics of the deviation will be dictated by exactly the same differential operator as the wave function itself. Putting this mathematically, an inaccuracy Δx^μ in the orbital functions will result in an inaccuracy $\Delta\bar{S}^{lm}_{ZM,RW}$ in the source of the Zerilli-Moncrief and Regge-Wheeler equations,

$$x^\mu(\tau) \to x^\mu(\tau) + \Delta x^\mu(\tau) \qquad \Rightarrow \qquad \bar{S}^{lm} \to \bar{S}^{lm} + \Delta\bar{S}^{lm}, \tag{5.2}$$

which in turn will lead to an inaccuracy $\Delta\Psi^{lm}_{ZM,RW}$ in the wave function which then, due to the fact that the wave equation is linear, will solve a differential equation similar to the Zerilli-Moncrief and Regge-Wheeler equations,

$$\left(-\partial_t^2 + \partial_{r_*}^2 - \bar{V}^l(r)\right)\Delta\Psi^{lm}_{ZM,RW} = \Delta\bar{S}^{lm}. \tag{5.3}$$

This allows the inaccuracy $\Delta\Psi^{lm}_{ZM,RW}$ to be calculated in at least three ways.
One possibility is to use a similar numerical algorithm as was used to solve the Regge-Wheeler and Zerilli-Moncrief wave equations, *i.e.* the Lousto-Price algorithm discussed in Chapter 3. Some modifications to the algorithm need to be made, however, as the inaccuracy Δx^μ will make the source $\Delta\bar{S}_{ZM,RW}$ be of a different form than in Eq. (4.32).

Instead, it will be of the form

$$\Delta\bar{S}^{lm}_{ZM,RW} = G^{lm}(r)\,\delta(r-r_p(t)) + F^{lm}(r)\,\partial_r\delta(r-r_p(t)) + H^{lm}(r)\,\partial_r^2\delta(r-r_p(t))\,, \quad (5.4)$$

due to the fact that a first-order Taylor expansion needs to be made around $\Delta x^\mu = 0$. The appearance of the new term $\propto \partial_r^2\delta(r-r_p(t))$ changes the outcome of the integration of the source over a single grid cell. Indeed, following the methods of Appendix D, it is found that the left hand side of Eq. (4.32) must be supplemented by

$$\begin{aligned} &+ \int_{t_b}^{t_t} dt\ \partial_r^2\left(\frac{H^{lm}(r)}{f(r)}\right)\Bigg|_{r=r_p(t)} \\ &\mp \left(\frac{1}{f(r)}\partial_r\left(\frac{H^{lm}(r)}{f(r)}\right) + \partial_r\left(\frac{H^{lm}(r)}{f^2(r)}\right)\right)\Bigg|_{r=r_p(t_b)} \cdot \frac{1}{1\mp\dot{r}_{*p}(t)}\Bigg|_{t=t_b} \\ &\mp \left(\frac{1}{f(r)}\partial_r\left(\frac{H^{lm}(r)}{f(r)}\right) + \partial_r\left(\frac{H^{lm}(r)}{f^2(r)}\right)\right)\Bigg|_{r=r_p(t_t)} \cdot \frac{1}{1\pm\dot{r}_{*p}(t)}\Bigg|_{t=t_t}\,, \end{aligned} \quad (5.5)$$

in which, as in Section 4.3.3, t_b denotes the time at which the worldline of the test mass enters the cell, t_t the time it leaves the cell; in the first boundary term, the upper/lower sign must be chosen when the worldline enters the cell on the right/left and in the second boundary term the upper/lower sign must be chosen when the worldline leaves the cell on the right/left. With this modification, the Lousto-Price algorithm can be used to calculate the propagation of the inaccuracy $\Delta\Psi^{lm}_{ZM,RW}$.
A second method to solve Eq. (5.3) is by using some expansion series. For instance, using the dimensionless ratio $2M/r$ as the expansion parameter, the wave equation simplifies to lowest order to

$$-\partial_t^2\Delta\Psi^{lm}_{ZM,RW} + \partial_r^2\Delta\Psi^{lm}_{ZM,RW} - \frac{2}{r^2}(\lambda+1)\Delta\Psi^{lm}_{ZM,RW} = \Delta\bar{S}^{lm}_{ZM,RW}\,, \quad (5.6)$$

which can be solved by Green's function methods. It can be noted that this equation applies equally to the original Zerilli-Moncrief and Regge-Wheeler equation and can even serve as the starting point of a novel analytical solution method for the calculation of gravitational waves in a Schwarzschild spacetime. Of course, an expansion in the parameter $2M/r$ is physically one in the curvature of the Schwarzschild spacetime, making this method akin to the Post-Newtonian methods. This would be contrary to the premise of the geodesic deviation method as the latter does not require spacetime to be approximately uncurved; however, for the purposes of estimating the order of magnitude rather that the full solution, this approach suffices[1].

[1]Indeed, in Section 5.3.2 this will be seen explicitly, as there the energy per unit mass as calculated by the Zerilli-Moncrief/Regge-Wheeler formalism will be compared to the outcome obtained by a calculation in an uncurved spacetime (*i.e.* by using the Peters-Mathews equation). Typically, the outcomes agree up to some ten percent, which is enough to make a good estimate of the order of magnitude of the solution.

One last way to estimate the order of magnitude of the inaccuracy $\Delta\Psi^{lm}_{ZM,RW}$ is by making use once more of the fact that the Zerilli-Moncrief/Regge-Wheeler differential equation is linear. As a result of this property, any constant relative difference in the source $\bar{S}_{ZM,RW}$ will yield a constant relative difference in the solution $\Psi^{lm}_{ZM,RW}$ of the exact same size. Thus, once an estimate is made of the maximum error $\Delta\bar{S}^{lm}_{ZM,RW}$ due to the error of the orbital functions, the maximum error in the wave functions follows immediately. It will be this method that will be used to make an order of magnitude estimate of the accuracy of the Zerilli-Moncrief and Regge-Wheeler functions.

In order to do so, the general expressions for the source $\bar{S}^{lm}_{ZM,RW}$ can be used, Eqs. (4.36), (4.37). From this expression it can be seen that the source depends on the radial position $r_p(\tau)$ of the test mass via the various (inverse) powers of r_p and via the presence of the four-velocities u^μ_p. The latter holds true because, as was mentioned already in section 4.4, for geodesic motion the four-velocities are all completely fixed via Eq. (2.9) once the radial position is known. Furthermore, the source depends on the angular position φ_p via the spherical harmonics.
The response of the four-velocities on a relative change of the radial position $r_p(t)$ is that they change by a relative amount of the same order, and so it follows immediately that the source functions $\bar{S}^{lm}_{ZM,RW}$ experience a relative change of this order of magnitude as well. As for the response of the source functions to the introduction of an inaccuracy $\Delta\varphi$ in the angular orbital function φ_p, it needs only be realized that the angular coordinate solely appears as an argument in the spherical harmonics, in which they simply are (complex) exponents. Thus, when

$$\varphi_p \to \varphi_p + \Delta\varphi_p \,, \tag{5.7}$$

it follows by a first-order Taylor expansion that

$$Y^{lm}(\theta, \varphi_p) \to Y^{lm}(\theta, \varphi_p)\,(1 + im\Delta\varphi_p) \;, \tag{5.8}$$

(and likewise for the vectorial and tensorial spherical harmonics) which shows that adding a small *absolute* difference $\Delta\varphi_p$ to the angular position will translate to a *relative* difference in $\bar{S}^{lm}_{ZM,RW}$ of the order of magnitude of $m\,\Delta\varphi_p$.
Combining results, it follows that an order of magnitude estimate for $\Delta\bar{S}_{ZM,RW}/\bar{S}_{ZM,RW}$ is given as the sum of a few times the ratio $(r_p + \Delta r_p)/r_p$ and m times $\Delta\varphi_p$. It will be this rule that will be used to estimate the accuracy of the Zerilli-Moncrief and Regge-Wheeler functions in the examples that follow. As will be seen, for all cases for which the literature provides a quantitative value for the average energy per unit mass and angular momentum per unit mass sent out by these EMRI systems, the rules of estimate prove trustworthy. Finally, as the second-order epicycle expansion was seen in chapter 2 to give radial orbital functions that have an error of a few tenths of percents (at least for all cases considered), the estimate rules predict that the gravitational waves will have an error of this order of magnitude as well. It is for this reason that, as was remarked before, an intrinsic numerical error of the code of the order of tenths of percents will suffice.

5.3 Bound eccentric orbits

5.3.1 An explicit example: $e = 0.1$, $a = 10M$

In the previous section it was argued that the numerical inaccuracy can be made arbitrarily small but that in practice a value of 0.1% will be allowed. The attention will now be turned to bound *eccentric* orbits, which introduces a second source of inaccuracy which is extrinsic to the code as it stems from the fact that the sources of the Zerilli-Moncrief and Regge-Wheeler differential equations are now themselves an approximation. In this section, this inaccuracy will be investigated.
In order to do so, an orbit will be considered that is well studied in the literature and so can be used to compare the epicycle results to those of purely numerical calculations. This orbit is uniquely specified by the following values of the parameters $(e,\ a)$: $e = 0.1,\ a = 10M$. The average power and angular momentum for this orbit are known in the literature to a precision of about nine decimal places. It is therefore well suited to be used as a test of the accuracy of the gravitational waves as based on the epicycle expansion of the orbital functions.
The epicycle expansion of the orbit $(e = 0.1,\ a = 10M)$ was presented to first and to second order in detail in section 3.3.1, where it was found to be an excellent approximation to the real orbit: to second order the relative difference between the radial coordinate r and its numerical counterpart was seen to be 0.05% at most, and the absolute difference between the angular coordinate φ and its numerical counterpart was found to be 0.004 radians at most. These accurate results for the orbital functions suggest that the gravitational waveforms and the resulting power and angular momentum per unit time sent out by the system will be accurate as well. Indeed, the rules of error estimate of the last section predict that the inaccuracy due to the second-order epicycle expansion is of the order of a few tenths of a percent at most.
In order to test this, the Zerilli-Moncrief and Regge-Wheeler contributions are calculated up to mode $l = 4, m = \pm 3$; contributions of higher multipoles only add to the total outcomes (much) less than 0.1% and will therefore be ignored. In fact, the main contributions come from the $l = 2, m = \pm 2$ modes, as is to be expected from the quadrupole nature of free gravitational waves. The average power and angular momentum per unit time contributed by each individual mode are listed in table 5.2. Plots of the Zerilli-Moncrief and Regge-Wheeler functions of the most contributing modes are given in figures 5.1 and 5.2, along with the plots of their resulting power and angular momentum.
In the plots, it can be seen that the power and the angular momentum follow a periodic pattern that has twice the frequency as the bound orbit of the test mass. There is also some distorted data points around $t \approx 510M$, which is around the time the gravitational wave (emitted at $t = 0$ and moving with the speed of light) arrives at the position of the observer (who is located at $r = 500M$, which in tortoise coordinates is around $r_* = 511M$). The distorted data points are the result of the initial conditions taken for the Zerilli-Moncrief and Regge-Wheeler functions at $t = 0$, or, physically, the amount of gravitational waves already present in the system before the bound orbit of the test mass commences. In

making the plots above, both the Zerilli-Moncrief and Regge-Wheeler functions (as well as their derivatives with respect to time) have been taken to be zero at $t = 0$. This is unphysical, because the presence of the test mass indicates that it has either been brought at its starting position from afar, or that it has been in this bound orbit indefinitely, either possibility of which would have produced gravitational waves. Setting these zero implies that the test mass spontaneously came into existence at its starting position, and it is this assumption that produces the distorted data points.
Despite being unphysical, the initial conditions are of little consequence due to the combination of the following two reasons: firstly, the fact that the Zerilli-Moncrief and Regge-Wheeler differential equations are linear means that the initial gravitational wave will propagate to spatial infinity without having an effect on the propagation of the gravitational waves emitted by the EMRI system; secondly, the fact that the effect of the loss of energy and angular momentum on the shape of the orbit is not yet taken into account means that the test mass will move in its bound orbit indefinitely. Thus, the chosen initial

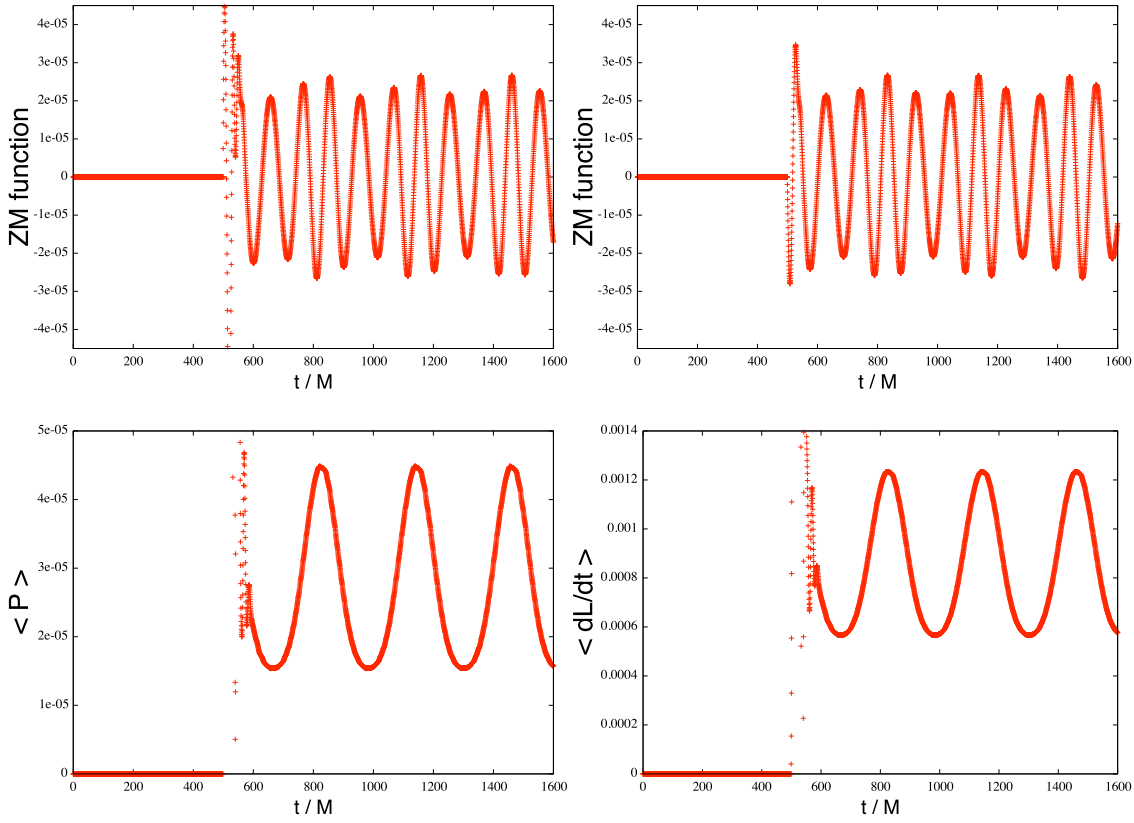

Figure 5.1: Upper: The real (left) and imaginary (right) parts of the $l = 2, m = 2$ mode of the Zerilli-Moncrief function as a function of Schwarzschild time t for the case of an orbit $(a,\, e) = (10M,\, 0.1)$. Lower: The power (left) and time derivative of the angular momentum (right) emitted by this mode, as a function of Schwarzschild time t. The observer is situated at $r = 500M$. In this plot, the mass of the black hole was taken to be $M = 10$, and the mass ratio was taken to be $(\mu/M) = 10^{-5}$.

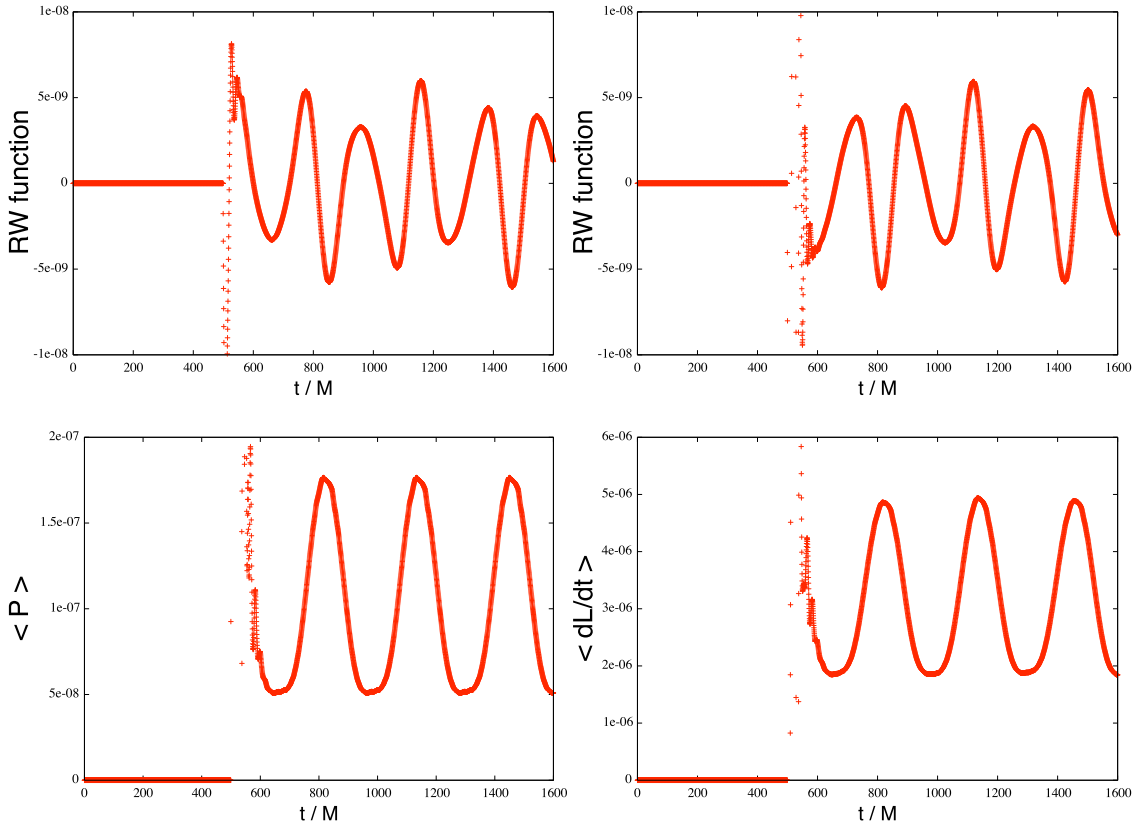

Figure 5.2: Upper: The real (left) and imaginary (right) parts of the $l = 2, m = 1$ mode of the Regge-Wheeler function as a function of Schwarzschild time t for the case of an orbit $(a,\, e) = (10M,\, 0.1)$. Lower: The power (left) and time derivative of the angular momentum (right) emitted by this mode, as a function of Schwarzschild time t. The observer is situated at $r = 500M$. In this plot, the mass of the black hole was taken to be $M = 10$, and the mass ratio was taken to be $(\mu/M) = 10^{-5}$.

condition for the Zerilli-Moncrief and Regge-Wheeler functions will have ample time to propagate away from the system and hence remove themselves from the results. Indeed, in the plots, the distorted data points have vanished around the time $t \approx 600M$. In all other examples of this chapter, the same assumption will be made.
Adding all contributions listed in table 5.2 gives the following values for the average power and angular momentum emitted per unit time

$$< P > = 6.294 \cdot 10^{-5} \left(\frac{\mu}{M}\right)^2 , \qquad < \dot{L} > = 1.949 \cdot 10^{-3} \left(\frac{\mu^2}{M}\right), \tag{5.9}$$

which are in good agreement with the values obtained by the purely numerical calculations of [40], [41]:

$$< P > = 6.318 \cdot 10^{-5} \left(\frac{\mu}{M}\right)^2 , \qquad < \dot{L} > = 1.953 \cdot 10^{-3} \left(\frac{\mu^2}{M}\right), \tag{5.10}$$

mode	$\langle P \rangle$	$\langle \dot{L} \rangle$
$l = 2, \lvert m \rvert = 2$	$5.492 \cdot 10^{-5}$	$1.703 \cdot 10^{-3}$
$l = 2, \lvert m \rvert = 1$	$2.045 \cdot 10^{-7}$	$6.262 \cdot 10^{-6}$
$l = 3, \lvert m \rvert = 3$	$6.730 \cdot 10^{-6}$	$2.067 \cdot 10^{-4}$
$l = 3, \lvert m \rvert = 2$	$5.216 \cdot 10^{-8}$	$1.583 \cdot 10^{-6}$
$l = 4, \lvert m \rvert = 4$	$1.033 \cdot 10^{-7}$	$3.134 \cdot 10^{-5}$
$l = 4, \lvert m \rvert = 3$	$9.915 \cdot 10^{-9}$	$2.982 \cdot 10^{-7}$
total	$6.294 \cdot 10^{-5}$	$1.949 \cdot 10^{-3}$

Table 5.2: Average power and angular momentum emitted in gravitational waves by a system of a star of mass μ in a bound orbit of eccentricity $e = 0.1$ and semi-major axis $a = 10M$ around a black hole, per mode (l, m) as listed in the first column (where $|m|$ denotes the sum of the two modes $\pm m$). The second column presents the power in the second order epicycle approximation, whereas the third column presents the average angular momentum. The powers are given in units $(\mu/M)^2$, the derivative of the angular momenta in units (μ^2/M). The ratio of these masses is taken to be $(\mu/M) = 10^{-5}$.

the relative differences being a mere 0.4% and 0.2%, respectively.
In making the plots and calculating the power and angular momentum, the cell size has been chosen small enough for the power and angular momentum not to change anymore when going to even smaller cell size. From this it can be concluded that the 0.4% and 0.2% deviations found are solely due to the epicycle approximation. This is in good agreement with the expectation.

5.3.2 Power emitted for $e = 0.1$, various a

Having investigated the accuracy of the method used, the average powers of a series of examples can now be calculated. The examples considered in this section will be those presented before in section 3.3, *i.e.* a series of bound geodesic orbits with a fixed eccentricity $e = 0.1$ and decreasing value of the semi-major axis a, all the way to the orbit at $a = 66$ that has its periastron grazing the ISCO. The accuracy of the epicycle expansions was presented in table 3.1; additional details of the orbits can be found in Appendix C.
Table 5.3 presents in the second and third columns the average power $< P >_{epicycles}$ as calculated by the epicycle expansion and numerical algorithm. Finally, for comparison, the last column shows the average power $< P >_{PM}$ as calculated with the Peters-Mathews equation. In all cases, the size Δ of the cells of the spacetime was chosen such that setting a smaller size still would have no effect on the power at the level expected by the error of the epicycle expansion. In this way, the errors in the results for the power are purely due to the error of the epicycle expansions. Using the error estimate rules, the inaccuracy of the epicycle results is of the order of a percent or less.
As can be seen, both at large distances and close to the ISCO, the power computed by the epicycle procedure exceeds that of the Newtonian approximation, while in intermediate regions the power is lower. This can be understood by the opposite effect of two factors:

on the one hand the precession of the periastron shows that the orbital velocity and acceleration in the relativistic orbit is higher than that in the Newtonian orbit; on the other hand, in the relativistic case the redshift of the gravitational waves lowers the power as measured by a distant observer.

a/M	$\langle P \rangle_{epicycle}$	$\langle P \rangle_{PM}$	rel. diff.
20.0	$2.033 \cdot 10^{-6}$	$2.033 \cdot 10^{-6}$	< 0.1 %
15.0	$8.139 \cdot 10^{-6}$	$8.555 \cdot 10^{-6}$	-5.1%
10.0	$6.294 \cdot 10^{-5}$	$6.496 \cdot 10^{-5}$	-3.2%
9.0	$1.083 \cdot 10^{-4}$	$1.100 \cdot 10^{-4}$	-1.6%
8.5	$1.475 \cdot 10^{-4}$	$1.464 \cdot 10^{-4}$	-0.5%
8.0	$1.991 \cdot 10^{-4}$	$1.983 \cdot 10^{-4}$	$+0.4\%$
7.5	$2.944 \cdot 10^{-4}$	$2.738 \cdot 10^{-4}$	$+7.6\%$
7.0	$4.209 \cdot 10^{-4}$	$3.865 \cdot 10^{-4}$	$+8.9\%$
6.6	$5.869 \cdot 10^{-4}$	$5.187 \cdot 10^{-4}$	$+13\%$

Table 5.3: Average power $\langle P \rangle$ emitted in gravitational waves by a system of a star of mass μ in a bound orbit of eccentricity $e = 0.1$ around a black hole of mass M for various values of a, as listed in the first column. The second column presents the power in the second-order epicycle approximation, whereas the third column presents the power as calculated by the Peters-Mathews equation. The third column presents the relative difference in percents. All powers are computed to a numerical accuracy of the level of 0.1% and are stated in units $(\mu/M)^2$. The ratio of the masses is taken to be $(\mu/M) = 10^{-5}$.

5.3.3 Higher eccentricities

As a next example, the energy per unit mass and angular momentum per unit mass will be calculated for an EMRI system that has an eccentricity of the order of $e = 0.2$. For such bound orbits, the second-order epicycle expansion was seen in chapter 2 to be an order of magnitude less accurate than for the orbits with an eccentricity of $e = 0.1$. Indeed, table 3.4 showed that the maximum relative difference in the radial coordinate was about half of a percent, whereas the maximum absolute difference in the angular coordinate is about 0.2 radians and usually much less. By the error estimate rules of section 5.2.2, it is expected that the resulting gravitational waves (and the energy per unit mass and angular momentum per unit mass they take away from the system) will be mostly off due to the inaccuracy of the angular coordinate, and is expected to be of the order of percents to a few tens of percents. This would make the second-order epicycle expansion considerably less accurate to describe gravitational waves in EMRI systems of eccentricity 0.2 than of eccentricity 0.1.
This will now be demonstrated explicitly by considering a bound orbit with semi-major axis $a = 7.50478M$ and eccentricity $e = 0.188917$, as this is one of the cases for which the literature states the purely numerically calculated values for the energy per unit mass and angular momentum per unit mass.

By the methods of section 2.2, the physical characteristics (energy per unit mass ε, angular momentum per unit mass ℓ, the periastron r_{pa}, the apastron r_{aa}, periastron shift $\delta\varphi$ and proper time between two successive periastra $\Delta\tau$) are given by

$$\varepsilon = 0.9483, \quad \ell = 3.55M, \quad r_{pa} = 6.312M, \quad r_{aa} = 9.253M, \quad \delta\varphi = 7.92, \quad \Delta\tau = 232.3M\,, \tag{5.11}$$

and by the methods of section 3.2, the epicycle parameters $(R, \sigma, \Delta_n, \Delta_m)$ needed for the most accurate second-order epicycle approximation are found to be

$$R = 7.9876M, \qquad \sigma = -0.31103M, \qquad \Delta_n = -2.8862, \qquad \Delta_m = -21.9232\frac{1}{M}\,, \tag{5.12}$$

yielding the second-order epicycle expansions

$$\begin{aligned} t(\tau) &= 1.2843\,\tau + 2.2008M\sin\left((\omega+\sigma\omega_1)\tau\right) + 0.14769M\sin\left(2(\omega+\sigma\omega_1)\tau\right), \\ r(\tau) &= 7.8249M - 1.47025M\cos\left((\omega+\sigma\omega_1)\tau\right) - 0.042359M\cos\left(2(\omega+\sigma\omega_1)\tau\right), \\ \varphi(\tau) &= 0.0611436\frac{\tau}{M} + 0.572787\sin\left((\omega+\sigma\omega_1)\tau\right) + 0.042723\sin\left(2(\omega+\sigma\omega_1)\tau\right), \end{aligned} \tag{5.13}$$

in which the frequencies are given by

$$\omega = 0.02796\frac{1}{M}\,, \qquad \sigma\omega_1 = -0.000916\frac{1}{M}\,, \qquad \omega + \sigma\omega_1 = 0.02704\frac{1}{M}\,. \tag{5.14}$$

The accuracy of this second-order epicycle expansion is of the same order of magnitude as the orbits in table 3.4: the maximum relative difference of the radial function compared to its numerical counterpart is 0.18%, and the maximum absolute difference of the angular function with its numerical counterpart is 0.29 radians. Figure 5.3 presents the comparison of the second-order epicycle approximations to the purely numerical orbital functions.

The error estimate rules then state that, indeed, there will be an error in the power and angular momentum of the order of tens of percents, and that this will be most dominantly due to the inaccuracy of the angular coordinate. This can be confirmed when the power and angular momentum are calculated by the methods of chapter 4; this is done for all modes up to $(l, m) = (4, \pm 3)$. The resulting power and angular momentum are stated per mode in table 5.4; the Zerilli-Moncrief function and Regge-Wheeler function that contributes most to the total outcomes are shown in figures 5.4, 5.5 along with the power and angular momentum they carry as a function of time. Adding the contributions in the table gives the total average energy per unit mass and angular momentum per unit mass sent out by the system per unit time

$$< P > = \; 2.6534 \cdot 10^{-4} \left(\frac{\mu}{M}\right)^2, \qquad\qquad < \dot{L} > = \; 5.4782 \cdot 10^{-3} \left(\frac{\mu^2}{M}\right), \tag{5.15}$$

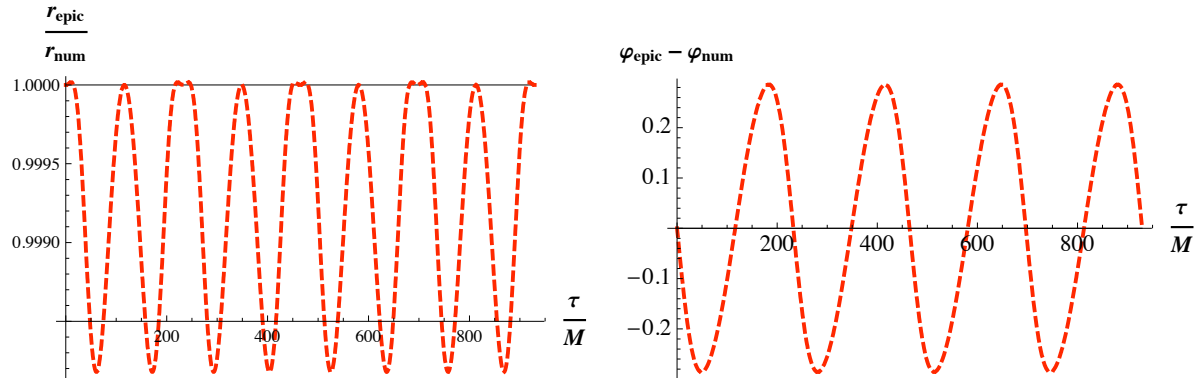

Figure 5.3: Left: The radial function $r(\tau)$ in epicycle approximation up to second order, divided by the numerical one, as a function of proper time τ. Right: The angular function $\varphi(\tau)$ in radians as given by the epicycle approximation up to second order, minus the numerical one, as a function of proper time τ.

mode	$\langle P \rangle$	$\langle \dot{L} \rangle$
$l = 2, \lvert m \rvert = 2$	$2.2200 \cdot 10^{-4}$	$4.5827 \cdot 10^{-3}$
$l = 2, \lvert m \rvert = 1$	$1.1332 \cdot 10^{-6}$	$2.3560 \cdot 10^{-5}$
$l = 3, \lvert m \rvert = 3$	$3.4911 \cdot 10^{-5}$	$7.2113 \cdot 10^{-4}$
$l = 3, \lvert m \rvert = 2$	$3.6867 \cdot 10^{-7}$	$7.6500 \cdot 10^{-6}$
$l = 4, \lvert m \rvert = 4$	$6.8352 \cdot 10^{-6}$	$1.4124 \cdot 10^{-4}$
$l = 4, \lvert m \rvert = 3$	$8.9265 \cdot 10^{-8}$	$1.8502 \cdot 10^{-6}$
total	$2.6534 \cdot 10^{-4}$	$5.4782 \cdot 10^{-3}$

Table 5.4: Average power and angular momentum emitted in gravitational waves by a system of a star of mass μ in a bound orbit of eccentricity $e = 0.188917$ and semi-major axis $a = 7.50478M$ around a black hole, per mode (l, m) as listed in the first column (where $|m|$ denotes the sum of the two modes $\pm m$). The second column presents the power in the second order epicycle approximation, whereas the third column presents the average angular momentum. The powers are given in units $(M/\mu)^2$ and the angular momenta in units (M/μ^2). The mass ratio was taken to be $(\mu/M) = 10^{-5}$.

whereas the purely numerical results state

$$< P > = \; 3.1770 \cdot 10^{-4} \left(\frac{\mu}{M}\right)^2, \qquad < \dot{L} > = \; 5.9329 \cdot 10^{-3} \left(\frac{\mu^2}{M}\right). \tag{5.16}$$

The relative differences are about 19% and 8%, respectively, which is of the expected order of magnitude.
From this example, it can be concluded that the epicycle expansion taken to second order does not suffice to accurately calculate the gravitational waves emitted by an EMRI system when the eccentricity is of the order of 0.2: the inaccuracy of the angular orbital function causes the source of the Zerilli-Moncrief and Regge-Wheeler functions to be off by a few tens of percents, leading to inaccuracies in the emitted energy per unit mass and angular momentum per unit mass that are of the same order of magnitude. As discussed at the

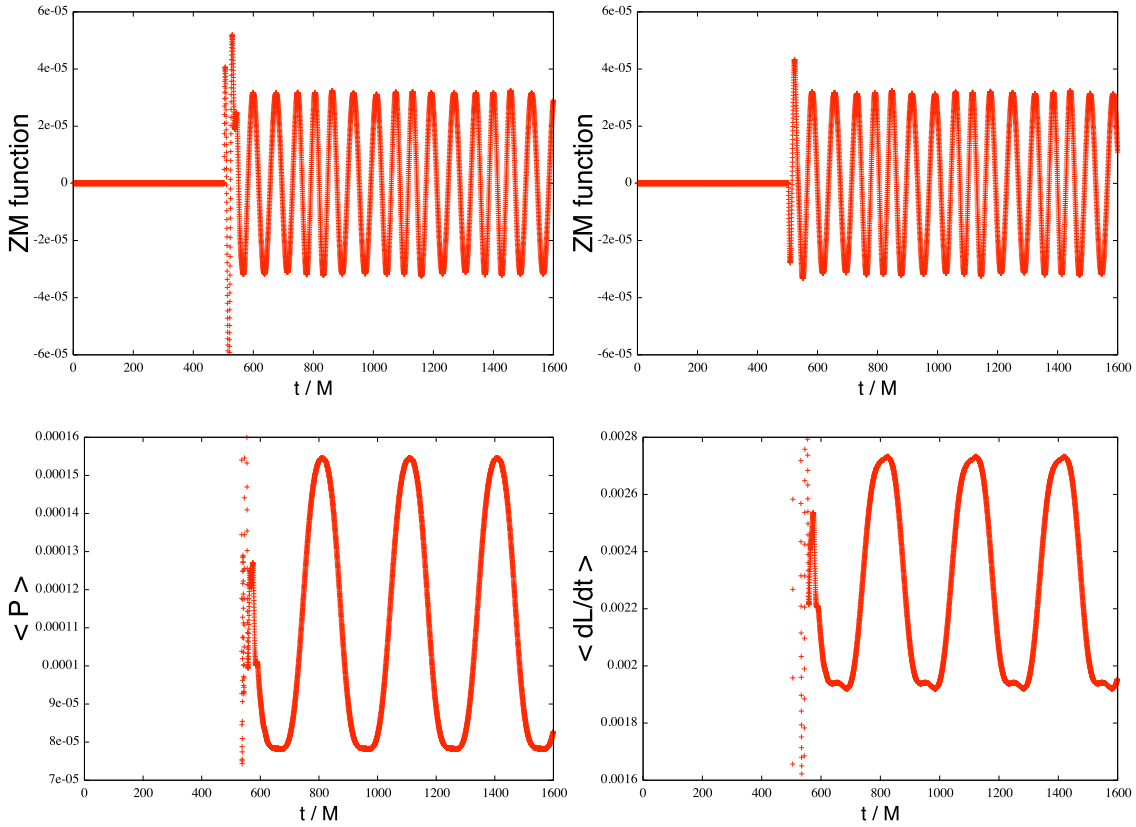

Figure 5.4: Upper: The real (left) and imaginary (right) parts of the $l = 2, m = 2$ mode of the Zerilli-Moncrief function as a function of Schwarzschild time t for the case of an orbit $(a, e) = (7.50478M, 0.188917)$. Lower: The power (left) and time derivative of the angular momentum (right) emitted by this mode, as a function of Schwarzschild time t. The observer is situated at $r = 500M$. In this plot, the mass of the black hole was taken to be $M = 10$, and the mass ratio was taken to be $(\mu/M) = 10^{-5}$.

end of section 3.5, this can be remedied by sacrificing one boundary condition on the radial coordinate in favor of one on the angular coordinate, but it is preferable to better constrain both the radial coordinate and the angular coordinate by adding another (*i.e.* third or higher) order to the epicycle expansion with the methods of chapter 2.

5.4 Gravitational waves from an EMRI system with radiative self force

The examples of the last section showed that the combination of the second-order epicycle expansion and the Regge-Wheeler/Zerilli-Moncrief formalism yields accurate results for the gravitational waves and the energy per unit mass and angular momentum per unit mass emitted by an EMRI system, as long as the eccentricity of the bound orbit is taken to be

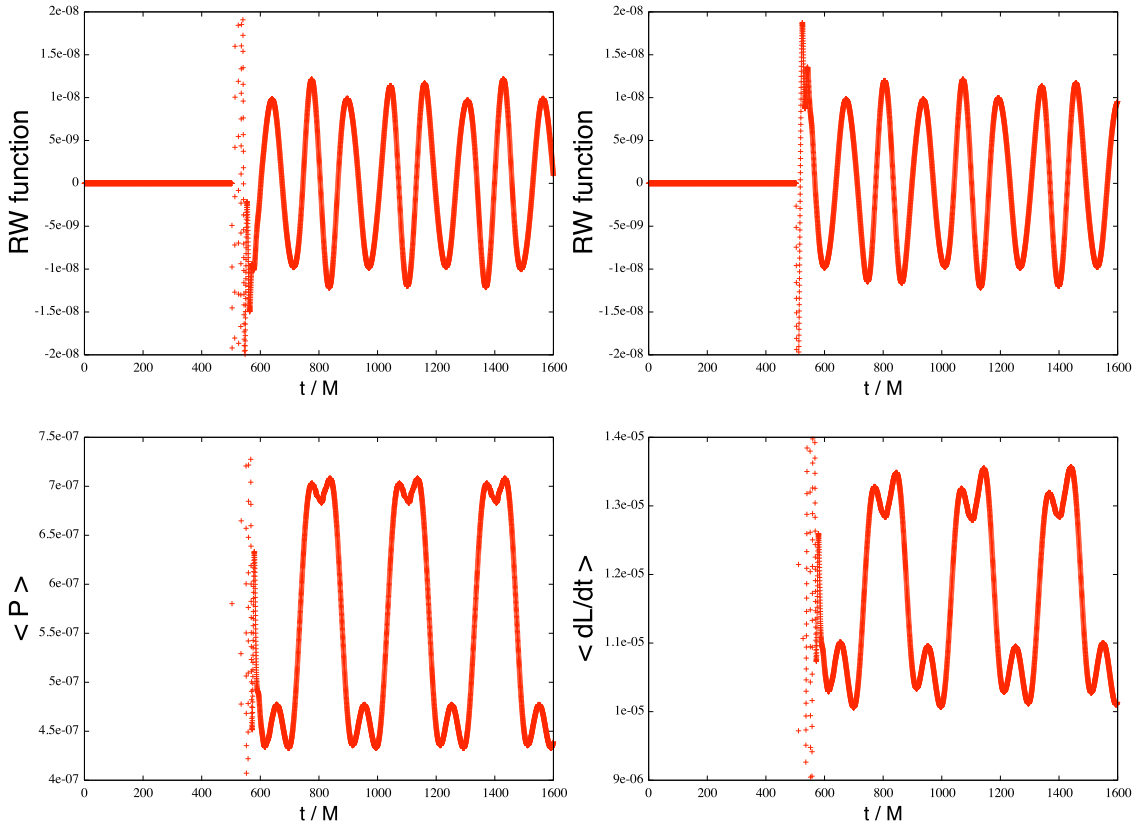

Figure 5.5: Upper: The real (left) and imaginary (right) parts of the $l = 2, m = 1$ mode of the Regge-Wheeler function as a function of Schwarzschild time t for the case of an orbit $(a, e) = (7.50478M, 0.188917)$. Lower: The power (left) and time derivative of the angular momentum (right) emitted by this mode, as a function of Schwarzschild time t. The observer is situated at $r = 500M$.In this plot, the mass of the black hole was taken to be $M = 10$, and the mass ratio was taken to be $(\mu/M) = 10^{-5}$.

limited (*i.e.* of the order of 0.1). It also showed that higher eccentricities (*i.e.* of the order of 0.2) still yield reasonably accurate results for the orbits, but not for the gravitational waves and the emitted energy per unit mass and angular momentum per unit mass. It has been argued several times throughout this thesis that this is not a drawback of the epicycle expansion, as the condition of small eccentricity is naturally fulfilled in all but the most extreme natural cases. This is due to *circularisation*: under the emission of gravitational waves, eccentric geodesic orbits tend to become increasingly less eccentric. This is effectively because gravitational waves do not only carry away energy from the binary system, but also angular momentum.

Circularization has been studied generally in Ref. [46] and is found in Post-Newtonian calculations as well as purely numerical calculations. It can also be demonstrated within the fully relativistic context of the epicycle expansion scheme, and this is what will be done next. It serves not only to demonstrate that bound geodesic orbits circularize under emission of gravitational waves, but also as the major justification of the practical utility

a/M	e	$< P >$	$< \dot{L} >$	$\Delta a/a$	$\Delta e/e$	$\Delta t/\mu$	max.rel.diff. r	max.abs.diff. φ
12.00	0.1500	$2.536 \cdot 10^{-5}$	$0.996 \cdot 10^{-3}$	n.a.	n.a.	n.a.	0.20%	0.0085
11.64	0.1447	$2.951 \cdot 10^{-5}$	$1.125 \cdot 10^{-3}$	3.1%	3.7%	$4.021 \cdot 10^{11}$	0.18%	0.0080
11.28	0.1410	$3.451 \cdot 10^{-5}$	$1.258 \cdot 10^{-3}$	3.2%	2.6%	$3.526 \cdot 10^{11}$	0.16%	0.0080
10.93	0.1378	$4.051 \cdot 10^{-5}$	$1.410 \cdot 10^{-3}$	3.2%	2.4%	$3.121 \cdot 10^{11}$	0.15%	0.0081
10.58	0.1349	$4.785 \cdot 10^{-5}$	$1.589 \cdot 10^{-3}$	3.3%	2.2%	$2.756 \cdot 10^{11}$	0.14%	0.0083
10.23	0.1322	$5.683 \cdot 10^{-5}$	$1.794 \cdot 10^{-3}$	3.4%	2.0%	$2.423 \cdot 10^{11}$	0.13%	0.0087
9.87	0.1300	$6.774 \cdot 10^{-5}$	$2.039 \cdot 10^{-3}$	3.6%	1.8%	$2.123 \cdot 10^{11}$	0.12%	0.0094
9.52	0.1287	$8.193 \cdot 10^{-5}$	$2.326 \cdot 10^{-3}$	3.7%	1.0%	$1.850 \cdot 10^{11}$	0.11%	0.011
9.16	0.1273	$9.853 \cdot 10^{-5}$	$2.661 \cdot 10^{-3}$	3.9%	1.1%	$1.604 \cdot 10^{11}$	0.11%	0.013

Table 5.5: A series of eccentric orbits parametrized by a and e, as listed in the first two columns. The orbits are related by the emission of gravitational waves in an adiabatic way, as explained in the main text. The average power emitted is given in the third column in units $(\mu/M)^2$, and the average angular momentum emitted per unit time is given in the fourth column in units $\left(\mu^2/M\right)$. The fifth and sixth columns list the percentual change in a and e compared to the next larger orbit, showing explicitly the inspiral and circularization due to the emission of gravitational waves. The seventh column presents the Schwarzschild time taken to make the discrete step from the previous orbit to the current. The eighth column presents the maximum relative difference between the second-order epicycle radial orbital function $r(\tau)$ and its numerical counterpart; the last column presents the maximum absolute difference between the second-order epicycle angular orbital function $\varphi(\tau)$ and its numerical counterpart. The mass ratio was taken to be $(\mu/M) = 10^{-5}$.

of the epicycle expansion.
The calculation of the emitted power and angular momentum per unit time for a series of eccentric orbits that are adiabatically related to each other by the emission of gravitational radiation proceeds as follows. The average emitted power and angular momentum for each given eccentric orbit is calculated by the second-order epicycle expansion and numerical code, and these values are subsequently used to update the values of ε and ℓ in a discrete step; the newly found values for ε and ℓ then correspond to the next orbit in the series. The discrete step is chosen as follows: the next orbit will always be chosen to be the one that has a value ℓ that is 1% smaller than that of the current orbit. In this way, it is found in practice that successive orbits have a percentual change in periastra of less than 4%, which justifies the adiabatic approximation. The results are shown in table 5.5. As before, the size of the grid was chosen such that the values for $< P >$ and $< \dot{L} >$ do not change more than at the 0.1% level, and the estimate rules of section 5.2.2 state that the found values are accurate to the order of a percent.
Although in this example the amount of successive orbits is limited and the results are accurate to the order of a percent, this suffices to conclude that circularization takes place. Indeed, figure 5.6 depicts the decrease of the eccentricity e as a function of time, and shows that it does so nearly linearly, at least on the timescale considered. At the same time, the right panel of the plot shows that also the semi-major axis a decreases and that it does so exponentially. This indicates that, at least for the case considered, the test mass quickly reaches the ISCO of the black hole and has, by comparison, little time to circularize. However, as was shown explicitly in chapter 2, the accuracy of the second-order

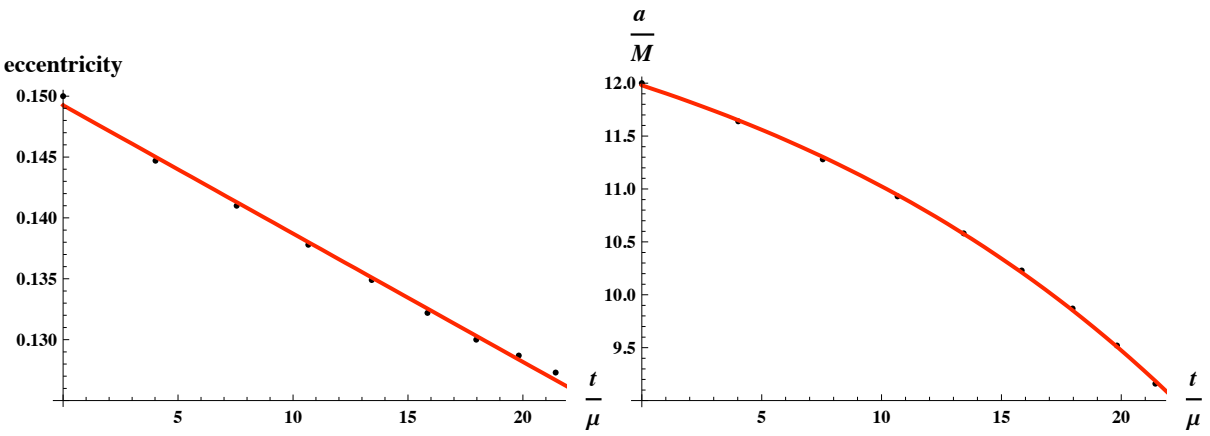

Figure 5.6: Left: the evolution of the eccentricity e of the adiabatically related bound orbits, as explained in the main text, as a function of Schwarzschild time t/μ. The best linear fit of the data points is given by $0.14925 - 0.001054 \cdot t/\mu$. Right: the evolution of the semi-major axis a/M of the adiabatically related bound orbits, as explained in the main text, as a function of the Schwarzschild time t/μ. The best exponential fit of the data points is given by $13.505 - 14.25 \cdot \exp(0.0486\, t/\mu)$. In both plots, the time t/μ is measured in units 10^{11}.

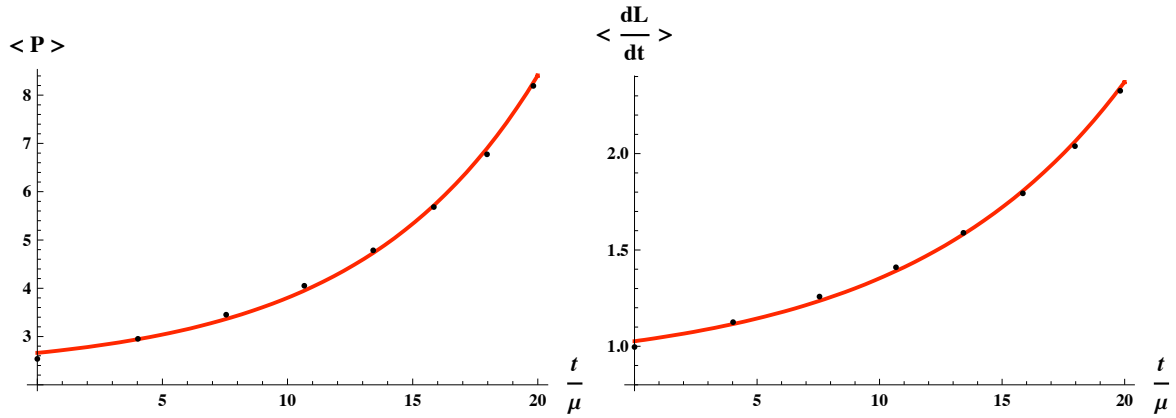

Figure 5.7: Left: the evolution of the average power $< P >$ of the adiabatically related bound orbits, as explained in the main text, as a function of Schwarzschild time t. The best exponential fit of the data points is given by $2.283 + 0.3766 \cdot \exp(0.1395\, t/\mu)$, and $< P >$ is given in units $10^{-5}\,(\mu/M)^2$. Right: the evolution of the average time derivative $< dL/dt >$ of the adiabatically related bound orbits, as explained in the main text, as a function of the Schwarzschild time t/μ. The best exponential fit of the data points is given by $0.8726 + 0.1536 \cdot \exp(0.1139\, t/\mu)$, and $< dL/dt >$ is given in units $10^{-3}\,(\mu^2/M)$. In both plots, the time t/μ is measured in units 10^{11}.

epicycle expansion suffers only little from a close proximity to the black hole, and hence the fact that the decrease of the semi-major axis proceeds more rapidly than the process of circularization is of little consequence on the accuracy of the expansion.
Rather, the epicycle expansion is expected to become increasingly accurate for successive orbits, and indeed this is seen to be the case. To wit: the radial orbital function r becomes

almost twice as accurate in the course of the orbits considered. In contrast, the angular coordinate φ does not improve in accuracy, but instead remains mostly fixed. An increase in angular accuracy was not to be expected. This is because the second-order epicycle expansion allows for four boundary conditions to restrict the orbital functions, two of which are needed to make sure successive periastra are reached in a given time interval and with a given value for the periastron shift, leaving only two boundary conditions to restrict the orbital functions r and φ. In the calculation presented, these remaining two boundary conditions were used to fix the values of the radial positions of the periastron and apastron, which in practice also makes the orbital function φ very accurate, but a priori does not guarantee that this accuracy increases with decreasing eccentricity. Indeed, the table shows that the absolute difference between the orbital function φ as calculated by the second-order epicycle expansion and its purely numerically calculated counterpart, is around the value of 0.008 radians. For almost all practical applications, this accuracy is excellent.
Finally, the fact that the semi-major axis decreases under influence of the emission of gravitational waves suggests (for example by assuming the Peters-Mathews equation, Eq. (1.46), to give reasonably accurate results in the Schwarzschild spacetime, as was quantitatively demonstrated in section 5.3.2) that the emission of energy will increase exponentially. This is indeed the case, and likewise so for the angular momentum, as can be seen in figure 5.7.

5.5 Summary

In this chapter, the methods developed throughout this thesis have been used to calculate gravitational waves for bound eccentric orbits in an EMRI system. A number of test cases were investigated first: by calculating the average power and angular momentum emitted by an EMRI with a perfectly circular orbit and comparing the outcomes to those stated in the literature, the correct working of the code was confirmed. It was seen that the intrinsic numerical error could effortlessly be made of the order of 0.1% and smaller still. Next, the error due to the fact that the epicycle expansion is an approximation itself, was quantified. This rule was tested by calculating the average power and angular momentum emitted by an EMRI system for one specific well-known eccentric orbit. It was found that here too the results agree well with those stated in the literature, with a relative difference of the order of 0.1%; this was in agreement with the error estimate rule.
The methods were then used to straightforwardly calculate the gravitational waves for a number of orbits of eccentricity 0.1% that were not known in the literature, all of which have a total error (*i.e* intrinsic and extrinsic) of the order of 0.1% to a percent. The results for the powers were compared to the ones obtained by using the Peters-Mathews equation, showing, as expected, good agreement when the orbit has a semi-major axis much greater than the typical size of the black hole. Closing in, however, the Peters-Mathews equation becomes less accurate due to the interplay of two opposing relativistic effects: the true orbit has a greater quadrupole moment due to the periastron shift than expected on the basis of a Newtonian premise, whereas the curvature of spacetime gives the emitted grav-

itational waves a gravitational redshift that decreases the energy as measured at infinity. The former effect becomes dominant when in close proximity to the black hole, making the Peters-Mathews equation underestimate the power in gravitational waves by about ten percent in the case investigated.
The gravitational waves due to a bound orbit of eccentricity $e = 0.1889$ was investigated as well, and it was found that the epicycle error in the angular coordinate makes the accuracy of the emitted power and angular momentum significantly less than in the $e \approx 0.1$ case. This was seen to be due to the strong dependence of the spherical harmonics on the error in the angular coordinate.
Finally, the effect of the emission of gravitational waves on the shape of the bound orbits was investigated. It was found that, due to the loss of energy and angular momentum, the orbits circularize, *i.e.* they become increasingly less eccentric. This not only justified the use of the epicycle expansion in the first place, but it was also explicitly shown that the resulting orbits naturally become more and more accurate under the emission of gravitational waves.

Chapter 6

Conclusions & outlook

This thesis concerned the fully relativistic calculation of bound geodesic motion in EMRI systems and the resulting gravitational waves, with the aid of the geodesic deviation method. This last chapter summarizes the methods as explained in detail in the previous chapters, lists the conclusions of the thesis, and presents a number of directions of possible future research.

The geodesic deviation method provides a way to calculate geodesics in an expansion scheme that does not assume that gravity is weak. Rather, it takes all relativistic effects into full account, so that the outcomes should be accurate regardless of high velocities or strong gravitational fields. It assumes the initial geodesics to be simple (*i.e* meaning that they can be written down in analytical form as a function of time) and complements this with small deviations in order to find the more general geodesics as a function of time.
This method can be applied to many physical systems, by which is meant several background spacetimes and several simple geodesics as starting point of the expansion. In this thesis, the emphasis has been on the physical system of an EMRI: a heavy non-spinning central mass (called the black hole throughout this thesis) around which a smaller companion star is in bound orbit. Because of the high mass-ratio of the black hole and the companion star, the background spacetime can be taken to be Schwarzschild, and as starting geodesic a circular orbit was taken because this is the simplest bound orbit that can be written as an explicit function of time, and because all bound eccentric geodesic motion around a Schwarzschild black hole becomes increasingly circular due to the emission of gravitational waves. The result gives rise to the epicycle expansion: bound geodesic motion around a Schwarzschild black hole can be approximated by adding periodic and secular contributions to a perfectly circular orbit, in which the eccentricity of the orbit is related to the expansion parameter.
The periodic contributions were studied in the literature before, but the secular contributions have always been omitted because they were not thought to have any physical significance. In this thesis, however, it was shown that the secular contributions are needed to make the approximation already accurate at first order. More specifically: it was shown that the inclusion of secular contributions amounts to one extra constant of integration

with every next order added to the expansion, allowing for one extra boundary condition to constrain the resulting orbit. In the first-order expansion, this already gives enough constants of integration to make sure the resulting bound orbit is properly synchronized with the exact geodesic that is approximated; omission of the secular term always results in a lag, and makes the description of bound geodesic orbits considerably less accurate.
Going to higher orders, the inclusion of secular contributions were seen to have the mathematical complication to lead to Poincaré resonances when solving the geodesic deviation equations. These were removed by applying the Poincaré-Lindtsted method and the result was an expansion series for bound geodesics that, by construction, solves the geodesic equations, the geodesic deviation equations, and has a four-velocity that is properly normalized. The results given in previous literature are thus shown to be only a special and limited case of the most general expressions presented here.
In this thesis, the epicycle expansion has been pursued to second order. In practice, this allows for four boundary conditions to constrain the orbit, two of which are used to make the resulting orbit be synchronized with the true geodesic, and two of which are used to fix the radial distances of the periastron and apastron of the orbit. As such, the second order epicycle expansion was seen to produce accurate approximations to the radial distance between black hole and the companion star if the eccentricity of the orbit was small.
For example, if the eccentricity is around 0.1, the relative difference between epicycle approximation and the numerically calculated radial coordinate is typically a tenth to a hundredth of a percent. The angular coordinate was seen to be excellently approximated as well, with the absolute difference between epicycle approximation and the numerically calculated angular coordinate being typically of the order of a hundredth to a thousandth of a radian. As expected, it was seen that the accuracy does not suffer from close proximity to the black hole. Orbits of higher eccentricity are less well approximated by the second-order epicycle expansion: increasing the eccentricity by a factor of two decreases the accuracy of the second-order epicycle approximation by an order of magnitude.
The epicycle expansions were subsequently used to calculate the gravitational waves emitted by the EMRI system. This was done by using the Zerilli-Moncrief/Regge-Wheeler formalism to derive differential equations that have the two polarizations of the gravitational waves as their solutions. The sources of these differential equations require the orbits to be known as analytical functions of time, and because such expressions are given by the epicycle expansion, this thesis presented analytical functions for the sources for the first time.
However, solving the Zerilli-Moncrief and Regge-Wheeler differential equations is a task that still needed to be done numerically. For this, a numerical program has been implemented in the language C++, allowing for the calculation of gravitational waves produced in the EMRI system and the energy and angular momentum they carry away from the system. The code principally can produce outcomes of any desired accuracy, but as the epicycle approximation has a finite accuracy itself, outcomes were calculated accurate to 0.1% level. It was found that the epicycle approximated outcomes agree to this accuracy level with the purely numerical ones stated in literature for all cases considered in which the second order epicycle expansion is justified. Outcomes for new cases of such eccentric-

ity were calculated effortlessly and rapidly.
For bound orbits of eccentricity around 0.2, the gravitational waves yield values for the emitted energy and angular momentum per unit mass that have an error of the order of percents to tens of percents, and this was seen to be mainly due to the inaccuracy of the angular coordinate as given by the second-order epicycle expansion.
Finally, it was studied how the emission of gravitational waves changes the bound orbits, by using the calculated values for the emitted energy and angular momentum to update the parameters that uniquely specify the orbit. This was done in an adiabatic way, by updating the orbital parameters in discrete steps small enough to justify this approximation. It was found that orbits become smaller (to which the accuracy of the epicycle expansion is very much resistant) and circularize (which makes the epicycle expansion more accurate). To conclude, the epicycle expansion developed in this thesis is very well suited to describe bound orbits around a Schwarzschild black hole, as its accuracy is virtually independent of relativistic effects due to close proximity of the star to the black hole, and the emission of gravitational waves naturally leads to orbits of small eccentricity for which the epicycle expansion is well-justified and yields excellent results.

There are several directions for future research foreseeable. For instance, the epicycle expansion can be taken to third or higher order. Considering the previous conclusion about the high accuracy of the second-order epicycle expansion and the fact that bound motion naturally becomes more circular, this does not seem a priority for practical purposes. There are, however, at least two other motivations to do so. Firstly, the second-order epicycle expansion allows for boundary conditions to constrain the resulting orbit, which are used to synchronize the resulting orbit to the true geodesic and to fix the radial distances between successive periastra, but do not yet guarantee that the angular coordinate is accurate between periastra as well. In practice it was found that the angular coordinate is well-approximated already at second order by the boundary conditions on the radial coordinate for orbits with eccentricities of about 0.1, but it can be guaranteed by adding third- or higher-order terms in the epicycle expansion by using the resulting extra constants of integration to fix the value of the angular coordinate at apastron. This would also greatly increase the accuracy of the gravitational waves calculated using the epicycle expansion. Secondly, in this thesis the accuracy of the second-order epicycle expansions was quantified by comparing the orbits to the ones calculated by purely numerical means; adding third- or higher-order terms allows a measure of accuracy of the expansion that is intrinsic. Thus, in order to be able to accurately approximate bound orbits of eccentricity of the order of 0.2 and higher, and, additionally, to provide an intrinsic measure of the resulting orbital functions and their resulting gravitational waves, it is worthwhile to take the epicycle expansion to higher orders. It is recommended that the expansion is taken to fourth order, so that one order can be used to fix the value of the angular coordinate at apastron (thereby greatly increasing the accuracy of the angular approximation and hence of the resulting gravitational waves), and the remaining extra order can be used as an intrinsic measure of the obtained results. With the methods explained in this thesis, calculating third- and higher-order terms is a straightforward, albeit tedious, exercise.

Another direction of future research is the application of the geodesic deviation method to different physical systems. This is particularly straightforward when the geodesic deviation equations for such systems have only constant coefficients, as then the analysis presented in this thesis applies directly. This is the case, for example, when considering the bound orbits of electrically charged test masses around a Schwarzschild black hole surrounded by an axially symmetric magnetic field. What's more, it is straightforward to modify the C++ code to calculate the resulting emission of both gravitational waves and electromagnetic waves, the results of which are of value in multimessenger astronomy.
Finally, a future direction of research is in finding analytical expressions for the gravitational waves emitted by the EMRI system. In the present case, the calculation of these waves was done numerically because there are no known analytical general solutions to the Zerilli-Moncrief and Regge-Wheeler equations. However, the current case of the epicycle expansion supplying the source of these differential equations, there is only the need for a solution in case the orbit is a small deviation from a circular one. It might be interesting to investigate whether the Zerilli-Moncrief and Regge-Wheeler differential equations can be solved analytically for that particular case. If that is to succeed, a fully analytical calculation scheme would be available for both the geodesic orbits as the gravitational waves in the Schwarzschild spacetime, of which outcomes can be checked by the results given in this thesis. This would be a very interesting alternative to the Post-Newtonian techniques, as it does away with the assumption that gravity is weak and/or velocities are small.

Appendix A

Source terms for the second-order geodesic deviation equation

This appendix presents the explicit expressions for the coefficients (a^μ, b^μ, c^μ) in the expansion of the source terms $\Sigma^\mu[n]$ for the second-order deviations, Eq. (2.66). Using these results, the coefficients U_i^μ of the second-order solutions Eq. (2.84) will be expressed in terms of the four epicycle parameters $(\sigma, R, \Delta_n, \Delta_m)$.

The general expression for the source $\Sigma^\mu[n]$ of the second-order deviation equation is given by Eq. (2.62),

$$\Sigma^\mu[n] = S^\mu[n] + \frac{\omega_1}{\omega}\, T^\mu[n], \tag{A.1}$$

in which $S^\mu[n]$ is given in Eq. (2.32) after substitution $\tau \to \lambda$, and $T^\mu[n]$ is defined by

$$T^\mu[n] = -4\,\frac{d^2 n^\mu}{d\lambda^2} - 4\bar{\Gamma}_{\lambda\nu}^{\ \ \mu}\, u^\lambda \frac{dn^\nu}{d\lambda}. \tag{A.2}$$

After substitution of the first order solutions Eq. (2.64) in Eq. (2.32) with $\tau \to \lambda$, the expression for $S^\mu[n]$ becomes of the form of Eq. (2.56),

$$S^\mu[n] = A_c^\mu \cos 2\omega\lambda + A_s^\mu \sin 2\omega\lambda + B_c^\mu \cos\omega\lambda + B_s^\mu \sin\omega\lambda + C^\mu,$$

in which the coefficients $A_c^t = A_s^r = A_c^\varphi = 0$ vanish, and:

$$\begin{aligned}
A_s^t &= a^t = -\frac{2\omega\alpha}{R}\,\frac{1}{1-\frac{2M}{R}}\,(n_c^r)^2\,,\\
A_c^r &= a^r = -\frac{M}{R^4}\,\frac{3-\frac{M}{R}-\frac{18M^2}{R^2}}{\left(1-\frac{2M}{R}\right)\left(1-\frac{3M}{R}\right)}\,(n_c^r)^2\,,\\
A_s^\varphi &= a^\varphi = -\frac{3\omega\eta}{R}\,(n_c^r)^2\,.
\end{aligned} \tag{A.3}$$

Next, $B_c^t = B_s^r = B_c^\varphi = 0$, and:

$$\begin{aligned} B_s^t &= -\frac{\omega\alpha}{R}\frac{1}{\left(1-\frac{2M}{R}\right)\left(1-\frac{3M}{R}\right)}\left(4-\frac{13M}{R}+\frac{6M^2}{R^2}\right)\Delta_n n_c^r, \\ B_c^r &= -\frac{2M}{R^4}\frac{1}{\left(1-\frac{2M}{R}\right)\left(1-\frac{3M}{R}\right)^2}\left(7-\frac{36M}{R}+\frac{48M^2}{R^2}\right)\Delta_n n_c^r, \\ B_s^\varphi &= -\frac{\omega\eta}{R}\frac{1}{1-\frac{3M}{R}}\left(5-\frac{12M}{R}\right)\Delta_n n_c^r. \end{aligned} \tag{A.4}$$

In addition there is a constant term in the r-component:

$$C^r = -\frac{3M}{R^4}\frac{1+\frac{M}{R}}{1-\frac{3M}{R}}\left(n_c^r\right)^2 - \frac{3M}{2R^4}\frac{5-\frac{34M}{R}+\frac{75M^2}{R^2}-\frac{54M^3}{R^3}}{\left(1-\frac{3M}{R}\right)^3}\left(\Delta_n\right)^2. \tag{A.5}$$

The Lindtsted-Poincaré correction terms (A.2) are, after substitution of the first order solutions Eq. (2.64), of the form:

$$T^\mu[n] = D_s^\mu \sin\omega\lambda + D_c^\mu \cos\omega\lambda + E^\mu, \tag{A.6}$$

in which it follows that $D_c^t = D_s^r = D_c^\varphi = 0$ and:

$$\begin{aligned} D_s^t &= -2\omega\alpha n_c^r, \\ D_c^r &= -\frac{4M}{R^3}\frac{1}{1-\frac{3M}{R}}\,n_c^r, \\ D_s^\varphi &= -2\omega\eta n_c^r, \end{aligned} \tag{A.7}$$

while $E^t = E^\varphi = 0$ and:

$$E^r = -2\kappa\,\Delta_n. \tag{A.8}$$

Combining the results to compute:

$$b^t = B_s^t + \frac{\omega_1}{\omega}D_s^t, \quad b^r = B_c^r + \frac{\omega_1}{\omega}D_c^r, \quad b^\varphi = B_s^\varphi + \frac{\omega_1}{\omega}D_s^\varphi,$$

the coefficients b^μ are found to be of the form (2.74) with:

$$\begin{aligned} F^t &= -\omega\alpha\,\frac{4-\frac{13M}{R}+\frac{6M^2}{R^2}}{\left(1-\frac{2M}{R}\right)\left(1-\frac{3M}{R}\right)}, \\ F^r &= -\frac{2M}{R^3}\frac{7-\frac{36M}{R}+\frac{48M^2}{R^2}}{\left(1-\frac{2M}{R}\right)\left(1-\frac{3M}{R}\right)^2}, \\ F^\varphi &= -\omega\eta\,\frac{5-\frac{12M}{R}}{1-\frac{3M}{R}}, \end{aligned} \tag{A.9}$$

and:

$$\begin{aligned} G^t &= 2\omega\alpha, \\ G^r &= \frac{4M}{R^3}\frac{1}{1-\frac{3M}{R}}, \\ G^\varphi &= 2\omega\eta. \end{aligned} \tag{A.10}$$

It then follows by Eq. (2.75), that:

$$\frac{\omega_1}{\omega} = -\frac{3}{2}\frac{1-\frac{10M}{R}+\frac{18M^2}{R^2}}{\left(1-\frac{3M}{R}\right)\left(1-\frac{6M}{R}\right)}\frac{\Delta_n}{R}. \tag{A.11}$$

Finally, the constant c^r in the source terms $\Sigma^r[n]$ is given by:

$$c^r = C^r + \frac{\omega_1}{\omega}E^r. \tag{A.12}$$

Using the value (A.11) for the ratio ω_1/ω, this leads to the result:

$$c^r = -\frac{3M}{R^4}\frac{1+\frac{M}{R}}{1-\frac{3M}{R}}(n_c^r)^2 + \frac{3M}{2R^2}\left(\frac{\Delta_n}{R}\right)^2\frac{1-\frac{26M}{R}+\frac{165M^2}{R^2}-\frac{396M^3}{R^3}+\frac{324M^4}{R^4}}{\left(1-\frac{3M}{R}\right)^3\left(1-\frac{6M}{R}\right)}. \tag{A.13}$$

By collecting results from this appendix and chapter 2, the expressions for the coefficients U_i^μ of Eq. (2.84) can be written solely in terms of the four epicycle parameters $R, \sigma, \Delta_n, \Delta_m$ and the mass M of the black hole. The result for U_i^t is:

$$\begin{aligned} U_0^t &= \frac{1}{\sqrt{1-\frac{3M}{R}}} - \sigma\nu\cdot\Delta_n - \frac{1}{2}\sigma^2\nu\cdot\left(\Delta_m - \frac{(n_c^r)^2}{R}\frac{1+\frac{M}{R}}{1-\frac{2M}{R}} - \frac{2-\frac{3M}{2R}}{1-\frac{3M}{R}}\frac{\Delta_n^2}{R}\right), \\ U_1^t &= -\sigma\lambda\cdot n_c^r - \frac{1}{2}\sigma^2\lambda\cdot\left(\frac{n_c^r\Delta_n}{R}\frac{3-\frac{34M}{R}+\frac{72M^2}{R^2}}{\left(5-\frac{18M}{R}\right)\left(1-\frac{2M}{R}\right)}\right), \\ U_2^t &= \frac{1}{2}\sigma^2\lambda\cdot\frac{(n_c^r)^2}{2R}\frac{2-\frac{15M}{R}+\frac{14M^2}{R^2}}{\left(1-\frac{2M}{R}\right)\left(1-\frac{6M}{R}\right)}, \end{aligned} \tag{A.14}$$

in which

$$\nu \equiv \frac{3M}{2R^2}\frac{1}{\left(1-\frac{3M}{R}\right)^{3/2}}, \qquad \lambda \equiv 2\sqrt{\frac{M}{R}}\frac{1}{\left(1-\frac{2M}{R}\right)\sqrt{1-\frac{6M}{R}}}, \qquad n_c^r + \Delta_n = \sqrt{1-\frac{2M}{R}}\,. \tag{A.15}$$

For U_i^r the result is:

$$\begin{aligned} U_0^r &= R + \sigma\Delta_n + \frac{1}{2}\sigma^2\Delta_m, \\ U_1^r &= \sigma n_c^r + \frac{1}{2}\sigma^2\left(\frac{4n_c^r\Delta_n}{R}\frac{2-\frac{15M}{R}+\frac{30M^2}{R^2}}{\left(5-\frac{18M}{R}\right)\left(1-\frac{2M}{R}\right)\left(1-\frac{6M}{R}\right)}\right), \\ U_2^r &= -\frac{1}{2}\sigma^2\frac{(n_c^r)^2}{R}\left(\frac{1-\frac{7M}{R}}{1-\frac{6M}{R}}\right). \end{aligned} \tag{A.16}$$

And for U_i^φ, the result is:

$$\begin{aligned} U_0^\varphi &= \sqrt{\frac{M}{R^3}}\frac{1}{\sqrt{1-\frac{3M}{R}}} \\ &\quad -\sigma\kappa\Delta_n - \frac{1}{2}\sigma^2\kappa\cdot\left(\Delta_m - \frac{\Delta_n^2}{2R}\frac{5-\frac{20M}{R}+\frac{24M^2}{R^2}}{\left(1-\frac{2M}{R}\right)\left(1-\frac{3M}{R}\right)} - \frac{(n_c^r)^2}{R}\frac{1+\frac{M}{R}}{1-\frac{2M}{R}}\right), \\ U_1^\varphi &= -\sigma\mu\cdot n_c^r + \frac{1}{2}\sigma^2\mu\cdot\left(\frac{2n_c^r\Delta_n}{R}\frac{1-\frac{7M}{R}+\frac{18M^2}{R^2}}{\left(5-\frac{18M}{R}\right)\left(1-\frac{2M}{R}\right)}\right), \\ U_2^\varphi &= \frac{1}{2}\sigma^2\mu\cdot\left(\frac{(n_c^r)^2}{4R}\frac{5-\frac{32M}{R}}{1-\frac{6M}{R}}\right), \end{aligned} \tag{A.17}$$

in which

$$\kappa \equiv \frac{3}{2R^2}\sqrt{\frac{M}{R}}\frac{1-\frac{2M}{R}}{\left(1-\frac{3M}{R}\right)^{3/2}}, \qquad \mu \equiv \frac{2}{R}\frac{1}{\sqrt{1-\frac{6M}{R}}}. \tag{A.18}$$

Finally, the epicycle frequency $\bar{\omega}$,

$$\bar{\omega} \equiv \omega + \sigma\omega_1, \tag{A.19}$$

is expressed in (M, R, σ, Δ_n) via

$$\omega = \sqrt{\frac{M}{R^3}\frac{1-\frac{6M}{R}}{1-\frac{3M}{R}}}, \qquad \omega_1 = -\omega\,\frac{3\Delta_n}{2R}\frac{1-\frac{10M}{R}+\frac{18M^2}{R^2}}{\left(1-\frac{3M}{R}\right)\left(1-\frac{6M}{R}\right)}. \tag{A.20}$$

Appendix B

Retrieving the original epicycle expressions

This appendix investigates the relationship between the most general second-order solutions as stated in this thesis and the limited ones stated in the literature.

In the literature, the geodesic deviation method is applied to a number of cases, *i.e.* a number of different spacetimes and simple geodesics as starting point for the expansion. For the case of a Schwarzschild spacetime and a circular orbit as starting geodesic, the method is pursued to third order. The expressions for the second-order solutions are stated in, *e.g.* [21], and yield the following orbital functions:

$$
\begin{aligned}
t(\tau) &= \frac{1}{\sqrt{1-\frac{3M}{R}}}\tau + \frac{2\sqrt{M}n_0^r}{\sqrt{R}\left(1-\frac{2M}{R}\right)\sqrt{1-\frac{6M}{R}}}\sin(\omega\tau) + \frac{1}{2}\frac{M(n_0^r)^2}{R^3}\frac{1-\frac{2M}{R}}{\sqrt{1-\frac{3M}{R}}}\cdot \\
&\qquad \left(-\frac{3\left(2-\frac{5M}{R}+\frac{18M^2}{R^2}\right)}{\left(1-\frac{2M}{R}\right)^2\left(1-\frac{6M}{R}\right)^2}\tau + \frac{2-\frac{15M}{R}+\frac{14M^2}{R^2}}{\left(1-\frac{6M}{R}\right)\left(1-\frac{2M}{R}\right)^3\omega}\sin(2\omega\tau)\right), \\
r(\tau) &= R - n_0^r\cos(\omega\tau) + \frac{1}{2}\frac{(n_0^r)^2}{R\left(1-\frac{6M}{R}\right)}\cdot \\
&\qquad \left(\frac{5-\frac{33M}{R}+\frac{90M^2}{R^2}-\frac{72M^3}{R^3}}{\left(1-\frac{2M}{R}\right)\left(1-\frac{6M}{R}\right)} - \left(1-\frac{7M}{R}\right)\cos(2\omega\tau)\right), \\
\varphi(\tau) &= \frac{\sqrt{M}}{R^{3/2}\sqrt{1-\frac{3M}{R}}}\tau + \frac{2n_0^r}{R\sqrt{1-\frac{6M}{R}}} + \frac{1}{2}\omega\frac{(n_0^r)^2}{R^2\left(1-\frac{6M}{R}\right)^2}\cdot \\
&\qquad \left(-\frac{3\left(2-\frac{5M}{R}+\frac{18M^2}{R^2}\right)}{1-\frac{6M}{R}}\tau + \frac{5-\frac{32M}{R}}{2\omega}\sin(2\omega\tau)\right),
\end{aligned}
\tag{B.1}
$$

in which, as in this thesis,

$$\omega = \sqrt{\frac{M}{R^3}\frac{1-\frac{6M}{R}}{1-\frac{3M}{R}}}\,, \tag{B.2}$$

and the expansion parameter is n_0^r.
Going to third and higher order in the eccentricity will produce Poincaré resonances in the geodesic deviation equations, because the sources will contain, via Eq. (2.32), oscillatory terms that have the same frequency as the differential matrix.
These solutions are not the most general solutions to the first- and second-order geodesic deviation equations, as the secular contributions have not been taken into account. In contrast, the solutions given in this thesis do take these into account, as it was recognized in the main text of chapter 2 that these are not only mathematically allowed, but even necessary to ensure the resulting orbits produce the correct periastron shift, even already at first order. The price that has been paid for the inclusion of the secular constants is that the Poincaré resonances already appear when solving the *second* order geodesic deviation equations, rather than the third-and higher orders. This is explictly dealt with in the main text of chapter 2, and yields the solutions Eq. (2.83).
These are the most general solutions to the geodesic deviation equations up to second order. It should therefore be possible to choose the secular constants Δ_n, Δ_m such, that Eqs. (2.83) reduce to the ones stated in the literature, Eqs. (B.1). Indeed, by comparing the frequencies, it follows immediately that the secular constant Δ_n must be chosen to vanish,

$$\Delta_n = 0. \tag{B.3}$$

From the resulting expression for the radial function $r(\tau)$ it then follows that the expansion parameter σ is related to the parameter n_0^r via

$$\sigma = -\frac{n_0^r}{\sqrt{1-\frac{2M}{R}}}, \tag{B.4}$$

and that the secular constant Δ_m must be chosen as follows:

$$\Delta_m = \frac{1}{R}\left(\frac{5-\frac{33M}{R}+\frac{90M^2}{R^2}-\frac{72M^3}{R^3}}{\left(1-\frac{6M}{R}\right)^2}\right). \tag{B.5}$$

It is then straightforward to show that these values also make the orbital functions $t(\tau)$ and $\varphi(\tau)$ in Eq. (2.83) reduce to the ones stated in Eq. (B.1). Thus, it has now been explicitly shown that the solutions found in the literature are only a small subset of the general solutions obtained in this thesis.

Appendix C

Details of the bound orbits

This appendix presents the physical characteristics and values of the epicycle parameters as used in the epicycle expansions of the bound geodesic orbits considered in section 3.3, *i.e.* of the orbits around a Schwarzschild black hole of eccentricities $e = 0.075$, $e = 0.1$, $e = 0.15$, and $e = 0.2$ and various decreasing values of the semi-major axis a. It also presents the physical characteristics and values of the second order epicycle parameters of the adiabatically related orbits considered in section 5.4.

Tables C.1 and C.2 correspond to bound orbits with eccentricity $e = 0.1$. Table C.1 lists the following physical characteristics of the orbits: the energy per unit mass ε, the angular momentum per unit mass ℓ, the periastron r_{pa}, the apastron r_{aa}, the periastrion shift $\delta\varphi$, and the proper time between two successive periastra $\Delta\tau$. The first two of these are calculated using Eq. (2.21), the next pair follow from Eq. (2.18), and the last two parameters follow from Eqs. (2.22) and (2.23). As explained in the main text, the parameters ε and ℓ serve as a parametrization of bound orbits equivalent to (a, e), whereas the parameters r_{pa}, r_{aa}, $\delta\varphi$ and $\Delta\tau$ are used as boundary conditions for the epicycle expansions. The epicycle expansions themselves are, to first and second order in σ, given by Eqs. (2.50) and (2.83), respectively. Table C.2 present the (R, σ, Δ_n) for the first-order expansion and the parameters $(R, \sigma, \Delta_n, \Delta_m)$ for the second-order expansion. The accuracies of the expansions were already given in chapter 2.
In a similar manner, tables C.3 and C.4 list the information for bound orbits with eccentricity $e = 0.075$, C.5 and C.6 for bound orbits with eccentricity $e = 0.15$, and C.7 and C.8 for bound orbits with eccentricity $e = 0.2$.
Finally, tables C.9 and C.10 correspond to the adiabatically related bound orbits of various values for the parameters (a, e), as explained in the main text of section 5.4. Table C.9 lists the following characteristics of the orbits considered: the energy per unit mass ε, the angular momentum per unit mass ℓ, the periastron r_{pa}, the apastron r_{aa}, the periastrion shift $\delta\varphi$, and the proper time between two successive periastra $\Delta\tau$. Table C.10 lists the parameters $(R, \sigma, \Delta_n, \Delta_m)$ used to construct the second order epicycle expansions for these orbits.

a/M	ε	ℓ/M	r_{pa}/M	r_{aa}/M	$\delta\varphi$	$\Delta\tau/M$
20.0	0.97641	4.85214	18.181	22.222	1.2269	680.713
15.0	0.96925	4.33193	13.636	16.667	1.8291	427.277
10.0	0.95657	3.78235	9.0909	11.111	3.6560	266.105
9.0	0.95299	3.67730	8.1818	10.000	4.6087	242.749
8.5	0.95107	3.62771	7.7273	9.4444	5.3164	233.590
8.0	0.94911	3.58129	7.2727	8.8889	6.3069	227.268
7.5	0.94716	3.53947	6.8182	8.3333	7.8137	225.916
7.0	0.94534	3.50438	6.3636	7.7778	10.468	235.390
6.6	0.94412	3.48335	6.0000	7.3333	15.018	265.816

Table C.1: The physical characteristics of bound geodesic orbits of eccentricity $e = 0.1$ and various values of the semi-major axis a, as listed in the first column. Second and third columns list the values of the energy per unit mass ε and angular momentum per unit mass ℓ. The next two columns show the values of the periastron r_{pa} and apastron r_{aa}, and the last two columns show the periastron shift $\delta\varphi$ and the proper time $\Delta\tau$ between two successive periastra.

	first-order epicycles			second-order epicycles			
a/M	R/M	σ/M	Δ_n	R/M	σ/M	Δ_n	$\Delta_m M$
20.0	20.2062	-2.13271	0.01327	20.035	-1.93222	-0.08776	0.04842
15.0	15.1590	-1.63423	0.02047	15.016	-1.4596	-0.09603	0.05668
10.0	10.1274	-1.15699	0.05047	10.005	-0.97114	-0.12613	0.00228
9.0	9.13836	-1.08228	0.07685	9.01120	-0.85874	-0.14993	-0.05357
8.5	8.66094	-1.06466	0.107331	8.52420	-0.78830	-0.17940	-0.17797
8.0	8.23686	-1.10798	0.18396	8.07092	-0.66955	-0.27967	-0.70697
7.5	7.26501	-0.524878	-0.47662	7.31204	-0.96884	0.05307	0.69225
7.0	6.93534	-0.677709	-0.11382	6.90124	-0.78414	-0.04173	0.43238
6.6	6.56258	-0.674712	-0.03728	6.49392	-0.67525	-0.09367	0.34511

Table C.2: The parameters used in the epicycle expansions of bound geodesic orbits of eccentricity $e = 0.1$ and various values of the semi-major axis a, as listed in the first column. The first-order epicycle parameters (R, σ, Δ_n) are listed in the second to fourth column, whereas the second-order epicycle parameters (R, σ, Δ_n, Δ_m) are listed in the fifth to last column.

a/M	ε	ℓ/M	r_{pa}/M	r_{aa}/M	$\delta\varphi$	$\Delta\tau/M$
20.0	0.97632	4.85152	18.605	21.622	1.2269	624.199
15.0	0.96913	4.33114	13.954	16.216	1.8288	424.727
10.0	0.95640	3.78116	9.3023	10.811	3.6540	264.669
9.0	0.95281	3.67596	8.3721	9.7297	4.6047	241.501
8.5	0.95089	3.62627	7.9070	9.1892	5.3103	232.428
8.0	0.94892	3.57972	7.4419	8.6487	6.2965	226.178
7.5	0.94670	3.53775	6.9767	8.1081	7.7929	224.864
7.0	0.94515	3.50246	6.5116	7.5676	10.411	234.218
6.45	0.94358	3.47540	6.0000	6.9730	18.032	289.785

Table C.3: The physical characteristics of bound geodesic orbits of eccentricity $e = 0.075$ and various values of the semi-major axis a, as listed in the first column. Second and third columns list the values of the energy per unit mass ε and angular momentum per unit mass ℓ. The next two columns show the values of the periastron r_{pa} and apastron r_{aa}, and the last two columns show the periastron shift $\delta\varphi$ and the proper time $\Delta\tau$ between two successive periastra.

	first-order epicycles			second-order epicycles			
a/M	R/M	σ/M	Δ_n	R/M	σ/M	Δ_n	$\Delta_m M$
20.0	20.1155	-1.59207	0.00996	20.0185	-1.4805	-0.06515	0.0460
15.0	15.0891	-1.21925	0.01537	15.0093	-1.1226	-0.07071	0.0534
10.0	10.0716	-0.859283	0.03821	10.0021	-0.75666	-0.09167	-0.0208
9.0	9.0782	-0.799674	0.05882	9.00567	-0.67573	-0.10806	-0.0490
8.5	8.5920	-0.782078	0.08359	8.5132	-0.62738	-0.12823	-0.1604
8.0	8.1429	-0.807107	0.15242	8.0424	-0.54910	-0.19916	-0.6342
7.5	7.3398	-0.425673	0.40026	7.3804	-0.72670	-0.06120	0.8055
7.0	6.9624	-0.533942	-0.08420	6.9441	-0.59816	-0.02993	0.4272
6.45	6.4281	-0.515734	-0.00862	6.3699	-0.48123	-0.11200	0.3059

Table C.4: The parameters used in the epicycle expansions of bound geodesic orbits of eccentricity $e = 0.075$ and various values of the semi-major axis a, as listed in the first column. The first-order epicycle parameters ($R,\ \sigma,\ \Delta_n$) are listed in the second to fourth column, whereas the second-order epicycle parameters ($R,\ \sigma,\ \Delta_n,\ \Delta_m$) are listed in the fifth to last column.

a/M	ε	ℓ/M	r_{pa}/M	r_{aa}/M	$\delta\varphi$	$\Delta\tau/M$
20.0	0.97670	4.85393	17.391	23.529	1.2273	639.384
15.0	0.96961	4.33419	13.044	17.647	1.8301	434.718
12.0	0.96302	4.00501	10.435	14.118	2.6068	329.498
10.0	0.95705	3.78573	8.6957	11.765	3.6619	270.295
9.0	0.95349	3.68114	7.8261	10.588	4.6201	246.389
8.5	0.95159	3.63185	7.3913	10.000	5.3340	236.980
8.0	0.94964	3.58579	6.9565	9.4118	6.3369	230.445
7.5	0.94769	3.54441	6.5217	8.8235	7.8742	228.983
6.9	0.94554	3.50407	6.0000	8.1177	11.5005	323.726

Table C.5: The physical characteristics of bound geodesic orbits of eccentricity $e = 0.15$ and various values of the semi-major axis a, as listed in the first column. Second and third columns list the values of the energy per unit mass ε and angular momentum per unit mass ℓ. The next two columns show the values of the periastron r_{pa} and apastron r_{aa}, and the last two columns show the periastron shift $\delta\varphi$ and the proper time $\Delta\tau$ between two successive periastra.

	first-order epicycles			second-order epicycles			
a/M	R/M	σ/M	Δ_n	R/M	σ/M	Δ_n	$\Delta_m M$
20.0	20.4698	-3.24085	0.01988	20.0887	-2.7807	-0.13419	0.0539
15.0	15.3619	-2.48589	0.03061	15.0459	-2.0827	-014861	0.0642
12.0	12.3058	-2.04456	0.04647	12.0220	-1.6519	-0.16879	0.0632
10.0	10.2876	-1.77371	0.07424	10.0153	-1.3433	-0.20152	0.0282
9.0	9.3078	-1.6723	0.11047	9.0300	-1.1609	-0.24437	-0.0639
8.5	8.8489	-1.6568	0.14928	8.5581	-1.0377	-0.29768	-0.2202
8.0	8.4671	-1.7285	0.23245	8.1406	-0.83164	-0.46707	-0.8805
7.5	7.1187	-0.704007	-0.57916	7.1507	-1.4175	0.0237	0.5653
6.9	6.7877	-0.937917	-0.13668	6.6862	-1.0743	-0.0842	0.4309

Table C.6: The parameters used in the epicycle expansions of bound geodesic orbits of eccentricity $e = 0.15$ and various values of the semi-major axis a, as listed in the first column. The first-order epicycle parameters ($R,\ \sigma,\ \Delta_n$) are listed in the second to fourth column, whereas the second-order epicycle parameters ($R,\ \sigma,\ \Delta_n,\ \Delta_m$) are listed in the fifth to last column.

a/M	ε	ℓ/M	r_{pa}/M	r_{aa}/M	$\delta\varphi$	$\Delta\tau/M$
20.0	0.97710	4.85643	16.667	25.000	1.2278	655.832
15.0	0.97012	4.33736	12.500	18.750	1.8314	445.538
12.0	0.96362	4.00892	10.000	15.000	2.6100	337.356
10.0	0.95773	3.79049	8.3333	12.500	3.6701	276.384
9.0	0.95403	3.68654	7.5000	11.250	4.6362	251.677
8.5	0.95232	3.63767	7.0833	10.625	5.3588	241.905
8.0	0.95038	3.59211	6.6667	10.000	6.3796	235.059
7.5	0.94845	3.55135	6.2500	9.3750	7.9614	233.438
7.2	0.94733	3.53009	6.0000	9.0000	9.4491	237.323

Table C.7: The physical characteristics of bound geodesic orbits of eccentricity $e = 0.2$ and various values of the semi-major axis a, as listed in the first column. Second and third columns list the values of the energy per unit mass ε and angular momentum per unit mass ℓ. The next two columns show the values of the periastron r_{pa} and apastron r_{aa}, and the last two columns show the periastron shift $\delta\varphi$ and the proper time $\Delta\tau$ between two successive periastra.

	first-order epicycles			second-order epicycles			
a/M	R/M	σ/M	Δ_n	R/M	σ/M	Δ_n	$\Delta_m M$
20.0	20.8499	-4.39958	0.02648	20.181	-3.5711	-0.18067	0.059
15.0	15.6542	-3.37729	0.04070	15.097	-2.6478	-0.20309	0.0732
12.0	12.5515	-2.78281	0.06148	12.051	-2.0691	-0.23446	0.0745
10.0	10.5146	-2.42397	0.09701	10.038	-1.6439	-0.28634	0.0365
9.0	9.54135	-2.29614	0.14121	9.0638	-1.3803	-0.35560	-0.0747
8.5	9.09781	-2.28070	0.18553	8.6090	-1.1990	-0.44190	-0.2716
8.0	8.74451	-2.36595	0.27083	8.2220	-0.90799	-0.70266	-1.1121
7.5	6.98164	-0.866146	-0.64383	8.0069	-0.29761	-3.25667	-25.3034
7.2	6.89483	-1.06202	-0.3374	6.7763	-1.54511	-0.00669	0.485

Table C.8: The parameters used in the epicycle expansions of bound geodesic orbits of eccentricity $e = 0.2$ and various values of the semi-major axis a, as listed in the first column. The first-order epicycle parameters (R, σ, Δ_n) are listed in the second to fourth column, whereas the second-order epicycle parameters (R, σ, Δ_n, Δ_m) are listed in the fifth to last column.

a/M	e	ε	ℓ/M	r_{pa}/M	r_{aa}/M	$\delta\varphi$	$\Delta\tau/M$
12.00	0.1500	0.96302	4.00501	10.435	14.118	2.607	329.50
11.64	0.1446	0.96200	3.96496	10.170	13.610	2.747	317.41
11.29	0.1410	0.96096	3.92532	9.8899	13.138	2.903	305.99
10.93	0.1378	0.95988	3.88607	9.6072	12.677	3.077	295.05
10.58	0.1349	0.95877	3.84721	9.3208	12.227	3.274	284.58
10.23	0.1322	0.95761	3.80873	9.0315	11.784	3.498	274.60
9.87	0.1300	0.95640	3.77665	8.7379	11.348	3.757	265.13
9.52	0.1287	0.95515	3.73294	8.4335	10.925	4.061	256.25
9.16	0.1273	0.95184	3.69561	8.1260	10.497	4.427	247.96

Table C.9: The physical characteristics of bound geodesic orbits for various values of a and the eccentricity e, as listed in the first two columns. These orbits are related to each other by adiabatic emission of energy and angular momentum by gravitational waves, as explained in the main text. The third and fourth columns list the corresponding values of the energy per unit mass ε and angular momentum per unit mass ℓ. The next two columns show the values of the periastron r_{pa} and apastron r_{aa}, and the last two columns show the periastron shift $\delta\varphi$ and the proper time $\Delta\tau$ between two successive periastra.

a/M	e	R/M	σ/M	Δ_n	$\Delta_m M$
12.00	0.1500	12.022	-1.6519	-0.1688	0.0632
11.64	0.1446	11.659	-1.5525	-0.1658	0.0600
11.29	0.1410	11.299	-1.4707	-0.1652	0.0561
10.93	0.1378	10.943	-1.3936	-0.1654	0.0510
10.58	0.1349	10.589	-1.3211	-0.1666	0.0440
10.23	0.1322	10.236	-1.2517	-0.1690	0.0342
9.87	0.1300	9.8838	-1.1852	-0.1731	0.0202
9.52	0.1287	9.5310	-1.1247	-0.1807	-0.0012
9.16	0.1273	9.1.772	-1.0606	-0.1917	-0.0360

Table C.10: The parameters used in the second-order epicycle expansions of bound geodesic orbits of various values for a and the eccentricity e, as listed in the first two columns. These orbits are related to each other by adiabatic emission of energy and angular momentum by gravitational waves, as explained in the main text. The second-order epicycle parameters (R, σ, Δ_n, Δ_m) are listed in the third to last columns.

Appendix D

Integrations over a grid cell

This appendix considers some of the integrals of the main text of chapter 4. The integrands contain delta functions and its derivative, and the integrations are to be done over an individual cell of the grid. They are therefore integrations over a finite region of spacetime, which requires a careful evaluation. Exactly this is what will be presented.

In Eq. (4.32) of the main text, an integration of the following form is done:

$$\int_{cell} \bar{S}^{lm}\, dr_* dt = \int_{cell} \left(G^{lm}(r)\delta(r - r_p(t)) + F^{lm}(r)\partial_r \delta(r - r_p(t)) \right) dr_* dt. \tag{D.1}$$

This integration consist of two different terms:

$$\int_{cell} G(r)\delta(r - r_p(t))\, dr_* dt, \qquad \int_{cell} F(r)\partial_r \delta(r - r_p(t))\, dr_* dt, \tag{D.2}$$

dropping the indices for notational convenience. Both will be evaluated now, starting with the first.

An integration over the finite region of spacetime of a single grid cell requires a parametrization of the integrations boundaries. These can be read off from Figure 4.2, from which it can be seen

$$\begin{aligned} \text{if:} \quad & -\Delta \le t \le 0 \quad \Rightarrow \quad -(t+\Delta) \le r_* \le +(t+\Delta), \\ \text{if:} \quad & 0 \le t \le \Delta \quad \Rightarrow \quad +(t-\Delta) \le r_* \le -(t-\Delta), \end{aligned} \tag{D.3}$$

where it has been assumed, without loss of generality, that the lowest point of the cell is located at $(t, r_*) = (-\Delta, 0)$. The integral thus splits up in two parts:

$$\begin{aligned} \int_{cell} G(r)\delta(r - r_p(t)) dr_* dt \;&=\; \int_{-\Delta}^{0} dt \int_{-(t+\Delta)}^{(t+\Delta)} dr_*\; G(r)\delta(r - r_p(t)) \\ &+\; \int_{0}^{\Delta} dt \int_{(t-\Delta)}^{-(t-\Delta)} dr_*\; G(r)\delta(r - r_p(t)). \end{aligned} \tag{D.4}$$

The two terms are very similar, and the evaluation of the first will be presented in detail. An integration over a delta function is straightforward by the well-known defining property of the delta function. However, in the present case, this property can not be used just yet as the argument of the delta function does not match the integration variable. This can be remedied by using the chain rule for delta functions [47]:

$$\delta(g(x)) = \left|\frac{dg(x)}{dx}\right|^{-1} \delta(x - x_0), \tag{D.5}$$

which holds for any well-behaved function $g(x)$, and in which x_0 is the zero point of the argument of the original delta function, *i.e.* it is defined by

$$g(x_0) = 0. \tag{D.6}$$

Applying this rule to the first term of Eq. (D.4) yields:

$$\int_{-\Delta}^{0} dt \int_{-(t+\Delta)}^{(t+\Delta)} dr_*\, G(r)\delta(r - r_p(t)) =$$

$$\int_{-\Delta}^{0} dt \int_{-(t+\Delta)}^{(t+\Delta)} dr_*\, G(r)\left|\frac{d}{dr_*}(r - r_p(t))\right|^{-1} \delta(r_* - r_{*0}(t)), \tag{D.7}$$

in which $r_{*0}(t)$ is the value of the tortoise coordinate r_* that corresponds to the zero point of the original delta function, *i.e.* it is the position of the particle in tortoise coordinates: $r_{*0} = r_{*p}(t)$. The absolute value signs can be dropped as the derivative returns $f(r)$, which is always positive. The integration variable now matches the argument of the delta function, so the integration can now be performed by using the defining property of the delta function. This should be done with some care, as the integration is not done over infinite range and hence vanishes if the zero point $r_{*p}(t)$ does not lie in the interval $\mp(t+\Delta)$. This can be taken into account by using theta functions:

$$\int_{-\Delta}^{0} dt \int_{-(t+\Delta)}^{(t+\Delta)} dr_*\, \frac{G(r)}{f(r)}\delta(r_* - r_{*0}(t)) = \int_{-\Delta}^{0} \frac{G(r_p(t))}{f(r_p(t))}\theta(t + \Delta - r_{*p}(t))\theta(t + \Delta + r_{*p}(t))\, dt. \tag{D.8}$$

The theta functions now serve to restrict the range of the remaining integration over t. The first of the theta functions only starts to contribute to the outcome when the world line of the particle crosses the line $t+\Delta$. As this line is the right lower boundary of the cell, the theta function only starts to contribute at the moment the world line of the test mass enters the cell at some time $t = t_b$. For that situation, the second theta function equals unity over the whole range of integration. Similarly, the second theta function only starts to contribute to the integral when the world line enters the cell at some time $t = t_b$ at the left lower boundary of the cell, in which case the first theta function always equals unity

over the range of integration. The integral of the first term of Eq. (D.4) is thus found to evaluate to

$$\int_{-\Delta}^{0} dt \int_{-(t+\Delta)}^{(t+\Delta)} dr_*\; G(r)\delta(r - r_p(t)) = \int_{t_b}^{0} \frac{G(r_p(t)}{f(r_p(t)}\, dt. \tag{D.9}$$

The second term of Eq. (D.4) can be evaluated similarly, yielding the outcome

$$\int_{0}^{\Delta} dt \int_{(t-\Delta)}^{-(t-\Delta)} dr_*\; G(r)\delta(r - r_p(t))\, dt = \int_{0}^{t_t} \frac{G(r_p(t)}{f(r_p(t)}\, dt, \tag{D.10}$$

in which t_t is the time at which the world line leaves the cell. The two outcomes can be taken into one single expression:

$$\int_{cell} G(r)\delta(r - r_p(t))\, dr_* dt = \int_{t_b}^{t_t} \frac{G(r_p(t))}{f(r_p(t))}\, dt. \tag{D.11}$$

This concludes the evaluation of the first type of integral of Eq. (D.2).

Next, integrations of the second type in Eq. (D.2) will be evaluated. The integration ranges of Eq. (D.3) apply again, and hence the integration splits up in two parts:

$$\begin{aligned} \int_{cell} F(r)\partial_r\delta(r - r_p(t))dr_*dt &= \int_{-\Delta}^{0} dt \int_{-(t+\Delta)}^{(t+\Delta)} dr_*\; F(r)\partial_r\delta(r - r_p(t)) \\ &+ \int_{0}^{\Delta} dt \int_{(t-\Delta)}^{-(t-\Delta)} dr_*\; F(r)\partial_r\delta(r - r_p(t)). \end{aligned} \tag{D.12}$$

The evaluation of the first term will be demonstrated in detail; the evaluation of the second term is done similarly.
In order to use the defining property of the delta function, the delta function needs to be taken outside of the derivative. This can be done by a partial integration, and this requires the derivative to be with respect to the same variable as the integration. Using the chain rule to write $\partial_r = f^{-1}(r)\,\partial_{r_*}$ allows the partial integration, and it follows

$$\begin{aligned} \int_{-\Delta}^{0} dt \int_{-(t+\Delta)}^{(t+\Delta)} dr_*\; F(r)\partial_r\delta(r - r_p(t)) &= \int_{-\Delta}^{0} dt\, \left(\frac{F(r)}{f(r)}\delta(r - r_p(t))\right)\Bigg|_{r_*=-(t+\Delta)}^{(t+\Delta)} \\ &- \int_{-\Delta}^{0} dt \int_{-(t+\Delta)}^{(t+\Delta)} dr_*\; \partial_{r_*}\left(\frac{F(r)}{f(r)}\right)\delta(r - r_p(t)). \end{aligned} \tag{D.13}$$

The second term is easily evaluated by first writing the derivative back to a derivative with respect to r and then using Eq. (D.11). The result is

$$\int_{-\Delta}^{0} dt \int_{-(t+\Delta)}^{(t+\Delta)} dr_*\; \partial_{r_*}\left(\frac{F(r)}{f(r)}\right)\delta(r - r_p(t)) = -\int_{t_b}^{0} dt\, \partial_r\left(\frac{F(r)}{f(r)}\right)\Bigg|_{r=r_p(t)}. \tag{D.14}$$

As for the first term, the two boundary terms $r_* \mp (t+\Delta)$ can only be substituted when the argument of the delta function is expressed in tortoise coordinates. This can be done using the chain rule Eq. (D.5), giving

$$\begin{aligned}\int_{-\Delta}^{0} dt\, \left(\frac{F(r)}{f(r)}\delta(r-r_p(t))\right)\Bigg|_{r_*=-(t+\Delta)}^{(t+\Delta)} &= \int_{-\Delta}^{0} \frac{F(r)}{f^2(r)}\delta(t+\Delta-r_{*p}(t))\,dt \\ &- \int_{-\Delta}^{0} \frac{F(r)}{f^2(r)}\delta(-t-\Delta-r_{*p}(t))\,dt. \quad \text{(D.15)}\end{aligned}$$

The integrations over t can be performed after the argument of the delta function is made to match the integration variable, which can be done by using once more the chain rule Eq. (D.5). This gives:

$$\begin{aligned}\delta(\pm(t+\Delta)-r_{*p}(t)) &= \left|\frac{d}{dt}\Big(\pm(t+\Delta)-r_{*p}(t)\Big)\right|^{-1}\delta(t-t_b) \\ &= \left|\frac{1}{\pm 1-\dot{r}_{*p}(t)}\right|\delta(t-t_b), \quad \text{(D.16)}\end{aligned}$$

in which an overdot denotes the derivative with respect to Schwarzschild time, and t_b is the time that corresponds to the zero point of the original delta function. It is the time at which the world line $r_{*p}(t)$ crosses the line $\pm(t+\Delta)$, *i.e.* the moment the world line enters the cell from the right (upper sign) or the left (lower sign). As the world line describes motion with a velocity smaller than that of light, $\dot{r}_{*p}(t) < 1$, the absolute value signs can be dropped when the correct overall sign is taken into account. Finally, the world line cannot enter the cell both at the right and at the left side, so one of the terms in Eq. (D.15) vanishes. The remaining integration is straightforward to evaluate, and Eq. (D.16) thus equals:

$$\int_{-\Delta}^{0} dt\, \left(\frac{F(r)}{f(r)}\delta(r-r_p(t))\right)\Bigg|_{r_*=-(t+\Delta)}^{(t+\Delta)} = \pm\,\frac{F(r_p(t_b))}{f^2(r_p(t_b))}\frac{1}{1\mp\dot{r}_{*p}(t)}\Bigg|_{t=t_b}. \quad \text{(D.17)}$$

Collecting results, the first term in Eq. (D.12) has now been shown to evaluate to the result:

$$\begin{aligned}\int_{\Delta}^{0}\int_{-(t+\Delta)}^{(t+\Delta)} dr_*\; F(r)\partial_r\delta(r-r_p(t))\,dt &= -\int_{T_b}^{0} dt\,\partial_r\left(\frac{F(r)}{f(r)}\right)\Bigg|_{r=r_p(t)} \\ &\pm\,\frac{F(r_p(t_b))}{f^2(r_p(t_b))}\frac{1}{1\mp\dot{r}_{*p}(t)}\Bigg|_{t=t_b}. \quad \text{(D.18)}\end{aligned}$$

The second term in Eq. (D.12) can be evaluated similarly, and yields the result:

$$\int_0^{\Delta}\int_{(t-\Delta)}^{-(t-\Delta)} dr_*\; F(r)\partial_r\delta(r-r_p(t))\,dt \;=\; -\int_0^{T_t} dt\,\partial_r\left(\frac{F(r)}{f(r)}\right)\Bigg|_{r=r_p(t)} \pm \frac{F(r_p(t_t))}{f^2(r_p(t_t))}\frac{1}{1\pm\dot r_{*p}(t)}\Bigg|_{t=t_t}, \tag{D.19}$$

in which t_t denotes the time at which the world line leaves the cell; the upper sign applies to leaving the cell at the right side, whereas the lower sign applies to leaving the cell at the left side. The last two results can be taken together in one expression,

$$\begin{aligned}\int_{cell} dr_*dt\; F(r)\partial_r\delta(r-r_p(t)) \;=\; &-\int_{t_b}^{t_t} dt\,\partial_r\left(\frac{F(r)}{f(r)}\right)\Bigg|_{r=r_p(t)} \pm \frac{F(r_p(t_b))}{f^2(r_p(t_b))}\frac{1}{1\mp\dot r_{*p}(t)}\Bigg|_{t=t_b} \\ &\pm \frac{F(r_p(t_t))}{f^2(r_p(t_t))}\frac{1}{1\pm\dot r_{*p}(t)}\Bigg|_{t=t_t},\end{aligned} \tag{D.20}$$

This concludes the evaluation of the second type of integral of Eq. (D.2).

Having evaluated both two types of integrals of Eq. (D.2), their resulting expressions can be taken together to give Eq. (D.1) as

$$\begin{aligned}\int_{cell}\bar S^{lm}\,dr_*dt \;=\; &\int_{t_b}^{t_t} dt\,\left(\frac{G^{lm}(r)}{f(r)}-\partial_r\Big(\frac{F^{lm}(r)}{f(r)}\Big)\right)\Bigg|_{r=r_p(t)} \pm \frac{F^{lm}(r_p(t_b))}{f^2(r_p(t_b))}\frac{1}{1\mp\dot r_{*p}(t)}\Bigg|_{t=t_b} \\ &\pm \frac{F^{lm}(r_p(t_t))}{f^2(r_p(t_t))}\frac{1}{1\pm\dot r_{*p}(t)}\Bigg|_{t=t_t},\end{aligned} \tag{D.21}$$

in which the indices lm have been reinstated. This is exactly Eq. (4.32) stated in the main text.
Finally, Eq. (4.35) of the main text can be proved as well. The first of these is straightforwardly shown to hold true by applying Eq. (D.11) to both sides and noting that their outcomes are the same. The second equation in Eq. (4.35) can be shown to hold true as follows: working out the derivative of its left hand side and applying Eqs. (D.11) and

(D.20) to the resulting terms, gives:

$$\begin{aligned}\int_{cell} b(r)\partial_r\Big(a(r)\delta(r-r_p(t))\Big)\,dtdr_* \;=\; & \int_{t_b}^{t_t} dt\,\frac{b(r)\partial_r a(r)}{f(r)}\bigg|_{r=r_p(t)} \\ & -\int_{t_b}^{t_t} dt\,\partial_r\left(\frac{b(r)a(r)}{f(r)}\right)\bigg|_{r=r_p(t)} \\ & \pm\frac{b(r_p(t_b))a(r_p(t_b))}{f^2(r_p(t_b))}\frac{1}{1\mp\dot{r}_{*p}(t)}\bigg|_{t=t_b} \\ & \pm\frac{b(r_p(t_t))a(r_p(t_t))}{f^2(r_p(t_t))}\frac{1}{1\pm\dot{r}_{*p}(t)}\bigg|_{t=t_t}\;. \qquad \text{(D.22)}\end{aligned}$$

The two integrals can be taken together to give:

$$\int_{t_b}^{t_t} dt\,\frac{b(r)\partial_r a(r)}{f(r)}\bigg|_{r=r_p(t)} - \int_{t_b}^{t_t} dt\,\partial_r\left(\frac{b(r)a(r)}{f(r)}\right)\bigg|_{r=r_p(t)} = -\int_{t_b}^{t_t} dt\,a(r_p(t))\frac{\partial_r b(r)}{f(r)}\bigg|_{r=r_p(t)}\;. \qquad \text{(D.23)}$$

The resulting expression for the left hand side of the second equation of Eq. (4.35) is then exactly equal to the expression that is found when Eq. (D.20) is applied to the right hand side. Both sides are thus equal, which is what was to be shown.

Bibliography

[1] A. Einstein
Die Grundlage der allgemeinen Relativitätstheorie (Annalen der Physik 49, 769 (1916))

[2] C.W. Misner, K.S. Thorne and J.A. Wheeler
Gravitation (Freeman, San Francisco; 1970)

[3] S. Weinberg
Gravitation and Cosmology (John Wiley & Sons, Inc.; 1972)

[4] J.B. Hartle
Gravity: An Introduction to Einstein's General Relativity (Addison Wesley; 2003)

[5] The Virgo Collaboration
Status and perspectives of the Virgo gravitational wave detector (Journal of Physics: Conference Series 203 (2010)

[6] M. Maggiore
Gravitational Waves. Volume 1: theory and experiments (Oxford University Press, 2007)

[7] A. Balakin, J.W. van Holten, R. Kerner
Motions and world-line deviations in Einstein-Maxwell theory (Class.Quant.Grav.17. 5009-5024 (2000))

[8] A. Einstein
Uber das Relativittsprinzip und die aus demselben gezogenen Folgerungen Jahrbuch der Radioaktivitt und Elektronik 4, 411462 (1907)

[9] G. Lemaitre
Expansion of the universe Monthly Notices of the Royal Astronomical Society, Vol. 91, 490-501 (1931)

[10] C.M. Will
Theory and Experiment in Gravitational Physics (Cambridge University Press, 1993)

[11] P.C. Peters and J. Mathews
Gravitational radiation from Point Masses in a Keplerian Orbit, Physical Review 131 (1963), 435

[12] T. Futamase and Y. Itoh
The Post-Newtonian Approximation for Relativistic Compact Binaries,
http://www.livingreviews.org/lrr-2007-2

[13] K. Schwarzschild
Uber das Gravitationsfeld eines Massenpunktes nach der Einsteinschen Theorie (Reimer, Berlin 1916, S. 189 ff. (Sitzungsberichte der Kniglich-Preussischen Akademie der Wissenschaften; 1916))

[14] J.T. Jebsen
Ark. Mat. Ast. Fys. 15, (1921)

[15] G.D. Birkhoff
Relativity and Modern Physics (Harvard University Press, 1923)

[16] E.F.Taylor, J.A. Wheeler
Exploring Black Holes Addison Wesley; 2000

[17] J. Droste *Het zwaartekrachtsveld van een of meer lichamen volgens de theorie van Einstein*; PhD thesis (Leiden University, Leiden; 1916)

[18] Atam P. Arya
Introduction to Classical Mechanics (Prentice Hall International Inc.; 1998)

[19] S. Chandrasekhar
The Mathematical Theory of Black Holes (Clarendon Press, Oxford; 1983)

[20] E. Poisson
A Relativist's Toolkit (Cambridge University Press; 2004)

[21] R. Kerner, J.W. van Holten, R. Colistete Jr.
Relativistic Epicycles: another approach to geodesic deviations (Class. Quantum Grav. 18 (2001), 4725; arXiv:gr-qc/0102099)

[22] J.W. van Holten
Worldline deviations and epicycles (Int. J. Mod. Phys. A17 (2002), 2645;
arXiv: hep-th/0201083)

[23] G. Koekoek, J.W. van Holten
Epicycles and Poincaré Resonances in General Relativity (arXiv:1011.3973)

[24] J.W. van Holten
Worldline deviations and epicycles (Int. J. Mod. Phys. A17 (2002), 2645;
arXiv: hep-th/0201083)

[25] R. Colistete, C. Leygnac and R. Kerner
Higher-order geodesic deviations applied to the Kerr metric (Class. Quantum Grav. 19 (2002), 4573; arXiv:gr-qc/0205019)

[26] R. Kerner, R. Martin, J. Mignemi and J.W. van Holten
Geodesic Deviation in Kaluza-Klein Theories, Phys. Rev. D63 (2001), 027502; arXiv:gr-qc/0010098

[27] David C. Lay
Linear Algebra and its Applications (Addison-Wesley; 1996)

[28] Ptolemy of Alexandria
Almagest (Ancient Egypt, 2^{nd} Century)

[29] A. Lindtsted
Abh. K. Akad. Wiss. (St. Petersburg) 31 (1882)

[30] H. Poincaré
Les méthodes nouvelles de la mechanique céleste II (Gauthiers-Villars, Paris; 1893)

[31] J.V. José and E.J. Saletan
Classical Dynamics, (Cambridge Univ. Press; 1998)

[32] K. Martel
Particles and black holes: time-domain integration of the equations of black-hole perturbation theory; Phd thesis (The University of Guelph, Guelph; 2004)

[33] K. Martel and E. Poisson
Gravitational perturbations of the Schwarzschild spacetime: a practical covariant and gauge-invariant formalism, Physical Review D. 71 (2005), 104003

[34] T. Regge, J.A. Wheeler
Stability of a Schwarzschild singularity (Phys.Rev. 108: 1063-1069 (1957))

[35] F.J. Zerilli
Effective potential for even-parity Regge-Wheeler gravitational perturbation equations (Phys.Rev.Lett. 24, 737-738 (1970))

[36] V. Moncrief
Gravitational perturbations of spherically symmetric systems. I. The exterior problem (Ann. Phys. 88, 323-342 (1974))

[37] R.A. Isaacson
Gravitational radiation in the limit of high frequency. I. The linear approximation and geometrical optics (Physical Review 166. 1272 (1968))

[38] P.P. Fizief
Exact Solutions of Regge-Wheeler Equation (J.Phys.Conf.Ser. 66, 012016 (2007))

[39] C.O. Lousto, R.H. Price
Understanding initial data for black hole collisions (Phys.Rev.D 56. 6438-6457 (1997))

[40] R. Fujita, W. Hikida, H. Tagoshi
An Efficient Numerical Method for Computing Gravitational Waves Induced by a Particle Moving On Eccentric Inclined Orbits around a Kerr Black Hole (Prog.Theor.Phys. 121. 843 (2009))

[41] S. Hopper, C. Evans
Gravitational perturbations and metric reconstruction: Method of extended homogeneous solutions applied to eccentric orbits on a Schwarzschild black hole (Phys.Rev.D 82. 084010 (2010))

[42] P. Zevenbergen
Gravitational waves: A numerical solution for radial infall on a Schwarzschild background. Master's thesis, Vrije Universiteit Amsterdam, 2008

[43] E. Poisson
Gravitational radiation from a particle in circular orbit around a black hole. VI. Accuracy of the post-Newtonian expansion Phys. Rev.D 52, 5719-5723 (1995)

[44] E. Poisson
Erratum and Addendum: Gravitational radiation from a particle in circular orbit around a black hole. VI. Accuracy of the Post-Newtonian expansion Phys. Rev.D 55, 7980-7981 (1997)

[45] C. Cutler et al.
Gravitational radiation reaction for bound motion around a Schwarzschild black hole, Physical Review D. 50 (1994), 3816

[46] A. Pound, E. Poisson, and B.G Nickel
Limitations of the adiabatic approximation to the gravitational self-force arXiv:gr-qc/0509122v2, 2005

[47] George B. Arfken and Hans J. Weber
Mathematical Methods for Physicists (Academic Press; 1995)

[48] J. de Boer, E. Gimon, K. Schalm and J. Wijnhout
Evidence for a gravitational Myers effect, Ann. Phys. 313 (2004), 402;
arXiv:hep-th/0212250

[49] M. Mohensi
Spinning particles in gravitational wave space time, Phys. Lett. A301 (2002), 382;
arXiv:gr-qc/0208072

[50] J.W. van Holten
Gravitatie en Kosmologie; lecture notes (VU University, Amsterdam; 2000) (in Dutch)

Summary

This is a thesis about gravity, and a number of the interesting effects it has on the motion of stars when they get in close proximity to each other. Describing such motions turns out to be a complicated problem, and this at first seems to be a remarkable statement. After all, gravity is a force that we human beings are very familiar with from every day experience. It is the force that keeps us with our feet on the ground, makes apples fall from trees, traps the Moon in an orbit around the Earth, and the Earth itself in an orbit around the Sun. The fact that research in gravity is nonetheless challenging, is due to the fact that gravity is conceptually very different from the three other fundamental forces that are known in physics (the electromagnetic force, the strong nuclear force, and the weak nuclear force), which reflects itself in the radically different mathematics involved. It is for this reason that it required the genius of two of the greatest scientific minds in history to provide us with an understanding of how things fall.

Gravity according to Newton and Einstein

Sir Isaac Newton (1642-1727) was the first to provide mankind with an accurate description of gravity. He considered it to be an 'action at a distance', a mysterious and invisible tendency of all matter to pull all other matter in the Universe closer. In 1687 he published a mathematical formula with which the pull could be calculated. This *Universal Law of Gravity* is very successful: for the first time in history, mankind had the means to accurately calculate the trek of the planets around the Sun, to predict solar- and lunar eclipses, and to solve the mystery of the tides. Despite these successes, however, a number of things were not quite exactly described by this theory. For example, very precise measurements on the orbit of Mercury show that the planet orbits the Sun slightly faster than predicted by the Universal Law of Gravity. Also, Newton's theory postulates that gravity is an instantaneous force, by which is meant that there is zero elapse of time between a cause and its gravitational effect. If, for example, the Sun were to magically disappear, the gravitational pull felt on the Earth would vanish at the exact same instant. This would indicate that the effects of gravity traversed the distance between the Sun and the Earth with an infinite velocity. This can not be, as it contradicts the *Special Theory of Relativity*. This is a theory, published in 1905 by Albert Einstein (1879-1955), which states that nothing can go faster than light. Gravity is not allowed to be an exception to this rule, and it thus became clear that Newton's Law of Universal Gravity had to be modified.

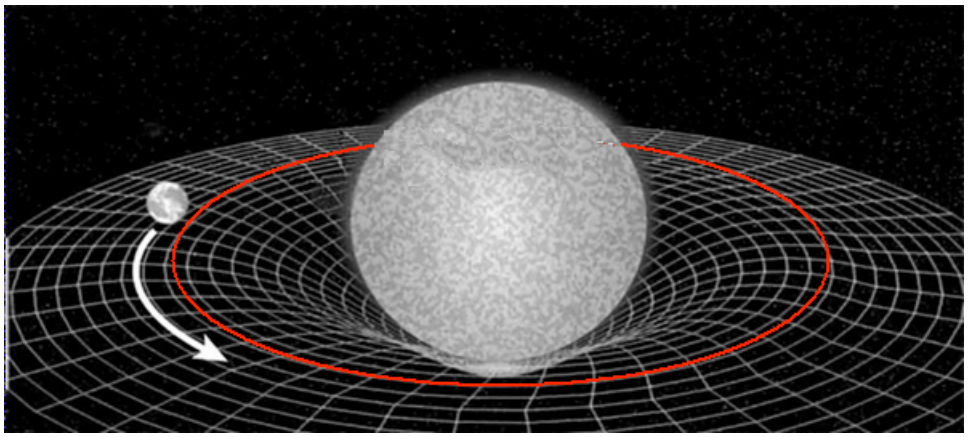

Figure D.1: The curvature of space due to the presence of a star (centre). The planet (left) follows a path that is wrapped around the star due to the curvature of space. The result is a closed orbit.

It was that same Special Theory of Relativity that suggested how this should be done. The theory states that the laws of physics should be the same for all observers moving with a constant velocity with respect to each other. It should therefore be possible to write the equations of physics in such a way that they can be used by all such observers regardless of their relative constant velocity. Einstein realized that this idea should also apply to observers who are *accelerating* with respect to each other, and was able to link this principle to the force of gravity. After all, he argued, if we are standing in an elevator that is accelerating upward, we feel that we are pushed to the floor of the elevator just as we would if there was a force of gravity pulling us down. With this insight, Einstein postulated that the phenomena of acceleration and gravity are fundamentally equivalent to each other, and formulated the *General Theory of Relativity* in 1916.
In the General Theory of Relativity, gravity is described as the curvature of space and time. Just as a meridian deviates from a straight line because the globe is spherically shaped, the path of a mass in motion will not follow a straight line if space is curved; the deviation from the straight line is what we ascribe to gravity. The way that space and time are curved is, in turn, determined by the presence of mass and energy: the more mass is present in space, the more space and time are curved, and the more the paths of masses in motion deviate from straight lines. An example of this is shown in Figure D.1, in which the presence of a heavy star curves space in such a way that the orbit of a planet is wrapped around the star. As a result, the planet follows a closed elliptical orbit instead of a straight line. Einstein published a formula that relates the curvature of space and time to the presence of mass and energy, and showed that when the curvature is not too extreme, the General Theory of Relativity exactly reduces to Newton's Universal Law of Gravity.

Black Holes and Gravitational Waves

The General Theory of Relativity is the most successful description of gravity that we have. It correctly predicts the orbit of the planet Mercury, the deflection of starlight when it grazes the Sun, the slowing down of time due to the presence of mass, and even the expansion of the Universe as a whole. All these predictions have, in a century of experiments, been accurately confirmed by observations. The theory makes two additional predictions that yet await experimental confirmation. The first is the existence of *black holes*: collapsed stars that are so massive that not even light can escape their gravitational pull and where time itself is slowed down to a standstill. Black holes are the most extreme examples of curved spacetime that we know.
The second unconfirmed prediction that the General Theory of Relativity makes is the existence of *gravitational waves*: microscopically small vibrations of space and time that are produced when two large masses move in each other's close proximity. These vibrations travel through the Universe with the speed of light, and we can reveal their presence by closely observing the relative position of two masses. Just as two bobbers will wobble with respect to each other when a little wave of water disturbs the pond, two masses will wobble with respect to each other when a gravitational wave disturbs space and time. The relative motion of the two masses is usually extremely small (the wobbles are typically of the order of a millionth of the size of a proton), and is biggest when the source of the gravitational wave has a very strong field of gravity. The production of the biggest gravitational waves is therefore expected to happen close to a very massive black hole.
Gravitational waves produced in this way contain a treasure trove of information about the black hole and allow us to test the General Theory of Relativity. It is for this reason that measuring gravitational waves is one of the biggest current challenges in physics. At this very moment, experiments such as VIRGO in Italy and LIGO in the United States are working to measure gravitational waves, and plans are in development to continue the effort underground in the upcoming Einstein Telescope, and in space in the upcoming LISA satellite experiment. In all cases, it is of absolute necessity to know in advance the exact shape of the gravitational waves in order to filter out the very small gravitational waves from the data collected by such experiments. This means that these must be calculated using the General Theory of Relativity.

Relativistic Epicycles...

It is not an easy task to calculate gravitational effects close to a black hole, as the mathematics needed to understand the General Theory of Relativity is very complicated. As such, solutions to the formulas are usually found only approximately. One of the ways that researchers do this is by first assuming that the gravitational field around the black hole is weak enough so as to describe it by Newton's Universal Law; the effects due to Einstein's curvature of space and time are subsequently added as corrections to Newton's solutions. A disadvantage of such a method is that it becomes less accurate when the star gets very close to the black hole. After all, it is in that region that the curvature of space and time

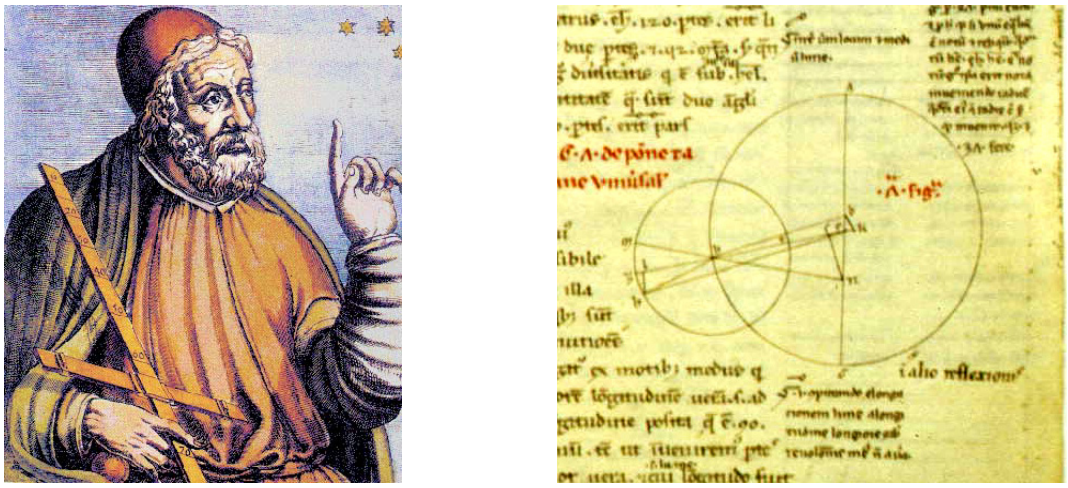

Figure D.2: Ptolemy (left) described the apparent motion of the planets, Sun, and Moon around the Earth by placing circles on top of circles, as is shown on a page (right) from his book *Almagest*.

is the most extreme and Newton's gravity does not suffice anymore. This is unfortunate, as it is also exactly this region where the strongest gravitational waves are produced.
In this thesis we present a novel method to calculate the gravitational waves produced when a star moves in close proximity to a black hole, in which we do not make the assumption that the gravitational field is weak. In our method, we assume instead that the orbit of the star around the black hole is simple enough to be described by a circle. By subsequently adding corrections to this circular orbit, we obtain the equations for more general orbits. The outcome of our calculations turns out to be akin to the system that the ancient egyptian sage Ptolemy (90-168) proposed to describe the apparent motion of the planets, Sun, and Moon around the Earth (which he thought the be at the centre of the Universe). He placed the planets on circles, on top of which he placed smaller circles called *epicycles*, in the manner shown in Figure D.2. Ptolemy's system is, of course, not correct (he made the incorrect assumption that the Earth is at the centre of the Universe, and he had no knowledge of the Theory of Relativity), but our research has shown that the motion of a star around a black hole can be described in a way very similar to Ptolemy's method. In our context, the corrections applied to a circular orbit are not themselves circles, but bear a more complicated shape that we have calculated accurately. We call our model *Relativistic Epicycles*.
In this model we never make any compromise on the strength of the gravitational field of the black hole: we do not assume it to be weaker than it really is. As a result, we expect our predictions for the orbit of the star to be accurate even when the star and the black hole are very close to each other. We found that this is indeed the case: as long as the orbit of the star does not deviate too much from a perfectly circular orbit, our results have an accuracy of more than 99%, and this regardless of how close the star is to the black hole.

...and the resulting gravitational waves

As the orbits of the star around the black hole could be accurately calculated, the next step in our research was to calculate the gravitational waves due to the star's motion in the gravitational field of the black hole. This turns out to be a complicated mathematical challenge: the first steps were already taken in 1957 (half a century ago!), and the final formalism was only published in 2004. This formalism requires that the orbit of the star is known as a function of time, and exactly this is provided by our method of Relativistic Epicycles. The resulting formulas for the gravitational waves we have subsequently solved by using a computer program that we have written ourselves. The gravitational waves we calculated in this way agree very well with the ones that were already known in the literature, and new ones we can calculate effortlessly and rapidly. Here too we found that the accuracy or our method is excellent, with accuracies being of the order of 99% when the orbits do not deviate too much from perfect circles.
Finally, as the last step in our research, we have investigated the limitations of our method of Relativistic Epicycles. The main disadvantage of our method is that we need to assume that the orbit of the star is close to circular; we have indeed found that our results become less accurate when the orbits become more eccentric. However, our calculations have also shown that, as the system sends out gravitational waves, the star's orbit becomes increasingly less eccentric and the predictions of our method are therefore rendered increasingly accurate. This means that the main disadvantage of our method is naturally nullified by the emission of gravitational waves! We therefore conclude that the method of Relativistic Epicycles is very well suited to describe the production of gravitational waves due to the motion of a star around a black hole, even when the star and black hole get in extremely close proximity.

Future research

There are numerous ideas for future research. For example, we could improve the accuracy of the Relativistic Epicycle even more by adding some more corrections on the orbit. Secondly, up to this point we have only taken into account the curvature of space and time due to the presence of the black hole, but it would be in order to also take into account the curvature due to the star. It would also be interesting to investigate whether the calculation of the gravitational waves could be done without invoking a computer, by replacing the outcome of the program by a mathematical formula. Finally, our calculations have shown that the method of Relativistic Epicycles also applies to the situation of electrically charged masses moving around a pulsar (which is a heavy star that is surrounded by a magnetic field that, like a lighthouse, periodically sends out flashes of light). The latter possibility is very interesting, as it allows the study of astrophysical objects by not just looking at the gravitational waves that they send out, but also at their electromagnetics waves. We have already taken the first steps in that direction, which will be the basis for future research.

Populair-wetenschappelijke samenvatting

Dit proefschrift gaat over zwaartekracht, en een aantal van de bijzondere effecten die zij heeft op de beweging van sterren wanneer die extreem dicht bij elkaar in de buurt komen. Dat blijkt een heel ingewikkelde situatie te zijn, en dat lijkt in eerste instantie verbazend. Zwaartekracht is immers een natuurkracht waar iedereen van jongs af aan mee bekend is: het houdt ons met onze benen op de grond, zorgt ervoor dat appels uit de bomen vallen, dwingt de maan in een baan rond de aarde, en de aarde in een baan rond de zon. Wat onderzoek in zwaartekracht desondanks een uitdaging maakt, is dat het een natuurkracht is die veel afwijkt van ons begrip van de rest van de natuurkunde: de zwaartekracht is conceptueel heel anders dan de drie andere fundamentele natuurkrachten (de elektromagnetische kracht, de sterke kernkracht, en de zwakke kernkracht) en haar beschrijving vereist een heel andere wiskunde. Het vereiste dan ook het intellect van twee van de grootste wetenschappelijke genieën uit de historie om inzicht te krijgen in het vallen der dingen.

Zwaartekracht volgens Newton en Einstein

Sir Isaac Newton (1642-1727) was de eerste die een accurate beschrijving wist te geven van de werking van de zwaartekracht. Hij beschouwde het als een 'action at a distance', een mysterieuze en onzichtbare neiging van materie om alle andere materie naar zich toe te trekken, en wist daar een wiskundige formule aan toe te kennen die hij publiceerde in 1687. Deze *Universele Wet van de Zwaartekracht* bleek erg succesvol: voor het eerst in de geschiedenis kon de mensheid nauwkeurig de banen van de planeten berekenen, Zons- en Maansverduisteringen voorspellen, en kenden de getijden geen geheimen meer. Toch bleek een aantal dingen niet helemaal te kloppen: zo laten metingen zien dat de planeet Mercurius iets sneller om de zon draait dan door de Universele Wet van de Zwaartekracht wordt beschreven. Bovendien zegt Newtons theorie dat zwaartekracht instantaan is: er gaat geen tijd verloren tussen oorzaak en gevolg. Bijvoorbeeld: als de Zon op magische wijze zou verdwijnen zou dat op aarde direct merkbaar zijn, wat zou betekenen dat de zwaartekracht de afstand tussen de zon en de aarde heeft overbrugd met een oneindig hoge snelheid. Dat is in strijd met de *Speciale Relativiteitstheorie*, die in 1905 is opgesteld door Albert Einstein (1879-1955) die zegt dat niets sneller kan gaan dan het licht. Zwaartekracht mag hierop geen uitzondering zijn, en dus moest Newtons Universele Wet worden aangepast!

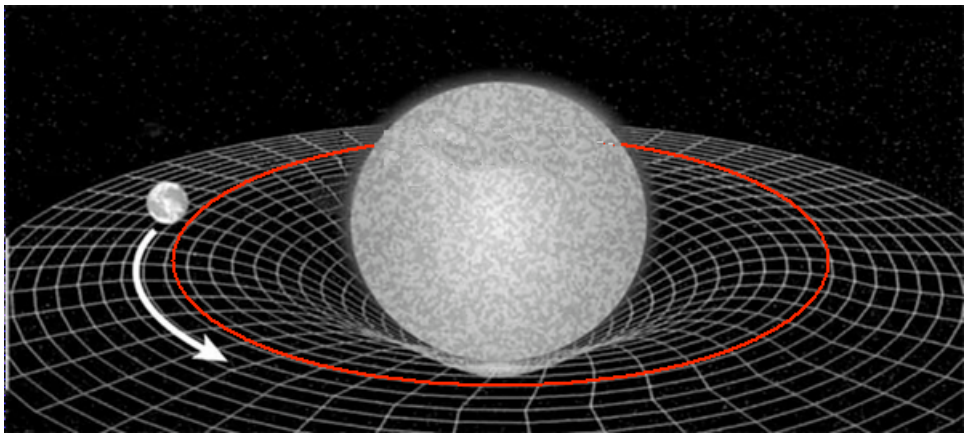

Figure D.3: De kromming van de ruimte door een ster (midden). De planeet (links) volgt een pad dat gebogen is door de kromming van de ruimte. Een gesloten baan rond de ster is het gevolg.

Hoe dat moest gebeuren, werd gesuggereerd door diezelfde Speciale Relativiteitstheorie. Deze zegt namelijk ook dat de wetten van de natuurkunde dezelfde moeten zijn voor alle waarnemers die ten opzichte van elkaar bewegen met constante snelheid. Einstein wist dit principe te verenigen met de zwaartekracht door te stellen dat er eveneens geen onderscheid bestaat tussen waarnemers die zich ten opzichte van elkaar *versnellen*. Immers, zo beredeneerde hij, iemand die in een lift staat die omhoog versnelt voelt dat hij met zijn voeten op de vloer wordt gedrukt, maar zou precies hetzelfde hebben gevoeld als het de zwaartekracht was die hem naar beneden trok. Met dit inzicht stelde Einstein de zwaartekracht equivalent aan versnelling, en formuleerde hij in 1916 de *Algemene Relativiteitstheorie*.
In deze theorie wordt zwaartekracht beschreven door een kromming van de ruimte en tijd. Zoals een meridiaan een gebogen pad volgt omdat de globe bolvormig is, zal een massa een gebogen baan volgen omdat hij beweegt in een ruimte die gekromd is; de buiging van het pad schrijven we toe aan zwaartekracht. De precieze vorm van de kromming van de ruimte en tijd wordt op zijn beurt gedicteerd door de aanwezigheid van massa: hoe meer massa er aanwezig is, hoe meer de ruimte en tijd gekromd zijn. Een voorbeeld hiervan is te zien in Figuur D.3; hierin kromt een zware ster de ruimte zodanig, dat de baan van de planeet om de ster heen gebogen wordt. De planeet volgt dan ook een gesloten baan rond de ster. Einstein publiceerde een formule waarmee de kromming van de ruimte en tijd berekend kan worden. Tenslotte liet hij zien dat, in het speciale geval dat de zwaartekracht niet al te sterk is, de Algemene Relativiteitstheorie weer netjes de Universele Zwaartekracht van Newton oplevert.

Zwarte Gaten en Gravitatiegolven

De Algemene Relativiteitstheorie is de meest succesvolle beschrijving van de zwaartekracht die we kennen. De theorie verklaart de afwijkingen van de baan van Mercurius, de afbuiging van licht door de Zon, de vertraging van de tijd door de aanwezigheid van massa, en zelfs de uitrekking van het Universum. Al deze voorspellingen zijn, vaak uiterst nauwkeurig,

bevestigd door experimentele waarnemingen. De theorie doet verder nog twee exotische voorspellingen. Een ervan is het bestaan van *zwarte gaten*: ineengestorte sterren die zoveel massa samenballen dat zelfs het licht niet aan de resulterende zwaartekracht kan ontsnappen en waar de tijd tot stilstand komt. Zwarte gaten zijn de sterkste bronnen van de kromming van ruimte en tijd die we kennen.
Verder voorspelt de Algemene Relativiteitstheorie het bestaan van *gravitatiegolven*: miniem kleine trillingen van de ruimte en tijd die worden opgewekt wanneer een massa beweegt in het zwaartekrachtsveld van een andere massa. Deze trillingen planten zich voort door het heelal met de snelheid van het licht, en we kunnen hun aanwezigheid meten door goed naar de onderlinge beweging van materie te kijken: zoals twee dobbers in een vijver zullen schommelen ten opzichte van elkaar wanneer er een watergolfje voorbij komt, zullen twee massa's in de ruimte dat doen door een gravitatiegolf. Deze schommelbeweging is echter heel erg klein (de relatieve verplaatsing van de massa's heeft een typische grootte van de kern van een waterstofatoom), en is het grootst wanneer de bron van de golven een heel sterk zwaartekrachtsveld heeft. Een van de sterkste bronnen van gravitatiegolven is dan ook wanneer een ster beweegt in het extreem sterke zwaartekrachtsveld van een zwart gat. Zulke gravitatiegolven bevatten een schat aan informatie over zwarte gaten en over de geldigheid van de Algemene Relativiteitstheorie, en het meten van deze golven is een van de grootste uitdagingen van de hedendaagse natuurkunde. Op dit moment wordt naarstig gezocht naar gravitatiegolven door o.a. de experimenten VIRGO in Italie, LIGO in de Verenigde Staten, en worden er voorbereidingen getroffen om de zoektocht voort te zetten buiten de aarde in het LISA experiment en onder de grond met de Einstein Telescope. Om de zeer kleine gravitatiegolven te herkennen in het meetsignaal en om daar informatie over zwarte gaten uit te concluderen, moet er wel een goede voorspelling paraat staan; dit betekent dat uit de Algemene Relativiteitstheorie berekend moet worden hoe de gravitatiegolven er precies uit zien.

Relativistische Epicykels...

Dat is geen gemakkelijke opgave: de wiskunde van de Relativiteitstheorie is erg ingewikkeld, en oplossingen worden vaak alleen bij benadering gevonden. Veelal wordt er daarbij gebruik gemaakt van de aanname dat de zwaartekracht in eerste instantie zwak genoeg is om beschreven te worden met Newtons Universele Zwaartekrachtswet; de effecten van Einsteins tijdruimtekromming worden daarna als correctie toegevoegd. Nadeel van deze aanpak is dat hij steeds minder goed werkt wanneer de ster steeds dichterbij het zwarte gat komt, omdat daar het zwaartekrachtsveld sterker en sterker wordt. Dat is jammer, omdat juist daar de grootste gravitatiegolven worden opgewekt.
In dit proefschrift presenteren wij een andere methode, die nergens aanneemt dat zwaartekracht zwak is. In plaats daarvan doen wij de aanname dat de beweging van de ster in eerste instantie eenvoudig genoeg is om beschreven te worden door een cirkelbaan, en voegen we daarna correcties op de baan toe om zo de werkelijke, ingewikkelder, beweging te vinden. De uitkomsten van onze berekeningen lijken op het model waarmee de Egyptische wijsgeer Ptolemeus (90-168) in de tweede eeuw na Christus de beweging van de Zon,

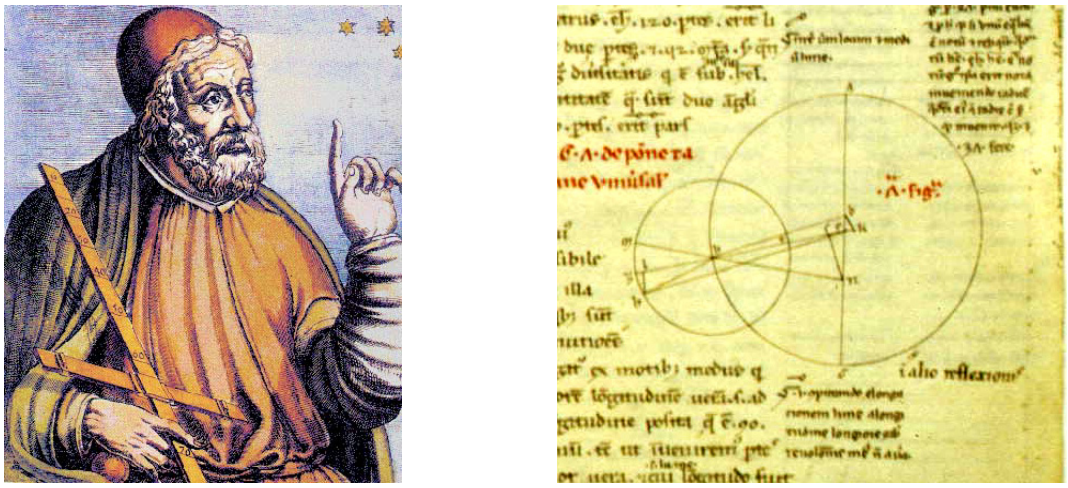

Figure D.4: Ptolemeus (links) beschreef de beweging van planeten en zon rond de aarde door cirkels bovenop cirkels te plaatsen, zoals te zien is op een bladzijde (rechts) uit zijn boek *Almagest*.

de Maan, en de planeten rond de aarde probeerde te verklaren. Hij plaatste daartoe de planeten op een cirkelbaan en voegde kleinere cirkels, de zogenaamde *epicykels*, toe ter correctie, zoals te zien is in Figuur D.4. Ptolemeus' model was, uiteraard, niet correct (zo was zijn aanname dat alle planeten en de zon rond de aarde draaien al verkeerd, laat staan dat hij kennis had van de Relativiteitstheorie), maar ons onderzoek heeft laten zien dat de Algemene Relativiteitstheorie dicteert dat de beweging van een ster rond een zwart gat op een soortgelijke manier te beschrijven is. In ons geval zijn de correcties niet cirkelvormig maar een ingewikkelder gesloten vorm, die we heel precies hebben uitgerekend. Wij noemen ons model *Relativistische Epicykels*.
Omdat wij het enorme zwaartekrachtsveld van het zwarte gat in vol ornaat meenemen, is de verwachting dat de uitkomsten van onze Relativistische Epicykels uiterst nauwkeurig zijn.. zelfs wanneer de ster extreem dicht bij het zwarte gat komt. We vinden dat dat inderdaad het geval is: zolang de banen niet te zeer afwijken van een cirkelbaan, komen onze uitkomsten typisch voor meer dan 99% overeen met de werkelijke banen.

...en de resulterende gravitatiegolven

Nu de banen bekend zijn, is de volgende stap het berekenen van de gravitatiegolven ten gevolge van de beweging van de ster rond het zwarte gat. Dit is een hele opgave gebleken: de eerste stappen werden al gezet in 1953, en een uiteindelijk formalisme is pas in 2004 gepubliceerd. Dit formalisme vereist dat de baan van de ster rond het zwarte gat in wiskundig precieze vorm bekend is als functie van de tijd, en onze Relativistische Epicykels stellen ons in staat dat te doen. De aldus verkregen formules voor de gravitatiegolven hebben we daarna door de computer laten oplossen, met behulp van een computerprogramma geschreven in de taal C++. De gevonden gravitatiegolven blijken goed overeen te komen met de uitkomsten die al in de literatuur bekend waren, en nieuwe uitkomsten berekenen

we nu snel en gemakkelijk. Ook hier geldt dat een nauwkeurigheid van ruim 99% gebruikelijk is.
Tenslotte hebben we onderzoek gedaan naar de beperkingen van onze Relativistische Epicykels. Het nadeel van onze methode is immers dat de baan van de ster rond het zwarte gat niet teveel mag afwijken van een cirkel; inderdaad vinden we dat onze uitkomsten minder nauwkeurig worden naarmate de ster een meer en meer eccentrische baan volgt. Echter, onze berekeningen laten ook zien dat de uitgezonden gravitatiestraling ervoor zorgt dat de baan van de ster van vorm verandert, en wel zodanig dat hij steeds cirkelvormiger wordt. Dit betekent dat onze uitkomsten steeds nauwkeuriger worden naarmate de ster dichterbij het zwarte gat komt! Het nadeel van onze methode wordt dus teniet gedaan door de natuurlijke cirkelvorming van een eccentrische baan ten gevolge van het uitzenden van gravitatiegolven. We concluderen dan ook dat onze Relativistische Epicykels erg geschikt zijn voor het beschrijven van de gravitatiegolven opgewekt door de beweging van een ster rond een zwart gat, zelfs wanneer de ster uiterst dichtbij het zwarte gat is.

Vervolgonderzoek

Ideeën voor vervolgonderzoek zijn er volop. Zo kan de nauwkeurigheid van de Relativistische Epicykels verder worden verhoogd door nog een aantal extra correcties op de baan uit te rekenen. Verder is tot nu toe louter de tijdruimtekromming van het zwarte gat beschouwd en dat van de ster verwaarloosd; een vervolgstap zou kunnen zijn deze extra tijdruimtekromming ook in rekening te brengen. Ook is het interessant te onderzoeken of de berekening van de gravitatiegolven niet zonder computer gedaan zou kunnen worden, door de berekening van het C++ programma te vervangen door een puur wiskundige formule. Tenslotte is uit onze berekeningen gebleken dat onze methode ook in staat is de beweging van elektrisch geladen deeltjes te beschrijven rond een pulsar (een zware ster met een magnetisch veld die, zoals een vuurtoren, regelmatig lichtflitsen uitzendt). Met name deze laatste mogelijkheid is bijzonder interessant, omdat pulsars ons in staat stellen multimessenger astronomy te doen: het bestuderen van de sterren door zowel naar gravitatiegolven te kijken als lichtgolven. De eerste stappen in die richting hebben we al gezet, en zal de basis zijn van vervolgonderzoek.

Gideon Koekoek,
2011.

Acknowledgments

Ever since I was little I have wanted to become someone who knows (or at least *studies*) the secrets of the Universe, the planets, and the stars. By finishing this thesis and officially ending my PhD-training, I seem to have reached that goal and it makes me happy. There are a number of people responsible for helping me to get to this point, and I would like to acknowledge them here.

First and foremost, there are my two promotors prof.dr. Jo van den Brand and prof.dr. Jan-Willem van Holten. When Jo started the Virgo group at Nikhef, I was one of the first PhD-students to work on this fascinating project. I would like to thank him for his support, which he gave from the early beginning of my research until the end, and after. Jan-Willem van Holten was my daily supervisor, whose insights in and knowledge of (seemingly) all of physics always proved highly inspirational to me. I would also like to thank both my promotors for letting me pioneer. The first years of my PhD-studies I spent investigating several possible ways to calculate gravitational waves, and I am grateful to Jo and Jan-Willem for allowing me to do so as I have found the efforts to be educational. Finally, my promotors also gave me ample opportunity to flaunt my love (and knack) for teaching. I especially have good memories of being Jan-Willem's teaching assistant (and, for one lecture series, the acting teacher) of the Gravitation & Cosmology course, and of writing and teaching the Quantum Universe course alongside Jo. I enjoyed that very much, and I am happy to say that the students did too.
My office mates Sipho, Paul 7 en Robb deserve a thanks for fun times, musical interruptions and discussions about physics, LOLcats, and the likes, and, in later years, allowing me to get my yoga on during working hours and to mumble along with EpicwapbattlitoryYy every now and then. I enjoyed sharing an office with those guys! Sipho especially I thank for putting up with me during the many years we have shared an office and an endless stream of B&B chuckles, and during the many conference trips we've made. Prima kantoorgenoot!
Paul deserves an extra mention for doing valuable preliminary work that made the numerical code possible. His initial implementation for the calculation of gravitational waves due to radially in-falling test masses cured me of my dislike for programming, and even though I spent quite some time to upgrade the code to allow the calculation of gravitational waves for *any* motion of the test mass, the original inception was Paul's.
Eric Laenen, R.Toor and Lisa the QB of the Nikhef theory group I would like to thank for

regularly regarding me as one of them whenever there was a group activity. Even though I gravitated towards the Virgo group more and more, it was nice to feel welcome.
The Virgo group of Nikhef has offered a motivational environment to do physics and I want to thank the people for happy times and interesting discussions. The same goes, of course, to all friends and colleagues at Nikhef, where I was happy to become a student so many years ago and where I have had such good times since. I wish Giuseppe d'Ambrosi similar times during his years at Nikhef, and I hope the work presented in this thesis will be a good starting point for his own PhD research.
Stepping outside of physics, a special mention is deserved by the YogaYatra studio lead by the inspirational Corine Leegwater. It is there where I have learned that the Universe has more to offer than a set of beautiful mathematical laws, as it is also a place of great comfort when you look at it the right way. This holds especially true when surrounded by like-minded people. So! ♫ Om Purnamadah Purnamidam[1] ♫.

And, on that note, I would like to end by thanking my friends, in & outside of physics. Life is not always easy, and it is due to your support that this thesis came to fruition. Thank you, my dear paranimfs, the good doctors E. Forest and the Z.Meister, for your friendship during our many shared years in physics.. and beyond! Many more people come to mind, all of whom I thank for being there both in happy times and in times of need. Annebol, Emka :E → :@, Voska, Dogless John, Noosh, Salvo Hedgehog & Marie, Handsome Mark, Besma, the De Boers, Molly Swanson, Don Diablo Marten, the list is long. I gladly dedicate this thesis to all of you.

[1]For the non-yogi and -yogini, in mathematics this mantra can be read as: $\infty - \infty = \infty$.